Numerical Investigation of Turbulent Fluid Flow Over a Porous Aerofoil Wing Design Within a Magnetic Field

Gideon Kimutai Kirui

2025-10
UoK
https://ir-library.kabianga.ac.ke/handle/123456789/1103

NUMERICAL INVESTIGATION OF TURBULENT FLUID FLOW OVER A POROUS AEROFOIL WING DESIGN WITHIN A MAGNETIC FIELD

GIDEON KIMUTAI KIRUI

A THESIS SUBMITTED TO THE BOARD OF GRADUATE STUDIES IN PARTIAL FULFILLMENT OF THE REQUIREMENTS FOR THE CONFERMENT OF THE DEGREE OF MASTER OF SCIENCE IN APPLIED MATHEMATICS OF THE UNIVERSITY OF KABIANGA

UNIVERSITY OF KABIANGA

OCTOBER, 2025

DECLARATION AND APPROVAL

DECLARATION

I hereby declare that this research thesis is my own original work and has not been presented for the conferment of a degree or award of a diploma in this or any other institution.

Signature…………………………………… Date……………………………...…...

Kirui Kimutai Gideon

PGC/AM/008/19

APPROVAL

This thesis has been submitted with our approval as university supervisors.

Signature…………………………………Date ………………………………………..

Wilys O. Mukuna, PhD

Department of Mathematics, Actuarial and Physical Sciences

University of Kabianga

Signature…………………………….……Date ………………………………………

Prof Maurice O. Oduor, PhD

Department of Mathematics, Actuarial and Physical Sciences

University of Kabianga

COPYRIGHT

DEDICATION

This thesis is dedicated to my students, my parents for their unfailing and unconditional love. And my friends, they have never left my side and are very special indeed.

I love you all dearly.

ACKNOWLEDGEMENT

Undertaking this research has been a truly life-changing experience for me and it would not have been possible without the support and guidance that I received from many people. There are a number of people without whom this thesis might not have been written, and to whom I am greatly indebted. Professor Maurice O. Oduor and Doctor Wilys O. Mukuna have been the ideal thesis Supervisors. Their sage advice, insightful criticism, and unstinting encouragement aided the writing of this thesis in innumerable ways. My deepest and higher gratitude goes to all my family members for their endless support, encouragement and spontaneous prayer during my study while I am away from home. I would also like to further thank, my colleagues, Mr Mukubwa and Boaz, for the many informative discussions we have held. More so, my regards are due to my classmates, Dorcas, Juma and Ongaro, whose steadfast support towards the success of this project was greatly needed and deeply appreciated. I am also very grateful to Kabianga School for their immense contribution which has left an everlasting footprint. It is necessary to acknowledge the goodness, generosity and the true sense of family-ship they have shown to me holistically as I came across in the academia from the onset of this program. I gratefully acknowledge the funding received towards my MSc. from Higher Education Loans Board – (HELB), which enabled me to pursue my study here at University of Kabianga.

ABOVE ALL YAHWEH

ABSTRACT

Aerofoil wings are an essential component of aircraft design, as they provide lift and enable flight. However, the flow of air over the wing is often turbulent, which can lead to decreased efficiency and performance. Porous aerofoil wings was proposed as a means of reducing turbulence, and the effects of such wings on fluid flow within a magnetic field have been investigated. A mathematical model of turbulent fluid flow over a porous aerofoil wing design within a magnetic field M=0.1 to M=2 was considered. The fluid flow was modeled using Navier Stokes equations for the conservation of momentum, energy and mass in cylindrical coordinates. The governing equations were then non-dimensionalized by the non- dimensional flow parameters such as magnetic parameter(M), Hall parameter(m), Prandtl number(Pr), and Grashof number (Gr) on fluid velocity and temperature distribution and gave rise to the non-dimensional parameters. Computational fluid dynamics (CFD) techniques were used to simulate the flow of air over a porous wing within a magnetic field strength. Examination of the effects of the magnetic field on key performance metrics such as lift, drag, and efficiency, as well as the overall flow structure of the wing was performed and found valuable insights into the use of porous aerofoil wings in the design of aircraft operating in high-magnetic field environments, such as those found in space or near the Earth's poles. Additionally, the outcomes of the research had wider implications for other domains investigating the impact of magnetic fields on fluid motion, such as in the design of magnetic resonance imaging systems or in the study of planetary motions. In this research, numerical investigation of the effects of a magnetic field on turbulent fluid flow over a porous aerofoil wing design was done. Variation of Prandtl number (from Pr = 0.7 to 3) significantly varied the temperature profile while it had no observable effect on the velocity profiles. It is evident from the results that the primary velocities increase when the magnetic parameter was reduced. It was also found that the lift force increase when the Grashof number and Prandtl number was decreased.

TABLE OF CONTENTS

LIST OF FIGURES

LIST OF ABBREVIATIONS

ANSYS	Analysis of Systems
BEM	Boundary Element Method
BTCS	Backward Time Central Space
CFD	Computational Fluid Dynamic
DES	Detached Eddy Simulation
DNS	Direct Numerical Simulation
EM	Electromagnetic
FDM	Finite Difference Method
FEM	Finite Element Method
FTCS	Forward Time Central Space
FVM	Finite Volume Method
IGA	Isogeometric Analysis
IVP	Initial Value Problem
LEP	leading Edge Protuberance
LES	Large-Eddy Simulation
MHD	Magnetohydrodynamics
MOO	Multi-Objective Optimization
NACA	National Advisory Committee for Aeronautics
NASA	National Aeronautics and Space Administration
NLH	Nonlinear Helmholtz Equation
ODE	Ordinary Differential Equation
PANS	Partially-Averaged Navier-Stokes
PDE	Partial Differential Equation
PEM	Porous Electromagnetism
PM	Porous Media

RANS	Reynolds-averaged Navier-Stokes
ROM	Reduced-Order Model
RSAs	Response Surface Approximations
RSM	Reynolds Stress Model
SAS	Spalart-Allmaras Model
SCR	Selective Catalytic Reduction
TR-PIV	Time-Resolved Particle Image Velocimetry
UAV	Unmanned Aerial Vehicles
UOK	University of Kabianga
UQ	Uncertainty Quantification
VLES	Very Large Eddy Simulation

LIST OF SYMBOLS

C_p	Specific heat at constant pressure, $J/\mathrm{kg/K}$
t	Time (s)
E_c	Eckert number
∇	Gradient operator, ($\nabla = i\ \frac{\partial}{\partial x} + j\frac{\partial}{\partial y} + k\frac{\partial}{\partial z}$)
$\frac{D}{Dt}$	Material derivative, ($\frac{D}{Dt} = \frac{\partial}{\partial t} + u\ \frac{\partial}{\partial x} + v\frac{\partial}{\partial y} + w\frac{\partial}{\partial z}$)
$\frac{\partial}{\partial t}$	Partial derivative with respect to time
P_{rt}	Turbulent Prandtl number
M	Magnetic parameter
Gr	Grashof number
Re	Reynolds number
R_t	Time parameter
Φ	Viscous dissipative function
(x, y, z)	Cartesian coordinates variables
(r, θ, z)	Dimensional cylindrical coordinates
(r, θ, φ)	Spherical coordinates variables
u, v, w	Velocity components in Cartesian coordinates (m/s)
$u_r,\ u_\theta,\ u_z$	Velocity components in cylindrical coordinates (m/s)
$u_r,\ u_\theta,\ u_\varphi$	Velocity components in spherical coordinates (m/s)
U^*, V^*, W^*	Dimensional mean velocity components, m/s
x^*, y^*, z^*	Dimensional Cartesian co-ordinates
t^*	Dimensional time, s

T^*	Dimensional temperature, K
T_∞^*	Temperature of the fluid in the free stream, K
T_w^*	Temperature of the fluid at the surface, K
U, V, W	Dimensionless mean velocity components
x, y, z	Dimensionless Cartesian co-ordinates
P	Pressure of the fluid
μ	Dynamic viscosity of the fluid
η	Viscosity
ν	Kinematic viscosity
B	Magnetic field strength, Width of the wing
A	Reference area of the wing (used to calculate lift and drag coefficients)
Q	Volumetric flow rate
α	Angle of attack
β	Angle of sideslip
γ	Angle of incidence
Δ	Difference or change in a quantity
τ	Shear stress
ω	Angular velocity

Ψ	Stream function
Ξ	Stream function for porous media flow
μ_0	Permeability of free space (magnetic constant)
ϵ_0	Permittivity of free space (electric constant)
σ	Electrical conductivity ($\omega^{-1}m - 1$)
ϵ	Permittivity
r	Distance from origin
T	Temperature (K)
L	Length of the wing
U	Velocity of the fluid flow
C	Chord length of the wing
ρ	Density of the fluid (kg/m^3)
Re	Reynolds number
C_d	Drag coefficient
C_L	Lift coefficient
AoA	Angle of attack of the wing
H_o	External applied transverse magnetic field intensity (wbm^{-2})
u', v', w'	Fluctuating components of velocity
H	Magnetic field intensity (wbm^{-2})
J	Current density vector

DEFINITION OF TERMS

Angle of attack is the angle between the wing and the direction of the flow of a fluid (such as air). The angle of attack determines the lift and drag generated by the wing.

Aerofoil is a streamlined body that is capable of generating significantly more lift than drag when moving in air.

Computational fluid dynamics (CFD) is a numerical method for simulating and analyzing fluid flow, heat transfer, and related phenomena.

Drag is the force exerted on an object in the direction of the flow of a fluid (such as air). Drag opposes the motion of the object and can reduce efficiency and performance.

Fluids are substances that are not in solid form and are sensitive to external pressure, they flow easily and are not rigid, but changes shape when a shear force is applied, no matter how small the force is.

Lift is the force exerted on an object that is perpendicular to the direction of the flow of a fluid (such as air). Lift is what enables an aircraft to generate upward force and become airborne.

Permeability is the ability of a porous material to allow fluids to flow through it. It is often characterized by the permeability coefficient, which is a measure of the ease with which a fluid can flow through the material.

Porous aerofoil wing an aerofoil wing with small holes or perforations in the surface, designed to alter the flow of air over the wing and reduce turbulence.

Turbulent flow is a type of fluid flow characterized by chaotic, turbulent eddies and fluctuations in velocity and pressure

CHAPTER ONE

INTRODUCTION

1.1 Overview

The concept of hydromagnetic turbulent fluid flow over a porous curved surface is introduced in this chapter. Statement of the problem is then presented. Objectives, significance, assumptions and approximations of this study are stated.

1.2 Background of the Study

The turbulent flow of fluid over aerofoil wings is an important area of research in the field of aerospace engineering, as it has the potential to improve the performance and efficiency of aircraft (Klose et al., 2018). Turbulent flow is a type of fluid flow characterized by chaotic, turbulent eddies and fluctuations in velocity and pressure, and it can lead to decreased lift and increased drag, reducing the overall performance of the wing.

One potential solution to this problem is the use of porous aerofoil wings, which have been shown to reduce turbulence in some cases (Fan et al., 2018). Porous aerofoil wings are designed with small holes or perforations in the surface of the wing, which allow some portion of the air flowing over the wing to pass through, rather than being deflected around the wing. This can alter the flow structure over the wing and reduce turbulence, leading to improved performance. However, the effects of porous aerofoil wings on turbulent fluid flow over a magnetic field have not been effectively investigated. This is an important area of study, as many aircraft operate in high-magnetic field environments, such as those found in space or near the Earth's poles.

Understanding the interaction between porous aerofoil wings and magnetic fields could enable the design of more efficient and effective aircraft for these environments.

In this study, a numerical exploration of the influence of a magnetic field on turbulent fluid flow through a porous wing design was conducted. Pore size of less than 5mm in diameter was uniformly spaced at 5mm on the wings. Computational fluid dynamics (CFD) techniques were used to simulate the flow of air over a porous wing within a range of magnetic field strengths, examined the effects on key performance metrics such as lift, drag, and efficiency, as well as the overall flow structure of the wing. The use of CFD in this study enabled us to effectively model and analyze the fluid flow over the wing in a computationally efficient manner. A range of CFD models, including Reynolds-Averaged Navier-Stokes (RANS) and Large-Eddy Simulation (LES), were used to capture the effects of turbulence on the flow. A consideration to the use of different porous media models to accurately represent the flow through the porous region of the wing was done (Wood et al., 2020).

This study has provided valuable insights into the use of porous aerofoil wings in the design of aircraft operating in high-magnetic field environments. Furthermore, the results of this study could potentially be applied to other fields where the effects of a magnetic field on fluid flow are of interest, such as in the design of magnetic resonance imaging systems or in the study of planetary atmospheres.

Poromechanics is the study of fluid-filled porous media. Porous materials are composed of a network of pores or cavities distributed in a solid or matrix. One way to think about this is to use a solid, such as a water-soaked sponge, similar to a porous ceramic block, except that it is saturated with liquid. A porous curved surface is a porous surface which is not flat but rounded, an object can have a porous surface all around it, and such objects have only one porous surface throughout it.

The images in figure 1.1 show some objects of porous curved surfaces

Figure 1.1: *Porous curved surfaces:(a) wings of the dove,(b) Aerofoil ,and (c) insect wing*

There are two main types of forces on a curved surface: vertical forces and horizontal forces. Vertical forces are determined by the weight of the liquid enclosed by the surface and the free horizontal surface of the liquid. These forces act in line with the center of gravity of the volume. On the other hand, horizontal forces operate at the pressure center of a curved surface's projected area and are equal to the forces applied to the surface's projected area.

Magneto Hydrodynamics, explores the interaction of fluids and magnetic fields at low frequencies, assuming minimal Maxwell bias and treating fluid as a continuum (Cortés-Dominguez, 2018). It holds significance in various technical areas, including MHD generators, plasma research, nuclear reactors, oil exploration, geothermal energy, and aerodynamics (Pandit, 2015).

1.2.1 Fundamental Fluid Dynamic Concepts

There are several fundamental concepts in fluid dynamics that are relevant to this study on the numerical investigation of turbulent fluid flow over a porous aerofoil wing design within a magnetic field. They include:

Continuity equation: This is a fundamental equation in fluid dynamics that states that the mass of a fluid flowing through a given region must be conserved. It is often expressed as an equation relating the mass flow rate, cross-sectional area, and velocity of the fluid (equation 3.1).

Navier-Stokes equations: Fundamental set of equations governing the movement of viscous fluids, play a crucial role in simulating fluid flow in computational fluid dynamics. They consist of a momentum equation and a mass conservation equation, and they involve terms representing the viscous forces acting on the fluid.

Boundary layer: This is a thin layer of fluid that forms adjacent to a solid boundary in a flowing fluid. The boundary layer is characterized by a gradual transition in velocity and other flow properties from the free-stream flow to the solid boundary (Goldstein, 2014).

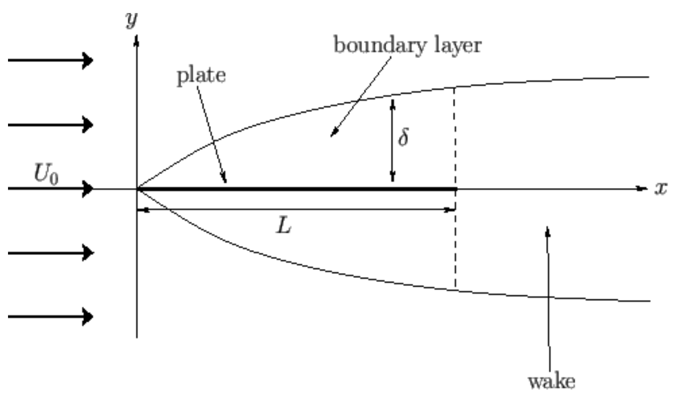

Figure 1.2: *Flow over a flat plate*

Turbulent flow: This is a type of fluid flow characterized by chaotic, turbulent eddies and fluctuations in velocity and pressure. Turbulence can significantly affect the performance of an aerofoil wing and is an important area of study in fluid mechanics. An understanding of these and other fundamental concepts in fluid dynamics is important for conducting a study on the proposed numerical investigation.

Free Stream Flow: Free stream flow refers to the natural motion of a fluid without any external influence or perturbation, except perhaps gravity. In the context of MHD, this typically implies a fluid moving in the absence of any applied magnetic fields or other external forces. In free stream flow, the fluid dynamics are governed solely by the inherent properties of the fluid, such as viscosity, density, and velocity (Goldstein, 2014).

Forced Stream Flow: Forced stream flow, on the other hand, involves the imposition of external forces or fields on the fluid to induce motion or alter its behavior. In MHD, this often entails the application of a magnetic field to the fluid, which can significantly influence its flow characteristics due to the interaction between the magnetic field and the conductive properties of the fluid. This interaction, known as the Lorentz force, can exert control over the fluid motion and lead to phenomena such as magnetohydrodynamic turbulence, flow stabilization, or flow control. In practical applications of MHD, both free stream flow and forced stream flow play crucial roles. Understanding the interplay between these two types of flow is essential for predicting and controlling fluid behavior in systems such as plasma confinement in fusion reactors, electromagnetic propulsion systems, and magnetic drug targeting, among others (Jha, et al., 2018).

1.2.2 Turbulent Fluid Flow

The Reynolds number is one of the metrics employed to distinguish laminar from turbulent fluid flow. A flow is considered laminar if the Reynolds number is up to 2300, and the properties of the fluid at each point of the flow remain constant--including velocity and pressure since viscous force is more prominent due to the slower flow rate. A flow is considered turbulent if the Reynolds number is greater than 3500. A faster and irregular flow path maximizes the inertial force in the system. Unlike laminar flow, the fluid layers in turbulent flow can cross paths due to the continuous change in the magnitude and direction of the flow. Eddies or swirls can be observed in turbulent flow, and the apparent erratic flow behavior makes the analysis of turbulent flow a challenge.

However, despite the challenges, turbulent flow analysis is important for industries, as most flows observed are turbulent. Due to the turbulence of the liquid, the momentum of the liquid changes over time, which is equal to the force generated at a certain distance. The change in velocity, that is, the properties of the fluid for a given point per unit of time in the system, causes periodic turbulence. Reynolds number(Re) increases proportionally with increasing fluid turbulence (Markatos, et al., 2015).

In aviation, aerofoils are used to alter airflow in order to create lift. The aerofoil has a curved leading edge, a pointed trailing edge and an upper and bottom surface. Straight line drawn from the trailing edge to the leading edge is the chord line. The angle of Attack is the angle between the chord line and the flow of relative wind. The angle of attack may be modified based on the situation. The flow across NACA 6412, 7412, and 8412 was examined by Manda et al.,(2020). The analysis concluded that the aerofoil 8412 has showed a better flow separation.

1.2.3 Magnetic Field Effect on Fluid Flow

The problem of free convective magnetohydrodynamic fluids is of great interest in such industries as MHD accelerators, aeromagnetic hydrodynamics, and space technologies such as celestial bodies. In petroleum engineering, MHD principles are applied in the development of technologies for cleaning and filtration processes, particularly those involving the flow of oil through porous rocks (Chebos et al., 2016). The magnetic field is created automatically by the moving charge, and the fluctuating magnetic field induces the Hall current. When researching the influence of magnetic fields on the temperature distribution of electrically conducting liquids, the Hall Effect is of significant interest. Magnetohydrodynamic(MHD) is the study of the flow of electrically conducting fluids in the presence of a magnetic field.

1.2.4 Numerical Solution of Turbulent Fluid Flow

Turbulent modeling and simulation is the key to solving fluid flow numerically because most practical fluid flows are turbulent. CFD is the art of rewriting the governing partial differential equations of fluid flow with numbers and advancing these numbers through space and time to produce a comprehensive numerical description of the flow field. Computational issues require the manipulation and solution of numbers (Argyropoulos, et al., 2015). It can be stated that the output of CFD is a collection of numbers accompanied by extensive analysis and discussion. When the turbulent model is combined with the control equation, terms like turbulent viscosity and turbulent thermal diffusivity are transformed into their laminar equivalents. The dimensionless and non-linear control equations for the partial differential will be sampled along with additional terms by the finite difference method and solved into a numerical solution with the help of mathematical computer software.

1.3 Statement of the Problem

The use of porous aerofoil wings has the potential to improve the performance and efficiency of aircraft by reducing turbulence in the flow of fluid over the wing. However, the effects of porous aerofoil wings on turbulent fluid flow within a magnetic field have not been investigated. This is a significant gap in existing literature, as many aircraft operate in high-magnetic field environments, such as those found in space or near the Earth's poles. Therefore, the problem that this research has addressed is, the effects of a magnetic field on turbulent fluid flow over a porous aerofoil wing design. This study has numerically investigated the effects of a magnetic field on turbulent fluid flow over a porous aerofoil wing design using Computational Fluid Dynamics (CFD) techniques. The effects of the magnetic field on key performance metrics such as lift, drag, efficiency, and the overall flow structure of the wing,has been examined.

1.4 General Objective of the Study

The general objective of this study was to numerically investigate the effects of a magnetic field on turbulent fluid flow over a porous aerofoil wing design using Computational Fluid Dynamics (CFD) techniques.

1.5 Specific Objectives of the Study

The specific objectives of this study were to :

(i). Model the Magnetohydrodynamic Stokes problem for curved surface using hydrodynamics' physical laws.

(ii). Simulate the flow of air over a porous aerofoil wing within a range of magnetic field strengths using Computational Fluid Dynamics (CFD) techniques .

(iii). Determine the effect of fluid properties, on flow variables with curved surface due to velocity variation and give the physical representation of each.

1.6 Significance of the study

The numerical investigation of turbulent fluid flow over a porous aerofoil wing design within a magnetic field is an important area of research in the field of aerospace engineering, as it has the potential to inform the design of more efficient and effective aircraft for use in high-magnetic field environments. Such environments are of particular interest in the aerospace industry, as many aircraft operate in these conditions, including those used for military, commercial, and space.

By better understanding the interaction between porous aerofoil wings and magnetic fields, we can design aircraft that are more resistant to turbulence and have improved performance and efficiency. This can lead to significant benefits for the aerospace industry, including reduced fuel consumption, lower operating costs, and improved safety.

In addition to the aerospace industry, the results of this study may also have broader applications in fields such as electromagnetism, engineering, and medical imaging. By gaining a deeper understanding of the effects of a magnetic field on fluid flow, we can better understand and model a wide range of phenomena involving magnetohydrodynamic (MHD) flows.

Overall, the significance of this study lies in its potential to contribute to the development of more efficient and effective aircraft and to advance our understanding of fluid flow in the presence of a magnetic field. The results of the study inform the design of aircraft specifically designed for use in high-magnetic field environments, such as those found in space or near the Earth's poles. This could lead to the development of more reliable and effective aircraft for these applications.

The study will help to identify optimal porous wing designs and porous media models for use in the presence of a magnetic field, enabling the design of more efficient and effective porous aerofoil wings. The findings of the study are of interest to researchers in other fields, such as electromagnetism and engineering, who are studying the effects of a magnetic field on fluid flow. This could lead to cross-disciplinary collaborations and the development of new research directions (Jin et al., 2022).

The study will help to improve our understanding of the physics of fluid flow in the presence of a magnetic field, including the mechanisms by which a magnetic field affects the flow structure and performance of a porous aerofoil wing. MHD is applicable in the field of Engineering including electromagnetic pumping, electric power generation and control of moving molten metals among others. In the realm of aerodynamics, this research demonstrates the value of cooperation, resulting in improved flow field designs. MHD is useful for describing unstable astrophysical systems and fluid flow. It has applications in astronomy, engineering, solar physics, and high-temperature aeronautics. The study benefits areas such as sunspots, the solar cycle, magnetic stars, and fluid-filled astronomical bodies. turbulent astrophysical flow, water evaporation, sewage, space heating and cooling, and solar energy technologies all exhibit Navier Stokes Issue (Wood, 2011). Therefore, the study is of great importance for Aerofoil Design, Astrophysics, Engineering, and general applications of MHD and heat transfer devices.

1.7 Assumptions and Approximations of the Study

In MHD, various assumptions and estimates were made to arrive at the final control equation. This section states the approximations and assumptions that took place during the modeling process.

1.7.1 Assumptions of the Study

It was assumed that:

i) The wing geometry and material properties used in the study were representative of real-world wings and do not significantly affect the results of the study.

ii) The flow over the wing is two-dimensional and does not significantly vary in the spanwise direction and the flow over the wing is steady and does not vary significantly over time.

iii) The magnetic field is does not vary significantly over the length of the wing.

iv) The flow over the wing was inviscid, meaning that viscous forces are not significant and can be neglected.

v) The flow over the wing is incompressible, meaning that the density of the fluid remained constant .

vi) The flow over the wing was isothermal, meaning that the temperature of the fluid remains constant and does not vary significantly.

vii) The magnetic Reynolds number is astronomically high, indicating that magnetic diffusion may be disregarded. The ion slip current is insignificant. The applied magnetic field is insufficient to generate a substantial ion leakage current.

viii) The velocity of the fluid, v, squared and the speed of light, c, squared have a negligible ratio. i.e. ($\frac{v^2}{c^2}$<<1)

ix) Since ideal fluids are regarded incompressible, their density is considered a space- and time-invariant constant.

1.7.2 Approximations of the Study

These approximations were necessary to simplify the problem and make it tractable to solve computationally. Here are a few examples:

i) It was necessary to use a simplified geometry for the wing, such as a flat plate or a NACA airfoil, rather than a more complex, realistic wing shape.

ii) Using a reduced-order model, such as a Reynolds-averaged Navier-Stokes (RANS) model, was used to simplify the mathematical description of the flow.

iii) The grid used had a limited number of cells to discretize the flow domain, which may not capture all of the fine-scale features of the flow. It may be necessary to use a porous media model that makes assumptions about the flow through the porous region of the wing, such as the Brinkman model or the Kozeny-Carman model.

iv) It has been necessary to assume that the flow over the wing is two-dimensional, meaning that the flow does not significantly vary in the spanwise direction. This simplification can significantly reduce the computational cost of the study.

CHAPTER TWO

LITERATURE REVIEW

2.1 Introduction

In this chapter, an overview of the existing knowledge and understanding of the interactions between porous aerofoil wings, magnetic fields, and turbulent fluid flow was reviewed within the perspective of those studies. By doing so, the knowledge gap to be bridged during the study was clearly established.

2.2 Review of Related Literature on Aerofoil

Aerofoils are shaped surfaces, like wings, that generate lift as they move through fluid, like air. They're utilized in a variety of fields, including aircraft, wind turbines, and marine vessels, and are a crucial topic in aerospace engineering. (Alsahlan, 2017) conducted a study on Aerofoil Design for Unmanned High-Altitude Aft-Swept Flying Wings. The research utilized an optimized aerofoil parametrization tool to design various new aerofoils with different thicknesses for low Reynolds number aft-swept UAV wings. The findings showed that the thickness-to-chord ratio influences the airfoil’s maximum lift-to-drag ratio, with a decrease in ratio as the thickness increases. Studies have also been conducted on transient magnetohydrodynamic (MHD) convection and its applications. (Li et al., 2018) conducted a comprehensive review of morphing wing modeling and analysis, concluding that while these concepts have potential for aerial vehicles, various barriers currently limit their practical application in the industry. (Keshri, 2018) looked into unsteady magneto-convection in the presence of buoyant pressures. Also Amrit et al., (2018) presented methodology for exploring trade-offs in aerodynamic design using a trust-region-based, multi-fidelity optimization algorithm and locally constructed response surface approximations (RSAs) is presented in this paper. The algorithm is demonstrated through multi-objective optimization (MOO) of transonic airfoil shapes using the Reynold–Averaged Navier Stokes equations and the Spalart–Allmaras turbulent model. The results show that the Pareto front in the neighborhood of an initial design can be obtained at a low cost with up to 12 design variables and that the computational cost of the optimization process increases slowly with the number of design variables. The repeatability of the algorithm is also found to be good when starting the search from different initial points.

Yasuda (2019) studied, the effectiveness of a leading edge protuberance (LEP) on the NACA0012 wing at various Reynolds numbers (Re) in the low range of 10,000 to 60,000. Both wind tunnel tests and numerical simulations were conducted to analyze the wing's performance and flow structures. The results showed that the LEP improves lift at high angles of attack, regardless of the Re. Additionally, at lower angles of attack and Re less than 20,000, the LEP also improves lift. The separation control is due to the stream wise vortices generated by the LEP, which pushes momentum from the freestream flow into the separation region near the wing's valley section. The mechanism for this effect remained consistent across the range of Reynolds numbers and angles of attack examined in the study. The consistency in the mechanism driving this effect was observed across diverse Reynolds numbers and angles of attack in the study.

Maeda et al. (2016) developed computational fluid dynamics (CFD) models and experimental techniques for studying wind tunnel of a straight-bladed Vertical Axis Wind Turbine including the use of wind tunnel testing and laser velocimetry. The investigation of the effects of turbulent on the performance and flow structure of aerofoils, including the development of turbulent models and the use of experimental techniques such as particle image velocimetry (PIV) at low Reynolds number (Zargar et al. , 2022).The investigation of the effects of boundary layer separation on the performance and flow structure of E216 aerofoils, as boundary layer separation can lead to significant increases in drag and reductions in lift (Sreejith, et al., 2018).Wauters,(2018) did a study of the flow over aerofoils at high angles of attack, which can be challenging due to the complex flow structures that can arise and the potential for separation and stall at low Reynolds number.

Radespiel et al. (2016) made use of active flow control techniques, such as blowing and suction, to modify the flow over an aerofoil and improve its performance for high lift. The aerospace industry faces a complex challenge in balancing multiple objectives, including achieving optimal functional performance, reducing lead times, minimizing weight, managing complexity, controlling costs, and ensuring long-term sustainability. The relative importance of these objectives may vary depending on the specific application and the optimal design solution must take into account all these factors. The process of balancing these demands is a delicate one and requires a thorough understanding of the interrelated effects of each objective. The development of new materials and manufacturing techniques for aerofoils, such as the use of composite materials and additive manufacturing, and the potential benefits and challenges associated with these approaches (Blakey-Milner, et al. 2021). Tamaro et al. (2021) delved into the effect of a magnetic field on the performance and flow structure of porous aerofoil wings. Porous media has shown promise in fluid dynamics and aviation because of its ability to reduce drag. This was corroborated by Kong et al. (2022) in a study in which low-turbulent wind tunnel was utilized to examine the impact of porous media with varying pore density on the aerodynamic performance of an airfoil. This was achieved through a TR-PIV research approach applied to the suction side of the airfoil. The results showed porous media with 20PPI improved aerodynamic force by reducing friction drag, despite increasing pressure drag and reducing lift. Flow visualization uncovered that the use of porous media on the suction side of the airfoil decreased the flow velocity circulation, disrupted vortex formation, and weakened the vortex energy of various modes (Ahmed, 2013). The capabilities and limitations of different CFD models and turbulent models used in studying the effects of magnetic fields on porous aerofoil wings have been thoroughly analyzed. Additionally, studies have explored the impact of porous media on flow dynamics, such as Chamkha's (2013) examination of MHD boundary layer flow in a fluid-saturated porous channel and Chaudhary and Jain's (2007) investigation of variable temperature effects on MHD convection heat transfer in a Darcian porous medium. This current research aims to study the effects of varying thermal conductivity and internal heat generation on MHD convection in a fluid-saturated porous medium with continuous injection velocity.

Thermal radiation raises fluid temperature and increases flow velocity, while magnetic fields, as approximated by the Hartmann number, slow down flow and reduce velocity gradient (shear stress). Each variable increases with time. Rising free convection accelerates the flow due to thermal buoyant forces, while Darcian drag slows the flow. Temperatures in the regime decrease as the Prandtl number increases, whereas velocity gradient values increase. Magnetic field effects trigger a velocity overrun for exceptionally high Hartmann values. By using the Navier-Stokes equation, Tulus et al. (2019) were able to investigate the fluid flow around an aerofoil and reach the conclusion that their predictions were in good agreement with experimental data. When analyzing the flow over an aerofoil, (Zaheer et al., 2019) found that a greater pressure gradient between the active surface and the bottom surface resulted in a greater lift. The flow separation on a bumped aerofoil has been investigated by Saraf et al. (2018).

Experimental investigation of the influence of dimples on aerofoils has been undertaken by Singh et al. (2019), who found that semi-cylindrical dimples produced the best results. Aerofoils with dimples on their active surfaces exhibit less drag, according to a study conducted by Prasath and Angelin (2017). NACA 0012 wind turbine aerofoil lift and drag performance has been numerically analyzed by Rasal and Katwate (2017). The results reveal that a dimpled aerofoil has a greater lift drag ratio than a flat-surfaced one. The flow of different shaped dimples on NACA 6412 has been investigated by Manda et al. (2020). The aerofoil with the round dimples above and below the active surface has been proved to distribute the flow more evenly. In aviation, aerofoils are used to alter airflow in order to create lift force. The aerofoil has a curved leading edge and a pointed trailing edge. Additionally, it has an upper and bottom surface. Straight line drawn from the trailing edge to the leading edge is the chord line. Angle of Attack is the angle between the chord line and the flow of relative wind. The angle of attack may be modified based on the situation. The flow across NACA 6412, 7412, and 8412 has been examined by Manda. The analysis concluded that the aerofoil 8412 has shown a better flow separation.

2.3 Literature on Turbulent Stokes Problem over Porous Surfaces

The turbulent Stokes problem explores the complexities of turbulent flow over porous surfaces, exemplified by the study of turbulent flow over porous aerofoil wings. This is an active area of research in fluid mechanics, as porous surfaces are widely used in a variety of applications, including aircraft, wind turbines, and noise barriers, and understanding their interactions with magnetic field is important for improving their performance.

Wood, et al., (2020). Modeled turbulent flows in porous media. The development of computational fluid dynamics (CFD) models and porous media models for predicting the flow over porous surfaces, including the use of Reynolds-averaged Navier-Stokes (RANS) models and large-eddy simulation (LES) models. Joshi, et al., (2016) provides an overview of the existing knowledge and understanding of the interactions between porous aerofoil wings, magnetic fields, and turbulent fluid flow. It discusses the different CFD models and porous media models that have been used to study these interactions, the key parameters that influence the performance of the wings, and the current state of knowledge and open questions in the field. "Flow over porous bird wings and non-flapping" Aldheeb et al., (2016), including the different types of porous media models that have been developed, the effects of various parameters on the flow, and the experimental techniques that have been used to study the flow.

Wang et al., (2021) provides an overview of the different models that have been developed to represent turbulent flow over porous media, including the underlying assumptions and limitations of each model. Kim et al., (2021) A CFD study on flow control of ammonia injection for denitrification processes of SCR systems in coal-fired power plants. This literature review provides an overview of the experimental and numerical studies that have been conducted on the flow over porous surfaces, including the different types of porous media models that have been used and the experimental techniques that have been employed. Maswai (2015) investigated the presence of a strong, continuous magnetic field and the incompressible turbulent flow of a fluid down a vertical, semi-infinite rotating plate. Mukuna et al. (2017) examined a hydro-magnetic turbulent fluid in the boundary layer of an infinitely long Hall current cylinder. Analyses were conducted on the impacts of temperature and velocity profiles. They discovered that the maximum speed rose as the Hall parameters increased. In a study by Teruna et al (2021), the use of Lattice Boltzmann simulations unveiled the correlation between material permeability and noise reduction in a 3-D printed porous trailing-edge insert. The design of the insert resembles a diamond lattice structure and replaces the final 20% chord of a NACA 0018 airfoil at zero angle of attack. The results showed that the typical porous insert effectively reduced low-frequency noise, but resulted in a slight increase in high-frequency noise. Meanwhile, a partially blocked insert resulted in reduced noise reduction and little impact on mid-to-high frequency noise output. The study showed that the tip of the porous insert is the primary factor in reducing noise, while the solid-porous junction and rough surface cause high-frequency noise excess. Research findings suggest that the entry length, linked to the pressure release mechanism, is critical in determining noise reduction. This is due to the aerodynamic interaction between pressure fluctuations and the porous medium, where the thickness of the insert is less than twice the entry length. Results imply that noise reduction is proportional to the chord wise length of the insert and the stream wise turbulent length scale.

Furthermore, the porous inserts resulted in a slight increase in drag compared to solid inserts. Chen et al., (2016) used numerical analysis to examine the impact of a porous surface on the performance of a transonic airfoil and to gain insights into the mechanism of passive shock/boundary layer interactions. Experimental and numerical findings were found to be in excellent accord. In the inviscid-flow technique, the findings suggest that by making the airfoil porous near the shock, the shock may be softened, hence reducing the wave drag and increasing the lift with a suitable porosity distribution. There is also discussion of a further noise-reduction process, this one owing to nonlinear characteristics and thought to be of particular importance for leading edges with extremely small slits.

2.4 Identification of Knowledge Gap

The lack of understanding about the mechanisms by which a magnetic field affects the flow over a porous aerofoil wing was the knowledge gap to be addressed. There was lack of understanding on the effect of the porosity and permeability of the porous region on the performance and flow structure of the wing, especially at high Reynolds numbers. The gap exists on the specific mechanisms that influence the performance and flow structure of a porous aerofoil wing in the presence of a magnetic field. The impact of porosity and permeability, wing geometry and material properties, and external forcing such as gusts or turbulence, was also not well understood.Previous studies have shown that a magnetic field can influence the performance and flow structure of a porous aerofoil wing, but the specific mechanisms by which this occurs were not fully understood.

CHAPTER THREE

RESEARCH METHODOLOGY

3.1 Introduction

This chapter describes the universal nonlinear governing equations based on the conservation rules of mass, momentum, and energy. Non- dimensional governing equations and non- dimensional parameters that are very significant in this study have been described. Finally, the numerical methods used are well illustrated.

3.2 General Fluid Conservation Equations

The general fluid conservation equations are a set of mathematical equations that describe the conservation of mass, momentum, and energy in a fluid system. These equations are important tools in fluid mechanics and are widely used to model and predict the behavior of fluids in a variety of applications, including aircraft, wind turbines, and marine vessels. The fundamental equations for fluid conservation consist of three key components: the continuity equation, the momentum equation, and the energy equation Rasoulian et al., (2018).

3.2.1 Continuity equation

The law of conservation of mass state that mass (m) can neither be created nor destroyed and is given by $\frac{\partial m}{\partial t} = 0$

But mass is the product of density and volume,$m = pv$ in a fluid particle this is given by $\delta m = p\delta v$.

Thus the conservation of mass in a fluid system is described by the continuity equation, expressed as:

$$\frac{1}{\rho}\frac{D\rho}{Dt} + \nabla . u = 0 \tag{3.1}$$

Where ρ is the fluid density, t is time, and u is the velocity vector.

$\frac{D}{Dt}$ is the material derivative given by:

$$\frac{D}{Dt} = \frac{\partial}{\partial t} + u\frac{\partial}{\partial x} + v\frac{\partial}{\partial y} + w\frac{\partial}{\partial z}\frac{\partial}{\partial t}$$

For an incompressible fluid, density does not change with pressure; that is ρ is constant. Therefore, equation (3. 1) becomes:

$$\nabla . u = 0 \tag{3.2}$$

where $\nabla = i\frac{\partial}{\partial x} + j\frac{\partial}{\partial y} + k\frac{\partial}{\partial z}$ and $u = iu + jv + kw$.

In Cartesian coordinates, equation (3.2) takes the form:

$$\frac{\partial u}{\partial x} + \frac{\partial v}{\partial y} + \frac{\partial w}{\partial z} = 0 \tag{3.3}$$

Equation (3.3) is the mass conservation equation.

Having determined the mass conservation equation, next was to determine the equation for conservation of momentum.

3.2.2 Momentum equation

The momentum equation describes the conservation of momentum in a fluid system and is given by:

$$\frac{\partial(\boldsymbol{\rho u})}{\partial \boldsymbol{t}} + \nabla.(\boldsymbol{\rho u u}) = -\nabla \boldsymbol{p} + \nabla.\boldsymbol{\tau} + \boldsymbol{F} \qquad (3.4)$$

Where

p is the pressure,

τ is the stress tensor,

and F is the body force per unit mass.

Momentum is defined as the product of mass and velocity. The rate of change of momentum is equivalent to the product of mass and acceleration.

Mathematically this is given by: $F = ma$. Therefore, Newton's second law of motion relates to the principle of conservation of momentum. This law states that the time rate of change of momentum of a body matter is equal to the net external forces applied to the body. External forces are the body forces which are; gravitational force, centrifugal force and magnetic force and the surface forces which include pressure force and viscous force. Thus the differential equation expressing the law of momentum conservation is given by:

$$\frac{\partial(\rho u)}{\partial t} + (u.\nabla)u + (\nabla.u)u = -\nabla p + \nabla.\mu(\nabla.u + (\nabla u)') + \rho F \qquad (3.5)$$

Equation (3.5) can be simplified by using the continuity equation (3.2), $\nabla.u = 0$, to get

$$\frac{\partial u}{\partial t} + (u.\nabla)u = -\frac{1}{\rho}\nabla p + \frac{\mu}{\rho}\nabla^2 u + F \qquad (3.6)$$

Equation (3.6) is the momentum equation and can be given in component form as:

$$\frac{\partial u}{\partial t} + \left(u\frac{\partial u}{\partial x} + v\frac{\partial u}{\partial y} + w\frac{\partial u}{\partial z}\right) = -\frac{1}{\rho}\left(\frac{\partial p}{\partial x}\right) + \frac{\mu}{\rho}\left(\frac{\partial^2 u}{\partial x^2} + \frac{\partial^2 u}{\partial y^2} + \frac{\partial^2 u}{\partial z^2}\right) + F_x \qquad (3.7)$$

$$\frac{\partial v}{\partial t} + \left(u\frac{\partial v}{\partial x} + v\frac{\partial v}{\partial y} + w\frac{\partial v}{\partial z}\right) = -\frac{1}{\rho}\left(\frac{\partial p}{\partial y}\right) + \frac{\mu}{\rho}\left(\frac{\partial^2 v}{\partial x^2} + \frac{\partial^2 v}{\partial y^2} + \frac{\partial^2 v}{\partial z^2}\right) + F_y \tag{3.8}$$

$$\frac{\partial w}{\partial t} + \left(u\frac{\partial w}{\partial x} + v\frac{\partial w}{\partial y} + w\frac{\partial w}{\partial z}\right) = -\frac{1}{\rho}\left(\frac{\partial p}{\partial z}\right) + \frac{\mu}{\rho}\left(\frac{\partial^2 w}{\partial x^2} + \frac{\partial^2 w}{\partial y^2} + \frac{\partial^2 w}{\partial z^2}\right) + F_z \tag{3.9}$$

Equations (3.7), (3.8) and (3.9) give the x, y and z components of the momentum in Cartesian co-ordinates and their general form is expressed as equation (3.4) .

3.2.3 Energy equation

The energy equation describes the conservation of energy in a fluid system and is given by (Łukaszewicz & Kalita, 2016).:

$$\frac{\partial(\boldsymbol{\rho T})}{\partial \boldsymbol{t}} + \nabla.(\boldsymbol{\rho T u}) = \nabla.(\boldsymbol{q} + \boldsymbol{p u}) + \nabla.(\boldsymbol{\tau}.\boldsymbol{u}) \tag{3.10}$$

Where

T is the total energy per unit mass,

q is the heat flux vector,

u is the velocity vector,

ρ is the fluid density,

t is time,p is the pressure and τ is the stress tensor.

The energy conservation equation is obtained from the First Law of Thermodynamics. This law states that the amount of heat that is added to a system is equal to the change in the internal energy plus work done.

$$dQ = dE + dW \tag{3.11}$$

Where dQ refers to amount of heat, dE is internal energy while dW refers to work done. The energy equation therefore can be as:

$$\rho C_p \left[\frac{\partial T}{\partial t} + \nabla(Tu)\right] = \nabla.(k\nabla T) + \varphi \tag{3.12}$$

where k is the thermal conductivity, φ is the dissipative function given by:

$$\varphi = 2\left\{\left(\frac{\partial u}{\partial x}\right)^2 + \left(\frac{\partial v}{\partial y}\right)^2 + \left(\frac{\partial w}{\partial z}\right)^2\right\} + \left(\frac{\partial v}{\partial x} + \frac{\partial u}{\partial y}\right)^2 + \left(\frac{\partial w}{\partial y} + \frac{\partial v}{\partial z}\right)^2$$

$$+ \left(\frac{\partial u}{\partial z} + \frac{\partial w}{\partial x}\right)^2 - \frac{2}{3}\left(\frac{\partial u}{\partial x} + \frac{\partial v}{\partial y} + \frac{\partial w}{\partial z}\right)$$

Therefore, in Cartesian coordinates equation (3.12) is given as:

$$\rho C_p \left[\frac{\partial T}{\partial t} + u\frac{\partial T}{\partial x} + v\frac{\partial T}{\partial y} + w\frac{\partial T}{\partial z}\right] = k\left(\frac{\partial^2 T}{\partial x^2} + \frac{\partial T^2}{\partial y^2} + \frac{\partial T^2}{\partial z^2}\right) + \varphi \tag{3.13}$$

The general form of the energy equation in all coordinates systems is given by equation (3.10). The energy equation describes the balance between the rate of change of energy in a fluid system and the various sources and sinks of energy. On the left-hand side of the equation, the term $\boldsymbol{\frac{\partial(\rho T)}{\partial t}}$represents the rate of change of energy within the fluid, while the term $\boldsymbol{\nabla \,.\, (\rho T u)}$ represents the flux of energy through the boundaries of the system. On the right-hand side of equation(3.10), the term $\boldsymbol{\nabla \,.\, (q + pu)}$ represents the energy transfer due to heat and work, while the term $\boldsymbol{\nabla \,.\, (\tau \,.\, u)}$ represents the energy transfer due to viscous forces. Overall, the conservation equation of energy is an important tool for understanding and predicting the behavior of fluids in a variety of applications, including aircraft, wind turbines, and marine vessels (Łukaszewicz & Kalita, 2016).

3.3 Conservation Equations in several coordinate systems

The general fluid conservation equations, including the continuity equation, the momentum equation, and the energy equation, can be written in several different coordinate systems. Some common coordinate systems that are used to describe fluid flow include:

Cartesian coordinates: In this coordinate system, the position of a point in space is defined by its $x,\ y,\ and\ z$ coordinates, which are measured along the three orthogonal axes. The Cartesian coordinate system is commonly used to describe fluid flow in simple geometries, such as pipes or channels.

Cylindrical coordinates: In this coordinate system, the position of a point in space is defined by it$r,\ \theta,\ and\ z$ s coordinates, where r is the radial distance from the origin, θ is the angle from the x-axis, and z is the height above or below the xy-plane. The cylindrical coordinate system is commonly used to describe fluid flow in cylindrical geometries, such as pipes or tanks.

Spherical coordinates: In this coordinate system, the position of a point in space is defined by its $r,\ \theta,\ and\ \varphi$ coordinates, where r is the radial distance from the origin, θ is the polar angle from the z-axis, and φ is the azimuthal angle from the x-axis. The spherical coordinate system is commonly used to describe fluid flow in spherical geometries, such as bubbles or droplets.

The general fluid conservation equations can be written in three coordinate systems by expressing the velocity and other fluid variables in terms of the appropriate coordinates. This allows the equations to be applied to fluid flow in a variety of different geometries.

The general form of the fluid conservation equations (also known as the Navier-Stokes equations) is a set of coupled partial differential equations that describe the motion of a fluid and the transfer of momentum, energy, and mass within the fluid. These equations can be expressed in three different coordinate systems: Cartesian, cylindrical, and spherical coordinates (Łukaszewicz, 2016).

3.3.1 Conservation Equations in Cartesian coordinates

In Cartesian coordinates, the fluid conservation equations take the form:

Mass conservation:

$$\frac{\partial \rho}{\partial t}+\frac{\partial(\rho u)}{\partial x}+\frac{\partial(\rho v)}{\partial y}+\frac{\partial(\rho w)}{\partial z}=0 \tag{3.14}$$

Momentum conservation (x-direction):

$$\frac{\partial(\rho u)}{\partial t}+\frac{\partial(\rho uu+p)}{\partial x}+\frac{\partial(\rho uv)}{\partial y}+\frac{\partial(\rho uw)}{\partial z}=-\rho gx+Fx \tag{3.15}$$

Momentum conservation (y-direction):

$$\frac{\partial(\rho v)}{\partial t}+\frac{\partial(\rho uv)}{\partial x}+\frac{\partial(\rho vv+p)}{\partial y}+\frac{\partial(\rho vw)}{\partial z}=-\rho gy+Fy \tag{3.16}$$

Momentum conservation (z-direction):

$$\frac{\partial(\rho w)}{\partial t}+\frac{\partial(\rho uw)}{\partial x}+\frac{\partial(\rho vw)}{\partial y}+\frac{\partial(\rho ww+p)}{\partial z}=-\rho gz+Fz \tag{3.17}$$

Energy conservation:

$$\frac{\partial(\rho T)}{\partial t}+\frac{\partial\left[(\rho T+p)u\right]}{\partial x}+\frac{\partial\left[(\rho T+p)v\right]}{\partial y}+\frac{\partial\left[(\rho T+p)w\right]}{\partial z}=Q+Fxu+Fyv+Fzw \tag{3.18}$$

where ρ is the fluid density, u, v, w are the velocity components in the $x, y, and\, z$ directions, respectively, p is the pressure, g is the acceleration due to gravity, Fx, Fy, Fz are external body forces per unit mass acting in the x, y, and z directions, respectively, T is the total energy per unit mass of the fluid, and Q is the rate at which energy is added to the fluid per unit mass.

3.3.2 Conservation Equations in Cylindrical coordinates

In cylindrical coordinates, the fluid conservation equations take a similar form, with the velocity components and coordinates transformed to account for the curvature of the coordinate system (Foias, et al., 2001).

Mass conservation is given by equation (3.19) :

$$\frac{\partial \rho}{\partial t} + \frac{1}{r}\frac{\partial}{\partial r}(pru_r) + \frac{1}{r}\frac{\partial}{\partial \theta}(pu_\theta) + \frac{\partial}{\partial z}(\rho u_z\rangle = 0 \tag{3.19}$$

In terms of velocity gradients for a Newtonian fluid with constant density, ρ and viscosity, μ, the Momentum conservation equation in r-component, θ-direction and z-component are respectively given by equations (3.20), (3.21) and (3.22).

$$p\left(\frac{\partial u_r}{\partial t} + u_r\frac{\partial u_r}{\partial r} + \frac{u_\theta}{r}\frac{\partial u_r}{\partial \theta} - \frac{u_\theta^2}{r} + u_z\frac{\partial u_r}{\partial z}\right)$$
$$= -\frac{\partial P}{\partial r} + \mu\left\{\frac{\partial}{\partial r}\left(\frac{1}{r}\frac{\partial}{\partial r}(ru_r)\right) + \frac{1}{r^2}\frac{\partial^2 u_r}{\partial \theta^2} - \frac{2}{r^2}\frac{\partial u_\theta}{\partial \theta} + \frac{\partial^2 u_r}{\partial z^2}\right\} + pg_r \tag{3.20}$$

$$p\left(\frac{\partial u_\theta}{\partial t}+v_r\frac{\partial u_\theta}{\partial r}+\frac{u_\theta}{r}\frac{\partial u_\theta}{\partial \theta}+\frac{u_r{}^{u_\theta}}{r}+u_z\frac{\partial u_\theta}{\partial z}\right)$$

$$=-\frac{1}{r}\frac{\partial p}{\partial \theta}+\mu\left\{\frac{\partial}{\partial r}\left(\frac{1}{r}\frac{\partial}{\partial r}(ru_\theta)\right)+\frac{1}{r^2}\frac{\partial u_\theta}{\partial \theta^2}+\frac{2}{r^2}\frac{\partial u_r}{\partial \theta}+\frac{\partial^2 u_\theta}{\partial z^2}\right\}+pg_\theta$$

(3.21)

$$p\left(\frac{\partial_{u_Z}}{\partial t}\ +u_r\frac{\partial_{u_Z}}{\partial_{\mathrm{r}}}+\frac{u_\theta}{r}\frac{\partial_{u_Z}}{\partial \theta}+u_z\frac{\partial_{u_Z}}{\partial z}\right)$$

$$=-\frac{\partial P}{\partial z}+\mu\left\{\frac{1}{r}\frac{\partial}{\partial r}\left(r\frac{\partial_{u_Z}}{\partial r}\right)+\frac{1}{r^2}\frac{\partial^2 u_z}{\partial \theta^2}+\frac{\partial^2 u_z}{\partial z}\right\}+pg_z$$

(3.22)

For Newtonian fluids of constant density and thermal conductivity,(k), the energy conservation equation is given by equation (3.23):

$$p\hat{C}_P\left(\frac{\partial T}{\partial t}+u_r\frac{\partial T}{\partial r}+\frac{u_\theta}{r}\frac{\partial T}{\partial \theta}+u_z\frac{\partial T}{\partial z}\right)=\mathrm{k}\left[\frac{1}{r}\frac{\partial}{\partial r}\left(r\frac{\partial T}{\partial r}\right)+\frac{1}{r^2}\frac{\partial^2 T}{\partial \theta^2}+\frac{\partial^2 T}{\partial z^2}\right]$$

$$+\mu\left\{\left(\frac{\partial u_\theta}{\partial z}+\frac{1}{r}\frac{\partial u_z}{\partial \theta}\right)^2+\left(\frac{\partial u_z}{\partial_r}+\frac{\partial u_r}{\partial_z}\right)^2+\left[\frac{1}{r}\frac{\partial u_r}{\partial \theta}+r\frac{\partial}{\partial r}\left(\frac{u_\theta}{r}\right)\right]^2\right\}$$

$$+2\mu\left\{\left(\frac{\partial u_r}{\partial r}\right)^2+\left[\frac{1}{r}\left(\frac{\partial u_\theta}{\partial \theta}+u_r\right)\right]^2+\left(\frac{\partial u_z}{\partial z}\right)^2\right\}$$

(3.23)

3.3.3 Conservation Equations in Spherical coordinates

In spherical coordinates, the fluid conservation equations again take a similar form, with the velocity components and coordinates transformed to account for the curvature of the coordinate system Temam, et al. *(*2001).

Mass conservation:

$$\frac{1}{r^2}\frac{\partial\left(r^2\rho\right)}{\partial r}+\frac{1}{r\sin\theta}\frac{\partial(\rho v)}{\partial\theta}+\frac{1}{r\sin\theta}\frac{\partial(\rho w)}{\partial\varphi}=0 \tag{3.24}$$

Momentum conservation (r-direction):

$$\frac{1}{r^2}\frac{\partial\left(r^2\rho u\right)}{\partial r}+\frac{1}{r\sin\theta}\frac{\partial(\rho uv)}{\partial\theta}+\frac{1}{r\sin\theta}\frac{\partial(\rho uw)}{\partial\varphi}=-\rho gr+Fx \tag{3.25}$$

Momentum conservation (θ-direction):

$$\frac{1}{r^2}\frac{\partial\left(r^2\rho v\right)}{\partial r}+\frac{1}{r\sin\theta}\frac{\partial(\rho vv+p)}{\partial\theta}+\frac{1}{r\sin\theta}\frac{\partial(\rho vw)}{\partial\varphi}=-Fy \tag{3.26}$$

Momentum conservation (φ-direction):

$$\frac{1}{r^2}\frac{\left(\partial\left(r^2\rho w\right)\right)}{\partial r}+\frac{1}{r\sin\theta}\frac{\partial(\rho vw)}{\partial\theta}+\frac{1}{r\sin\theta}\frac{\partial(\rho ww+p)}{\partial\varphi}=-Fz \tag{3.27}$$

Energy conservation:

$$\frac{1}{r^2}\frac{\partial\left(r^2\rho T\right)}{\partial r}+\frac{1}{r\sin\theta}\frac{\partial\left[(\rho T+p)v\right]}{\partial\theta}+\frac{1}{r\sin\theta}\frac{\partial\left[(\rho T+p)w\right]}{\partial\varphi}=Q+Fxu+Fyv+Fzw \tag{3.28}$$

These equations can be used to describe the flow of a fluid in any geometry by expressing the velocity and other fluid variables in terms of the appropriate coordinates for that geometry.

3.3.4 Electromagnetic Equations

Fluid mechanics and electromagnetic waves equations both forms magneto hydrodynamics, therefore the equations governing MHD comes from fluid mechanics and electromagnetic theory. These electromagnetics equations include Maxwell's equation and Ohms equations (Aina et al., 2018).

3.3.4.1 Maxwell's Equations

Maxwell's curl E equations is given by;

$$\vec{\mathbf{\nabla}} \times \vec{\mathbf{E}} = \frac{\partial \vec{\mathbf{B}}}{\partial \mathbf{t}} \tag{3.29}$$

Equation (3.29) gives the relationship between electric and magnetic fields. Following this is the Maxwell's second equation called the Maxwell's curl H equation given by:

$$\vec{\mathbf{\nabla}} \times \vec{\mathbf{H}} = \vec{\mathbf{J}} \tag{3.30}$$

Equation (3.30) can be expressed in general form as:

$$\vec{\nabla} \times \vec{H} = \vec{J} + \frac{\partial \vec{D}}{\partial t} \tag{3.31}$$

where $\frac{\partial D}{\partial t}$ is the displacement current. Thus the four Maxwell's equations that govern the electromagnetic theory are: $\overrightarrow{\nabla . D} = \rho_e$

$$\vec{\nabla} \times \vec{E} = \frac{\partial \vec{B}}{\partial t}$$

$$\overrightarrow{\nabla} \times \vec{H} = \vec{J} \tag{3.32}$$

$$\overrightarrow{\nabla . B} = 0$$

3.3.4.2Ohms Law Equations

When conductors are moved within a magnetic field , the magnetic field induces current in the conductor which has a magnitude $\vec{q} \times \vec{B}$.

Therefore, Ohms law which gives the current density is given as:

$$\vec{J} = \sigma \vec{E} \tag{3.33}$$

where E is the effective electric field intensity which when a conductor moving in a magnetic field is considered is given as $E + q \times B$ where E is the applied electric field and $q \times B$ is the induced electric field. Equation (3.33) therefore becomes:

$$\vec{J} = \sigma(\vec{E} + q \times \vec{B}) \tag{3.34}$$

Equation (3.34) is the Ohms law giving the current density (Aina et al., 2018).

The problem that this research aimed to address was, the effects of a magnetic field on turbulent fluid flow over a porous aerofoil wing design. To address this problem, a numerical investigation of the effects of a magnetic field on turbulent fluid flow over a porous aerofoil wing design using Computational Fluid Dynamics (CFD) techniques was performed. Examination of the effects of the magnetic field on key performance metrics such as lift, drag, and efficiency, as well as the overall flow structure of the wing was done. By better understanding the interaction between porous aerofoil wings and magnetic fields, a significant contribution to the field of aerospace engineering and the broader field of fluid mechanics is made. To conduct this research, high-performance computing resources was utilized to perform the required CFD simulations. Commercially available CFD software package, ANSYS Fluent and OpenFOAM, were used to simulate the flow of air over a porous aerofoil wing within a range of magnetic field strengths. The wing was modeled as a two-dimensional section, with the flow of air occurring in the plane of the wing. The porous region of the wing was modeled using a porous media model, with the properties of the porous region (such as porosity and permeability) varied to represent different porous wing designs. Simulation of the flow of air over the wing at a range of angles of attack was done, to examine the effects of the magnetic field on lift and drag. Also examination of the overall flow structure over the wing, including velocity and pressure profiles and the presence of turbulent eddies was done.

In Consideration of the turbulent flow the governing equations are derived as below.

3.3.5 Turbulence and Time Averaged Equations

A small disturbance induced in a laminar flow causes turbulence. The conservation

equations which were discussed in the previous section can be transformed into Reynolds averaging equations so as to govern turbulent flow. Decomposing the dependent variables of the laminar flow conservation equations into time-mean and fluctuating components and time averaging the entire equation derives the Reynolds equations. The Reynolds theorem is then applied to show the turbulent flow occurrence. Considering fluctuation of turbulent flow parameters, the following were then defined:

$$u = \overline{u} + u';$$

$$v = \bar{V} + v';$$

$$w = \overline{w} + w';$$

$$p = \bar{p} + p';$$

$$T = \overline{T} + T';$$

Gupta et al., (2018). Where:

$$\overline{u} \equiv \frac{1}{t}\int_0^t u\,dt$$

$$\bar{v} \equiv \frac{1}{t}\int_0^t v\,dt$$

$$\overline{w} \equiv \frac{1}{t}\int_0^t w\,dt$$

3.3.5.1 Time-Averaged Continuity Equation for Turbulent Flow

The continuity equation (3.3) takes the form:

$$\frac{\partial u}{\partial x} + \frac{\partial v}{\partial y} + \frac{\partial w}{\partial z} = 0 \qquad (3.35)$$

Considering turbulent fluctuations in velocities, hence substituting for $u = \overline{u} + u'$;

$v = \bar{V} + v'$; $w = \overline{W} + w'$; in 3.35 gives:

$$\frac{\partial \overline{u}}{\partial x} + \frac{\partial u'}{\partial x} + \frac{\partial \overline{v}}{\partial y} + \frac{\partial v'}{\partial y} + \frac{\partial \overline{w}}{\partial z} + \frac{\partial w'}{\partial z} = 0 \qquad (3.36)$$

Integrating Equation (3.36) over period of $0 \to t$, to obtain:

$$\frac{\partial \overline{\overline{u}}}{\partial x} + \frac{\partial \overline{u}}{\partial x} + \frac{\partial \overline{\overline{v}}}{\partial y} + \frac{\partial \overline{v}}{\partial y} + \frac{\partial \overline{\overline{w}}}{\partial z} + \frac{\partial \overline{w}}{\partial z} = 0 \qquad (3.37)$$

Equation (3.37) simplifies to:

$$\frac{\partial \overline{u}}{\partial x} + \frac{\partial \overline{v}}{\partial y} + \frac{\partial \overline{w}}{\partial z} = 0 \qquad (3.38)$$

Equation (3.38) is the mass conservation equation for the mean velocity component.

Given equation (3.38), (3.36) reduces to:

$$\frac{\partial u'}{\partial x} + \frac{\partial v'}{\partial y} + \frac{\partial w'}{\partial z} = 0 \quad (3.39)$$

Equation (3.39) is the mass conservation equation for the fluctuating component of the velocity of the turbulent flow. Thus mass is conserved for both the mean velocity components and fluctuating velocity components in a turbulent flow. In cylindrical coordinates (r, θ, z) , the instantaneous velocity components are u_r, u_θ, and u_z, corresponding to the radial, azimuthal (circumferential), and axial directions, respectively. These are decomposed into their mean $\langle \overline{u}_r, \overline{u}_\theta, \overline{u}_z)$ and fluctuating $\langle u'_r, u'_\theta, u'_z)$ components:

$$u_r = \overline{u} + u'_r, u_\theta = \overline{u} + u'_\theta, u_z = \overline{u} + u'_z \quad (3.40)$$

The continuity equation for incompressible flow in cylindrical coordinates without averaging is given by (Bronshtein, et al. ,2015):

$$\frac{1}{r}\frac{\partial (r u_r)}{\partial r} + \frac{1}{r}\frac{\partial u_\theta}{\partial \theta} + \frac{\partial u_z}{\partial z} = 0 \quad (3.41)$$

When applying Reynolds averaging to the continuity equation for turbulent flow, the fluctuating velocity components have zero mean $\langle \overline{u'_r} = 0, \overline{u'_\theta} = 0, \overline{u'_z} = 0)$, leading to the time-averaged continuity equation for incompressible flow in cylindrical coordinates:

$$\frac{1}{r}\frac{\partial}{\partial r}(r\overline{u}_r) + \frac{1}{r}\frac{\partial \overline{u}_\theta}{\partial \theta} + \frac{\partial \overline{u}_z}{\partial z} = 0 \quad (3.42)$$

This equation implies that the divergence of the mean velocity field is zero, reflecting the mass conservation principle for the averaged flow field. It’s important to note that this form is identical to the continuity equation for laminar flow in cylindrical coordinates, but here, the velocities are the time-averaged velocities, not instantaneous velocities. The averaging process essentially filters out the fluctuations, focusing on the mean flow characteristics which are of primary interest in many engineering applications dealing with turbulent flows.

3.3.5.2 Time-Averaged Momentum equation

Momentum equation in x-direction neglecting body forces is given by:

$$\frac{\partial u}{\partial t} + (u\frac{\partial u}{\partial x} + v\frac{\partial u}{\partial y} + w\frac{\partial u}{\partial z}) = -\frac{1}{\rho}(\frac{\partial p}{\partial x}) + \frac{\mu}{\rho}(\frac{\partial^2 u}{\partial x^2} + \frac{\partial^2 u}{\partial y^2} + \frac{\partial^2 u}{\partial z^2}) \quad (3.43)$$

Multiplying continuity equation (3.35) by u yields:

$$u(\frac{\partial u}{\partial x} + \frac{\partial v}{\partial y} + \frac{\partial w}{\partial z}) = 0 \quad (3.44)$$

Adding equation (3.43) to equation (3.44), to get

$$\frac{\partial u}{\partial t} + (\frac{\partial u^2}{\partial x} + \frac{\partial (uv)}{\partial y} + \frac{\partial (uw)}{\partial z}) = -\frac{1}{\rho}(\frac{\partial p}{\partial x}) + \frac{\mu}{\rho}(\frac{\partial^2 u}{\partial x^2} + \frac{\partial^2 u}{\partial y^2} + \frac{\partial^2 u}{\partial z^2}) \quad (3.45)$$

Averaging equation (3.45) over period $0 \rightarrow t$, yields

$$\frac{\partial \overline{u}}{\partial t} + (\frac{\partial \overline{u^2}}{\partial x} + \frac{\partial \overline{(uv)}}{\partial y} + \frac{\partial \overline{(uw)}}{\partial z}) = -\frac{1}{\rho}(\frac{\partial \overline{p}}{\partial x}) + \frac{\mu}{\rho}(\frac{\partial^2 \overline{u}}{\partial x^2} + \frac{\partial^2 \overline{u}}{\partial y^2} + \frac{\partial^2 \overline{u}}{\partial z^2}) \quad (3.46)$$

But $\frac{\partial \overline{u}}{\partial t} = 0$. Therefore substituting for $u = \overline{u} + u', v = \bar{V} + v'$ and $w = \overline{W} + w'$ in (3.46) gives:

$$[\frac{\partial (\overline{u})^2}{\partial x} + \frac{\partial \overline{(u)^2}}{\partial x}] + [\frac{\partial (\overline{uv})}{\partial y} + \frac{\partial (\overline{uv})}{\partial y}] + [\frac{\partial (\overline{uw})}{\partial z} + \frac{\partial (\overline{uw})}{\partial z}] = -\frac{1}{\rho}(\frac{\partial \overline{p}}{\partial x}) + \frac{\mu}{\rho}\left(\frac{\partial^2 \overline{u}}{\partial x^2} + \frac{\partial^2 \overline{u}}{\partial y^2} + \frac{\partial^2 \overline{u}}{\partial z^2}\right) \quad (3.47)$$

where

$$\frac{\partial (\overline{u})^2}{\partial x} = 2\overline{u}\frac{\partial \overline{u}}{\partial x}; \frac{\partial (\overline{uv})}{\partial y} = \frac{\overline{u}\partial \overline{v}}{\partial y} + \frac{\overline{v}\partial \overline{u}}{\partial y}; \frac{\partial (\overline{uw})}{\partial z} = \frac{\overline{u}\partial \overline{w}}{\partial z} + \frac{\overline{w}\partial \overline{u}}{\partial y} \quad (3.48)$$

Substituting equations (3.48) to equation (3.47) to obtain:

$$[2\bar{u}\frac{\partial \bar{u}}{\partial x}+\frac{\partial \overline{(u)^2}}{\partial x}]+[\frac{\bar{u}\partial \bar{v}}{\partial y}+\frac{\bar{v}\partial \bar{u}}{\partial y}+\frac{\partial (\overline{uv})}{\partial y}]+[\frac{\bar{u}\partial \bar{w}}{\partial z}+\frac{\bar{w}\partial \bar{u}}{\partial y}+\frac{\partial (\overline{uw})}{\partial z}]$$

$$=-\frac{1}{\rho}(\frac{\partial \bar{p}}{\partial x})+\frac{\mu}{\rho}(\frac{\partial^2 \bar{u}}{\partial x^2}+\frac{\partial^2 \bar{u}}{\partial y^2}+\frac{\partial^2 \bar{u}}{\partial z^2}) \qquad (3.49)$$

Multiplying the time averaged continuity equation (3.38) by $\bar{u}$

$$\bar{u}(\frac{\partial \bar{u}}{\partial x}+\frac{\partial \bar{v}}{\partial y}+\frac{\partial \bar{w}}{\partial z})=0 \qquad (3.50)$$

Subtracting equation (3.50) from equation (3.49) yields:

$$[\bar{u}\frac{\partial \bar{u}}{\partial x}+\frac{\partial \overline{(u)^2}}{\partial x}]+[\bar{v}\frac{\partial \bar{u}}{\partial y}+\frac{\partial (\overline{uv})}{\partial y}]+[\bar{w}\frac{\partial \bar{u}}{\partial y}+\frac{\partial (\overline{uw})}{\partial z}]=-\frac{1}{\rho}(\frac{\partial \bar{p}}{\partial x})+\frac{\mu}{\rho}(\frac{\partial^2 \bar{u}}{\partial x^2}+\frac{\partial^2 \bar{u}}{\partial y^2}+\frac{\partial^2 \bar{u}}{\partial z^2})$$

(3.51)

Rearranging equation (3.51) gives:

$$\bar{u}\frac{\partial \bar{u}}{\partial x}+\bar{v}\frac{\partial \bar{u}}{\partial y}+\bar{w}\frac{\partial \bar{u}}{\partial z}=-\frac{1}{\rho}(\frac{\partial \bar{p}}{\partial x})+\frac{\mu}{\rho}(\frac{\partial^2 \bar{u}}{\partial x^2}+\frac{\partial^2 \bar{u}}{\partial y^2}+\frac{\partial^2 \bar{u}}{\partial z^2})-(\frac{\partial \overline{(u)^2}}{\partial x}+\frac{\partial (\overline{uv})}{\partial y}+\frac{\partial (\overline{uw})}{\partial z}) \quad (3.52)$$

Similarly, y and z directional momentum can also be given by:

$$\bar{u}\frac{\partial \bar{v}}{\partial x}+\bar{v}\frac{\partial \bar{v}}{\partial y}+\overline{(w)^2}\frac{\partial \bar{u}}{\partial z}=-\frac{1}{\rho}(\frac{\partial \bar{p}}{\partial x})+\frac{\mu}{\rho}(\frac{\partial^2 \bar{v}}{\partial x^2}+\frac{\partial^2 \bar{v}}{\partial y^2}+\frac{\partial^2 \bar{v}}{\partial z^2})-(\frac{\partial (\overline{vu})}{\partial x}+\frac{\partial \overline{(v)^2}}{\partial y}+\frac{\partial (\overline{vw})}{\partial z})$$

(3.53)

$$\bar{u}\frac{\partial \bar{w}}{\partial x}+\bar{v}\frac{\partial \bar{w}}{\partial y}+\bar{w}\frac{\partial \bar{w}}{\partial z}=-\frac{1}{\rho}(\frac{\partial \bar{p}}{\partial x})+\frac{\mu}{\rho}(\frac{\partial^2 \bar{w}}{\partial x^2}+\frac{\partial^2 \bar{w}}{\partial y^2}+\frac{\partial^2 \bar{w}}{\partial z^2})$$

$$-(\frac{\partial (\overline{wu})}{\partial x}+\frac{\partial (\overline{wv})}{\partial y}+\frac{\partial \overline{(w)^2}}{\partial z}) \qquad (3.54)$$

Equations (3.52), (3.53) and (3.54) are the momentum equations for turbulent flow.

For an incompressible fluid flow in cylindrical coordinates (r, θ, z) , the conservation of momentum equations can be expressed in their time-averaged form to account for turbulence effects. Let $\overline{u}_r, \overline{u}_\theta, \overline{u}_z$ denote the time-averaged velocities in the $r,\ \theta,\ z$ directions, respectively, and let $\overline{p}$ denote the time-averaged pressure. The Reynolds stresses, which represent the momentum fluxes due to turbulence, are denoted as $-\rho\overline{u_i' u_j'}$, where u_i' and u_j' are the fluctuating components of the velocity field. The time-averaged momentum equations in cylindrical coordinates, incorporating the effects of turbulence via the Reynolds stresses, are given below for each coordinate direction.

Radial Direction (r):

$$\rho\left(\frac{\partial\overline{u}_r}{\partial t} + \overline{u}_r\frac{\partial\overline{u}_r}{\partial r} + \frac{\overline{u}_\theta}{r}\frac{\partial\overline{u}_r}{\partial\theta} - \frac{\overline{u}_\theta{}^2}{r} + \overline{u}_z\frac{\partial\overline{u}_r}{\partial z}\right) = -\frac{\partial\overline{p}}{\partial r} + \mu\left(\nabla^2\overline{u}_r - \frac{\overline{u}_r}{r^2} - \frac{2}{r^2}\frac{\partial\overline{u}_\theta}{\partial\theta}\right) -$$
$$\frac{\partial}{\partial r}\left(-\rho\overline{u_r' u_r'}\right) \quad - \frac{1}{r}\frac{\partial}{\partial\theta}\left(-\rho\overline{u_r' u_\theta'}\right) - \frac{\partial}{\partial z}\left(-\rho\overline{u_r' u_z'}\right) + \rho g_r \qquad (3.55)$$

Circumferential Direction (θ) :

$$\rho\left(\frac{\partial\overline{u}_\theta}{\partial t} + \overline{u}_r\frac{\partial\overline{u}_\theta}{\partial r} + \frac{\overline{u}_\theta}{r}\frac{\partial\overline{u}_\theta}{\partial\theta} + \frac{\overline{u}_r\overline{u}_\theta}{r} + \overline{u}_z\frac{\partial\overline{u}_\theta}{\partial z}\right) = -\frac{1}{r}\frac{\partial\overline{p}}{\partial\theta} + \mu\left(\nabla^2\overline{u}_\theta - \frac{\overline{u}_\theta}{r^2} + \frac{2}{r^2}\frac{\partial\overline{u}_r}{\partial\theta}\right) -$$
$$\frac{\partial}{\partial r}\left(-\rho\overline{u_\theta' u_r'}\right) - \frac{1}{r}\frac{\partial}{\partial\theta}\left(-\rho\overline{u_\theta' u_\theta'}\right) - \frac{\partial}{\partial z}\left(-\rho\overline{u_\theta' u_z'}\right) \qquad (3.56)$$

Axial Direction (z):

$$\rho\left(\frac{\partial\overline{u}_z}{\partial t} + \overline{u}_r\frac{\partial\overline{u}_z}{\partial r} + \frac{\overline{u}_\theta}{r}\frac{\partial\overline{u}_z}{\partial\theta} + \overline{u}_z\frac{\partial\overline{u}_z}{\partial z}\right) = -\frac{\partial\overline{p}}{\partial z} + \mu(\nabla^2\overline{u}_z) - \frac{\partial}{\partial r}\left(-\rho\overline{u_z' u_r'}\right) -$$
$$-\frac{1}{r}\frac{\partial}{\partial\theta}(-\rho\overline{u_z' u_\theta'}) - \frac{\partial}{\partial z}(-\rho\overline{u_z' u_z'}) + \rho g_z \qquad (3.57)$$

3.3.5.3 Time-Averaged Energy Equation

Energy equation, neglecting dissipative function is given by:

$$\rho C_p[\frac{\partial T}{\partial t} + u\frac{\partial T}{\partial x} + v\frac{\partial T}{\partial y} + w\frac{\partial T}{\partial z}] = k(\frac{\partial^2 T}{\partial x^2} + \frac{\partial^2 T}{\partial y^2} + \frac{\partial^2 T}{\partial z^2}) \quad (3.58)$$

Multiplying continuity equation (3.35) by T:

$$T(\frac{\partial u}{\partial x} + \frac{\partial v}{\partial y} + \frac{\partial w}{\partial z}) = 0 \quad (3.59)$$

And adding equation (3.58) to equation (3.59) and given that $k = \alpha\rho C_P$ you obtain:

$$\frac{\partial T}{\partial t} + \frac{\partial (uT)}{\partial x} + \frac{\partial (vT)}{\partial y} + \frac{\partial (wT)}{\partial z} = \alpha(\frac{\partial^2 T}{\partial x^2} + \frac{\partial^2 T}{\partial y^2} + \frac{\partial^2 T}{\partial z^2}) \quad (3.60)$$

Averaging over period $t \to 0$, to obtain:

$$\frac{\partial \overline{T}}{\partial t} + \frac{\partial (\overline{uT})}{\partial x} + \frac{\partial (\overline{vT})}{\partial y} + \frac{\partial (\overline{wT})}{\partial z} = \alpha(\frac{\partial^2 \overline{T}}{\partial x^2} + \frac{\partial^2 \overline{T}}{\partial y^2} + \frac{\partial^2 \overline{T}}{\partial z^2}) \quad (3.61)$$

But $\frac{\partial \overline{T}}{\partial t} = 0$. Hence substituting for $u = U + u(t), v = V + v(t)$ and $w = W + w(t)$ in(3.55) and rearranging gives:

$$[\overline{u}\frac{\partial \overline{T}}{\partial x} + \overline{T}\frac{\partial \overline{u}}{\partial x}] + [v\frac{\partial \overline{T}}{\partial y} + \overline{T}\frac{\partial \overline{v}}{\partial y}] + [w\frac{\partial \overline{T}}{\partial z} + \overline{T}\frac{\partial \overline{w}}{\partial z}] = \alpha(\frac{\partial^2 \overline{T}}{\partial x^2} + \frac{\partial^2 \overline{T}}{\partial y^2} + \frac{\partial^2 \overline{T}}{\partial z^2})$$

$$-(\frac{\partial (\overline{uT})}{\partial x} + \frac{\partial (\overline{vT})}{\partial y} + \frac{\partial (\overline{wT})}{\partial z}) \quad (3.62)$$

Since $\frac{\partial \overline{u}}{\partial x} = \frac{\partial \overline{v}}{\partial y} = \frac{\partial \overline{w}}{\partial z} = 0$, to obtain:

$$u\frac{\partial \overline{T}}{\partial x} + v\frac{\partial \overline{T}}{\partial y} + w\frac{\partial \overline{T}}{\partial z} = \alpha(\frac{\partial^2 \overline{T}}{\partial x^2} + \frac{\partial^2 \overline{T}}{\partial y^2} + \frac{\partial^2 \overline{T}}{\partial z^2}) - (\frac{\partial (\overline{uT})}{\partial x} + \frac{\partial (\overline{vT})}{\partial y} + \frac{\partial (\overline{wT})}{\partial z}) \quad (3.63)$$

Equation (3.57) is the energy equation for turbulent flow. Mass, momentum and energy are therefore conserved for velocity components in turbulent flow. Hereafter, non-dimensional parameters are discussed. The time-averaged energy equation for turbulent flow, when expressed in cylindrical coordinates $(r, \theta\ , z\ )$, accounts for the effects of mean flow and turbulence on the thermal energy distribution. The derivation of the time-averaged energy equation from the instantaneous energy equation involves Reynolds averaging, similar to the process used for deriving the Reynolds-Averaged Navier-Stokes (RANS) equations for momentum. The general form of the instantaneous energy equation for a fluid flow, assuming constant properties (density (ρ) and specific heat capacity $(c_p\ )$, and neglecting viscous dissipation and radiation, in cylindrical coordinates is:

$$\rho c_p\left(\frac{\partial T}{\partial t}+u_r\frac{\partial T}{\partial r}+\frac{u_\theta}{r}\frac{\partial T}{\partial \theta}+u_z\frac{\partial T}{\partial_z}\right)=k\left(\frac{\partial^2 T}{\partial r^2}+\frac{1}{r}\frac{\partial T}{\partial r}+\frac{1}{r^2}\frac{\partial^2 T}{\partial \theta^2}+\frac{\partial^2 T}{\partial_{z^2}}\right)+\Phi \qquad (3.64)$$

Where:

T is the temperature,

u_r, u_θ, and u_z are the components of velocity in the , θ, and z directions,

k is the thermal conductivity

Φ represents the volumetric heat sources within the fluid.

To obtain the time-averaged energy equation, the temperature and velocities were decomposed into their mean and fluctuating components ($T=\overline{T}+T'$, $u_i=\overline{u_i}+u_i$) and then apply Reynolds averaging. After averaging and assuming constant properties, the equation becomes:

$$\rho c_p\left(\frac{\partial \overline{T}}{\partial t}+\overline{u_r}\frac{\partial \overline{T}}{\partial r}+\frac{\overline{u_\theta}}{r}\frac{\partial \overline{T}}{\partial \theta}+\overline{u_z}\frac{\partial \overline{T}}{\partial_z}\right)=k\left(\frac{\partial^2 \overline{T}}{\partial r^2}+\frac{1}{r}\frac{\partial \overline{T}}{\partial r}+\frac{1}{r^2}\frac{\partial^2 \overline{T}}{\partial \theta^2}+\frac{\partial^2 \overline{T}}{\partial_{z^2}}\right)+\overline{\Phi}+\Phi_t \qquad (3.65)$$

Here, Φ_t represents the additional term arising from the turbulent fluctuations, often referred to as the turbulent heat flux. This term accounts for the enhanced mixing and transport of thermal energy due to turbulence and is modeled in various ways in different turbulence models. The exact form of Φ_t depends on the turbulence model being used and typically involves gradients of the mean temperature field and turbulent properties like turbulent kinetic energy and turbulent viscosity. Solving this equation, along with the RANS equations for momentum and the appropriate turbulence model equations, provides a comprehensive description of turbulent flow and heat transfer in cylindrical coordinates.

3.4 Non-Dimensional Parameters

There are several non-dimensional parameters that are commonly used in fluid dynamics to describe the behavior of a fluid and to simplify the fluid conservation equations. These parameters are defined as ratios of different physical quantities and can be used to compare different fluid flows or to analyze the relative importance of different terms in the equations. Dimensionless groups were used to allow for unit and scale independence (Rasool et al., 2022). The letters $U, P, L, t,$ and H represent the characteristic values of velocity, pressure, length, time, and magnetic field, respectively. Some common non-dimensional parameters in fluid dynamics include: Mach number, Magnetic Parameter, Prandtl Number, Turbulent Prandtl Number, Grashof Number, Reynolds Number, Eckert Number, Schmidt number, Rotational Parameter, Weber and Froude number

,3.4.1 Mach number (Ma)

Mach number is a dimensionless parameter that describes the ratio of the fluid velocity to the speed of sound in the fluid. It is defined as:

$$Ma = \frac{u}{a} \tag{3.66}$$

Where u is the fluid velocity and a is the speed of sound in the fluid.

3.4.2 Magnetic Parameter

Here, when given the magnetic force relative to the viscous force. For the magnetic parameter, these results are obtained. $M^2 = \frac{\sigma\mu_e^2 H_0^2 v}{\rho u_0^2}$; which can be written as

$$M = \sqrt{\left(\frac{\sigma\mu_e^2 H_0^2 v}{\rho u_0^2}\right)} \tag{3.67}$$

3.4.3 Prandtl Number

Prandtl number is a dimensionless parameter that describes the ratio of the momentum diffusivity (kinematic viscosity) to the thermal diffusivity of a fluid.

It is expressed as

$$Pr = \frac{\nu}{\alpha} \tag{3.68}$$

where ν is the kinematic viscosity and α is the thermal diffusivity.Kinematic viscosity-to-thermal diffusivity ratio refers to the relationship between the two properties. As a mathematical concept, it is described as;

$$P_r = \mu\frac{c_p}{k} \tag{3.69}$$

where $k = \frac{\mu}{\rho}, \quad and \ \ \alpha = \frac{k}{\rho C_p}$

3.4.4 Turbulent Prandtl Number

The turbulent Prandtl number, which quantifies the discrepancy between the eddy diffusivity of momentum and heat transfer, is crucial in understanding heat transfer in chaotic boundary layer flows.
Mathematically, it can be represented as;

$$\Pr t = \frac{E_M}{E_H} \tag{3.70}$$

Where $$\boldsymbol{E_M} = -2\boldsymbol{k}^2\boldsymbol{z}^2 \frac{\partial \boldsymbol{u}}{\partial \boldsymbol{z}}$$

3.4.5 Grashof Number

Grashof number (Gr) is a dimensionless parameter that describes the ratio of buoyancy forces to viscous forces in a fluid flow. It is defined as

$$Gr = \frac{g\beta L^3}{\eta^2} \tag{3.71}$$

Where $\boldsymbol{g}$ the acceleration due to gravity is,$\boldsymbol{\beta}$ is the coefficient of thermal expansion, $\boldsymbol{L}$is a characteristic length scale, and $\boldsymbol{\eta}$ is the dynamic viscosity of the fluid.

3.4.6 Reynolds Number

Reynolds number (Re) is a dimensionless parameter that describes the ratio of inertial forces to viscous forces in a fluid flow. It is defined as

$$Re = \frac{UL}{\eta}, \tag{3.72}$$

Where U is a characteristic velocity, L is a characteristic length scale, and η is the dynamic viscosity of the fluid.

3.4.7 Eckert Number (E_c)

Ratio of kinetic energy to the boundary layer. For high speed flows and high viscous dissipation

$$E_c = \frac{v_0^2}{c_p \Delta T} \tag{3.73}$$

3.4.8 Schmidt number

Schmidt number $(Sc)$is a dimensionless parameter that describes the ratio of the momentum diffusivity (kinematic viscosity) to the mass diffusivity of a fluid. It is defined as

$$\boldsymbol{Sc} = \frac{\boldsymbol{\nu}}{\boldsymbol{D}} \tag{3.74}$$

Where ν is the kinematic viscosity and D is the mass diffusivity.

3.4.9 Rotational Parameter

The ratio between rotational and translational kinetic energies.

The following provides kinetic energy:

$$E_r = \frac{Wu'}{U^2} \tag{3.75}$$

where Wu' is the drag force and U^2 represent cohesive force

3.4.10 Weber number

The Weber number is a dimensionless number used in fluid mechanics to describe the relative importance of inertial forces compared to surface tension forces in a fluid system.

It is defined as the ratio of inertial force to surface tension force. It is used to predict fluid behavior in systems with both fluid flow and surface tension, such as droplet formation and fluid instability.

The Weber number is mathematically expressed as:

$$We = \frac{\rho v^2 L}{\sigma} \tag{3.76}$$

where: ρ is the fluid density, v is the fluid velocity, L is a characteristic length and σ is the surface tension of the fluid.

3.4.11 Froude number

The Froude number is a dimensionless number used in fluid mechanics to describe the relative importance of inertial forces to gravitational forces in a fluid system. It is used to predict the behavior of flows with gravity effects, such as open channel flows and ship hydrodynamics. The Froude number is mathematically expressed as:

$$Fr = \frac{v}{(gL)^{0.5}} \tag{3.77}$$

Where: v is the fluid velocity, g is the acceleration due to gravity, L is a characteristic length typically the height of the channel or the draft of a ship.

These non-dimensional parameters were used to analyze the behavior of a fluid flow and to understand the relative importance of different physical effects in the flow. They were often used to simplify the fluid conservation equations and to study the behavior of fluid flows under different conditions.

3.5 Numerical Method of Solution

Fluid conservation equations can be solved using numerical methods. These involve discretizing the equations and solving them with computer software. Numerical methods include finite difference, finite element, and spectral element methods, which divide the flow domain into a grid and solve the equations at each grid point. The finite difference method is a numerical method that approximates the derivatives of a function using finite differences. It involves dividing the domain into a grid and then approximating the partial derivatives of the function at each point in the grid using finite difference approximations. The finite element method is a numerical method used to approximate solutions to Partial Differential Equations (PDEs). It involves discretizing the domain into a set of smaller elements and approximating the solution over each element. The method is useful for solving problems with complex geometries and irregular meshes.

The spectral element method is a numerical method used to approximate solutions to Partial Differential Equations (PDEs). Similar to the finite element method, it involves breaking the domain up into elements. However, spectral elements are typically polynomials, chosen to minimize approximation error and improve accuracy. The spectral element method works well when high accuracy is required, and when complex geometries need to be handled. It is widely applied in fluid dynamics problems.

The finite difference method is suitable for simple geometries and regular grids, the finite element method is best suited for complex geometries, and the spectral element method is useful for high accuracy problems and complex geometries. Numerical methods are used for complex flows or when analytical solutions are not possible. In fluid dynamics, numerical methods can be used to solve equations such as the Navier-Stokes and Euler equations using the finite volume and finite element methods, respectively. The advection-diffusion equation can be solved using the spectral element method. Programs are created in MATLAB to solve finite difference equations.

Finite difference methods are numerical techniques used to solve differential equations by approximating derivatives at discrete points (nodes) on a grid using the difference of function values at nearby nodes. This method can solve problems involving partial differential equations and is widely used in engineering and physics.

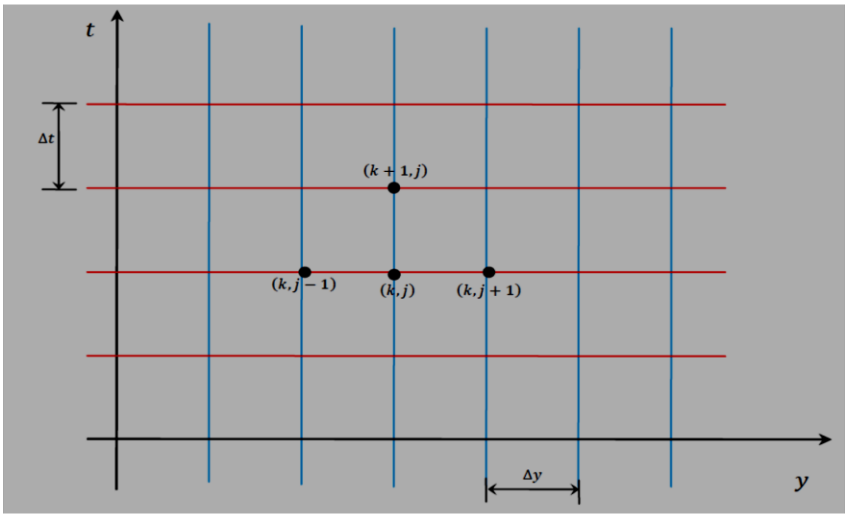

Figure 3.1: *Important point grid in explicit finite difference method*

Indeed, being concerned in the future propagation of the fluid's characteristics, taking the starting state (at time t = 0) into consideration. Each vertex is identified by a pair of indexes, j and k. Each node is used to determine the values of the given functions. Assuming a rectangular plane with the horizontal axis y and the vertical axis t. Let t vary from $0-a$ and y from $0-b$.Also let the intervals be divided into n and m sub-intervals each having width $\triangle t$ and $\triangle y$ respectively then a point (y_i, t_j) on the rectangular plane can be defined such that: $t_j = j \triangle t; j = 1,2,3, \dots$ $y_i = i \triangle y;$ $i = 1,2,3, \dots$The grid lines y_i and t_j intersecting at mesh points is illustrated in the figure above. The finite difference approximation for the first and second derivatives of U withrespect to y can now be given from the definition of mesh shown above. On applying Taylors series expansion and neglecting terms that have order which is higher than two. These neglected terms are the truncation error in approximation.

Applying Taylors series expansion in variables y and t at the points $\left(y_{i+1}, t_j\right)$

and$\left(y_{i-1}, t_j\right)$ about (y_i, t_j) you have:

$$U(i+1,j) = U(i,j) + U_y(i,j) \triangle y + \frac{1}{2} U_{yy}(i,j)(\triangle y)^2 + \cdots \tag{3.78}$$

$$U(i-1,j) = U(i,j) - U_y(i,j) \triangle y + \frac{1}{2} U_{yy}(i,j)(\triangle y)^2 + \cdots \tag{3.79}$$

$$U(i,j+1) = U(i,j) + U_t(i,j) \triangle t + \frac{1}{2} U_t t(i,j)(\triangle y)^2 + \cdots \tag{3.80}$$

$$U(i,j-1) = U(i,j) - U_t(i,j) \triangle t + \frac{1}{2} U_t t(i,j)(\triangle y)^2 + \cdots \tag{3.81}$$

where, $U(i,j) = U(y_i, t_j)$ and $U_y(i,j) = \frac{\partial U(y_i, t_{J'})}{\partial y}$

On eliminating Uyy from equations (3.78) and (3.79) the difference formula become :

$$\frac{\partial U(y_i, j)}{\partial y} = \frac{U(i+1,j) - U(i-1,j)}{2h} + o(h^2) \tag{3.82}$$

eliminating $U_t t$ from equations (3.80) and (3.81), becomes

$$\frac{\partial U(i,j)}{\partial t} = \frac{U(i,j+1)-U(i-1,j)}{2k} + o(k^2) \tag{3.83}$$

On eliminating U_y from equations (3.78) and (3.79), yields;

$$\frac{\partial^2 U(i,j)}{\partial y^2} = \frac{U(i+1,j)-2U(i,j)+U(i-1,j)}{h^2} + o(h^2) \tag{3.84}$$

and on eliminating U_t from equations (3.80) and (3.81), gives

$$\frac{\partial^2 U(i,j)}{\partial t^2} = \frac{U(i,j+1)-2U(i,j)+U(i,j-1)}{k^2} + o(k^2) \tag{3.85}$$

The equations (3.74), (3.75), (3.76) and (3.77) are then used to obtain approximate solutions for finite difference scheme for the differential equations. The order of the truncation errors are therefore minimized by taking small values of $\triangle t$ and $\triangle y$. Finite difference methods are of two types: explicit and implicit. Explicit methods solve for a node using only known values at that node and its neighbors, while implicit methods solve a system of equations at each node and depend on values at all nodes. Implicit methods are more stable but harder to implement, while explicit methods are simple but may be unstable for large step sizes. These methods can solve problems in heat transfer, fluid dynamics, and structural mechanics, and are useful for solving partial differential equations. They are widely used in engineering and physics and are a standard method for solving differential equations. There are various variations of finite difference methods such as finite difference in time and space, finite volume, and spectral methods, each suitable for specific types of problems. The two techniques for solving second-order PDEs are the fully explicit (FTCS) and fully implicit (BTCS) methods. A combination of implicit and explicit methods is proposed, with the Crank-Nicolson method being the popular and dependable implicit-explicit mixing approach. It's a general, powerful way to solve 2-D differential equations.

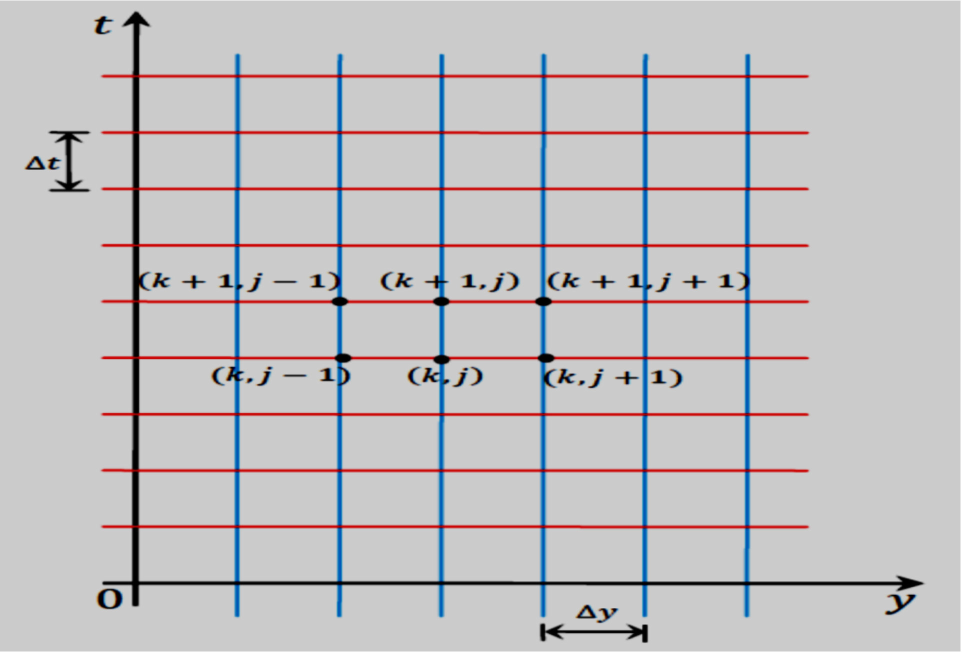

Figure 3.2: *Crank -Nicolson Formula*

(Johnson, O. B., 2020). The Crank-Nicolson method is a numerical method used to solve partial differential equations (PDEs) of the form:

$$\frac{du}{dt}=a\left(\frac{dx}{dt},x,t\right) \tag{3.86}$$

Where

u is the unknown function,

t is the time variable,

x is the space variable, and

a is a function that describes the spatial and temporal behavior of the system being modeled.

The Crank-Nicolson method is a finite difference method that uses a combination of implicit and explicit methods to approximate the solution to the PDE.The basic idea behind the Crank-Nicolson method is to divide the time interval into smaller time steps, and to use a weighted average of the solution at two successive time steps to obtain an estimate of the solution at the next time step. To do this, first divide the time interval into N equal subintervals of size Δt, and let,

$$t_i = i\Delta t \tag{3.87}$$

for $i = 0,1, \ldots, N$. (Johnson& Oluwaseun, 2020).

The solution at time t_i is approximated by u_i.Next, the Taylor series expansion was used to approximate the solution at time $t_{\{i+1\}}$. For example, if a first-order Taylor series expansion is used, equation (3.88) is obtained:

$$u\left(t_{\{i+1\}}, x\right) = u\left(t_i, x\right) + \Delta t * \frac{du}{dt}\left(t_i, x\right) + O\left(\Delta t^2\right) \tag{3.88}$$

The Crank-Nicolson method approximates the derivative term by taking a weighted average of the solution at two successive time steps:

$$\frac{\boldsymbol{du}}{\boldsymbol{dt}}\left(\boldsymbol{t}_i, \boldsymbol{x}\right) \approx \frac{\left(\boldsymbol{u}\left(\boldsymbol{t}_{\{i+1\}}, \boldsymbol{x}\right) - \boldsymbol{u}\left(\boldsymbol{t}_i, \boldsymbol{x}\right)\right)}{\boldsymbol{\Delta t}} \tag{3.89}$$

Using this approximation, the Crank-Nicolson method can be written as:

$$\boldsymbol{u}_{\{i+1\}} = \left(1 - \boldsymbol{\lambda}\right) * \boldsymbol{u}_i + \boldsymbol{\lambda} * \boldsymbol{u}_{\{i+1\}} \tag{3.90}$$

where

$$\boldsymbol{\lambda} = \boldsymbol{a}\left(\frac{\boldsymbol{dx}}{\boldsymbol{dt}}, \boldsymbol{x}, \boldsymbol{t}_{\{i+1\}}\right) * \boldsymbol{\Delta t}/2$$

The Crank-Nicolson method is an implicit method because the solution at time $t_{\{i+1\}}$ is dependent on the solution at time $t_{\{i+1\}}$. To solve for $u_{\{i+1\}}$, there is need to iterate the solution using a numerical method such as the Newton-Raphson method or a matrix solver until the solution converges.

The Crank-Nicolson method is widely used in numerical simulations of PDEs because it is relatively simple to implement and has good stability properties. However, it can be computationally expensive, especially for large problems, because it requires iterative solution of implicit equations at each time step.

3.6 Mathematical Model

Turbulent unsteady MHD flow over a porous aerofoil wing within a magnetic field is consider. The flow is considered in a 2 –Dimensional cylindrical geometry. The porous wing is assumed to have non-end effects. The porous wing is taken to be along the x-axis and the streamline body to be along the y-axis while the z-axis is taken normal to the porous aerofoil wing. The fluid used is air. The fluid flow is along a horizontal infinitely long porous aerofoil wing lying in the x-y plane. The porous aerofoil wing is immersed in the ionized air. The axis of the porous wing is in the positive z-axis direction and the air flows through it in positive z-axis direction parallel to the axis of the wing. OpenFOAM was used to simulate the flow of air over a porous aerofoil wing within a range of magnetic field strengths. The wing was modeled as a two-dimensional section, with the flow of air occurring in the plane of the wing. The porous region of the wing was modeled using a porous media model, with the properties of the porous region (such as porosity and permeability) varied to represent different porous wing designs. This ionized air is assumed to be incompressible and viscous in the magnetic field. A strong magnetic field of uniform strength is applied normal to the direction of flow of the ionized air. The induced magnetic field is considered negligible and the plane is flying horizontal in air hence the force acting on the wings due to gravity is assumed to be zero as in figure 3.3. Simulation of the flow of air over the wing at a range of angles of attack was done, to examine the effects of the magnetic field on lift and drag. Also examination of the overall flow structure over the wing, including velocity and pressure profiles and the presence of turbulent eddies was done.

3.7 Geometry of the Problem

A three-dimensional geometry of the porous wing of the airplane was drawn with scaled in ANSYS Design Modular, and shown in figure 3.3

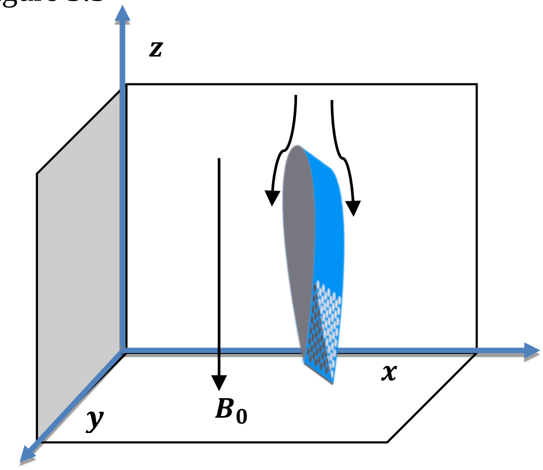

Figure 3.3: *PorousWings of the aerofoil*

Given that the flow is over porous wing, cylindrical coordinate form of the governing equations discussed in are used. The flow is considered to be along the axial and angular components. There is no radial flow. Thus the two dimensions of this flow are z and θ. From the geometry of the problem above, the porous airfoil wing is infinite such that the derivatives along r and θ are identically zero, more so there is no gravity force acting on the porous wing

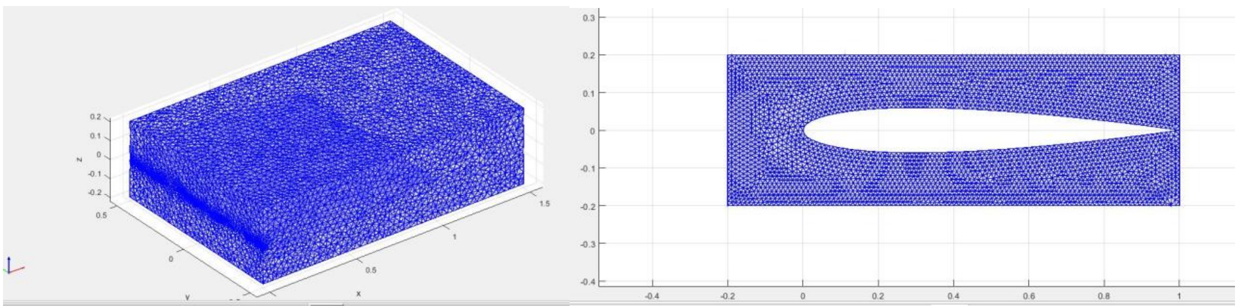

(a) Side view (b) front view

Figure 3.4: *Grid generations of Porous Wings of the aerofoil*

The above flow is governed by the following cylindrical coordinate equations:

$$\frac{\partial \overline{U_z}}{\partial t} + \overline{U_r}\frac{\partial \overline{U_z}}{\partial r} = -\frac{1}{\rho}\frac{\partial \overline{P}}{\partial z} + \nu\left(\frac{\partial^2 U_z}{\partial r^2} + \frac{1}{r}\frac{\partial U_z}{\partial r}\right) - \left[\frac{1}{r}\frac{\partial \overline{U_z' U_r'}}{\partial r}\right] + \rho g + \vec{J} \times B|_z \qquad (3.91)$$

$$\frac{\partial \overline{U_\theta^*}}{\partial t^*} + \overline{U_r}\frac{\partial \overline{U_\theta}}{\partial r} = V\left(\frac{\partial^2 \overline{U_\theta^*}}{\partial r^{*2}} + \frac{1}{r^*}\frac{\partial \overline{U_\theta^*}}{\partial r^*} - \frac{\overline{U_\theta^*}}{r^{*2}}\right) - \left[\frac{\partial \overline{U_r' U_\theta'}}{\partial r^*} - \frac{2\overline{U_\theta' U_r'}}{r^*}\right] + \vec{J} \times B|_\theta \qquad (3.92)$$

$$\rho C_p\left(\frac{\partial \overline{T^*}}{\partial t^*} + \overline{u_r}\frac{\partial \overline{T}}{\partial r}\right) = k\left(\frac{\partial^2 \overline{T^*}}{\partial r^{*2}} + \frac{1}{r^*}\frac{\partial \overline{T^*}}{\partial r^*}\right) - \rho C_p\left(\frac{\partial\left(\overline{U_r' T'}\right)}{\partial r^*}\right) \qquad (3.93)$$

It was noted that there was no pressure gradient in $\theta -$ direction and there is no gravitational force also. The boundary and initial conditions are:

$$t^* < 0: U_z^* = 0, U_\theta^* = 0, T^* = T_\infty^*, \text{ everywhere} \qquad (3.94)$$

$t^* \geq 0: U_z^* = U_0, U_\theta^* = 0, T^* = T_W^*$, at $r^* = \frac{L}{2}$ (is the chord Length of the porous aerofoil wing) (3.95)

$$U_z^* \to 0, U_\theta^* \to 0, T^* \to T_\infty^*, \text{ as } r^* \to \infty \qquad (3.96)$$

The pressure gradient in the z-axis direction results from the change in elevation up the porous wing. Thus: $\frac{\partial P}{\partial z} = -p_\infty g$ (3.97)

Hence equation (3.91) becomes:

$$\rho\frac{\partial \overline{U_z}}{\partial t} + \rho\overline{U_r}\frac{\partial \overline{U_z}}{\partial r} = (\rho_\infty - \rho)g + \mu\left(\frac{\partial^2 U_z}{\partial r^2} + \frac{1}{r}\frac{\partial U_z}{\partial r}\right) - \rho\left[\frac{1}{r}\frac{\partial \overline{U_z' U_r'}}{\partial r}\right] + \vec{J} \times B|_z \qquad (3.98)$$

The density difference $\rho - \rho_\infty$ may be expressed in terms of the volume coefficient of expansion β defined by:

$$\beta = \frac{1}{V}\left(\frac{\partial V}{\partial T}\right)_P = \frac{1}{V_\infty}\cdot\frac{V - V_\infty}{T_W - T_\infty} = \frac{p_\infty - p}{p(T_W - T_\infty)} \text{ (Frost,2013)} \qquad (3.99)$$

such that (3.98) becomes

$$\rho\frac{\partial \overline{U_z}}{\partial t} + \rho\overline{U_r}\frac{\partial \overline{U_z}}{\partial r} = \rho\beta g(T_w - T_\infty) + \mu\left(\frac{\partial^2 U_z}{\partial r^2} + \frac{1}{r}\frac{\partial U_z}{\partial r}\right) - \rho\left[\frac{1}{r}\frac{\partial \overline{U_z' U'}}{\partial r}\right] + \vec{J} \times B|_z \qquad (3.100)$$

which simplifies to

$$\frac{\partial \overline{U_z}}{\partial t} + \overline{U_r}\frac{\partial \overline{U_z}}{\partial r} = \beta g(T_w - T_\infty) + \nu\left(\frac{\partial^2 U_z}{\partial r^2} + \frac{1}{r}\frac{\partial U_z}{\partial r}\right) - \left[\frac{1}{r}\frac{\partial \overline{U_z' U'}}{\partial r}\right] + \vec{J} \times B|_z \qquad (3.101)$$

Using (*) to indicate dimension and $v = \mu/\rho$, equation (3.101) becomes.

$$\frac{\partial U_z^*}{\partial t^*} + \overline{U_r^*}\frac{\partial \overline{U_z^*}}{\partial r} = \beta g(T_w^* - T_\infty^*) + v\left(\frac{\partial^2 \overline{U_{zz}^*}}{\partial r^{*2}} + \frac{1}{r^*}\frac{\partial \overline{U_z^*}}{\partial r^*}\right) - \left[\frac{1}{r^*}\frac{\partial \overline{U_z' U_r'}}{\partial r^*}\right] + \vec{J} \times B|_z \qquad (3.102)$$

Next, was to establish the components of the electromagnetic force term in (3.102) and (3.92) that is the term: $\vec{J} \times \vec{B}$

The equation of conservation of charge $\nabla.J = 0$, gives $j_r = k$, a constant, where $\vec{J} = (j_r, j_\theta, j_Z)$. The constant is zero since, $j_r = 0$ at the aerofoil wing which is porous. Thus $j_r = 0$ everywhere in the flow. Neglecting the ion-slip and thermoelectric effects, generalized Ohm's law including the effects of Hall current gives:

$$\vec{J} + \frac{w_e \tau_e}{H_0}(\vec{J} \times \vec{H}) = \sigma(\vec{E} + \mu_0 \vec{q} \times \vec{H} + \frac{1}{e n_e}\nabla P_e) \qquad (3.103)$$

For the problem we seek to solve there is no applied electric field hence $\vec{E} = 0$ and thus neglecting electron pressure, equation (3.103) becomes:

$$\vec{J} + \frac{w_e \tau_e}{H_0}(\vec{I} \times \vec{H}) = \sigma\mu_0(\vec{q} \times \vec{H}) \qquad (3.104)$$

Given that $\vec{H} = (H_0, 0, 0)$ and taking $\vec{J} = (0, j_\theta, j_z), \vec{q} = (0, U_\theta, U_z)$ and $\vec{B} = \mu_0\vec{H}$ simplifying equation (3.104) and solving gives:

$$j_r = 0 \qquad (3.105)$$

$$j_\theta = \frac{\sigma\mu_0 H_0(U_Z + mU_\theta)}{1+m^2} \qquad (3.106)$$

$$j_Z = \frac{\sigma\mu_0 H_0(mU_Z - U_\theta)}{1+m^2} \qquad (3.107)$$

Where $m = w_e\tau_e$ is the Hall parameter.

Thus the electromagnetic force along θ and z-axis are respectively:

$$(I \times B)_\theta = \frac{\sigma\mu_0^2 H_0^2(mU_Z - U_\theta)}{1+m^2} \qquad (3.108)$$

$$(J \times B)_z = \frac{-\sigma\mu_0^2 H_0^2(U_Z + mU_\theta)}{1+m^2} \qquad (3.109)$$

Hence the governing equations (3.91) and (3.92) are respectively:

$$\frac{\partial \overline{U_z^*}}{\partial t^*} + \overline{U_r^*}\frac{\partial \overline{U_z^*}}{\partial r} = V\left(\frac{\partial^2 \overline{U_z^*}}{\partial r^{*2}} + \frac{1}{r^*}\frac{\partial \overline{U_z^*}}{\partial r^*}\right) - \left[\frac{1}{r^*}\frac{\partial \overline{U_z' U_r'}}{\partial r^*}\right] + \beta g(T_w^* - T_\infty^*)$$

$$- \frac{\sigma\mu_0^2 H_0^2\left(\overline{U_z^*} + m\overline{U_\theta^*}\right)}{1+m^2} \tag{3.110}$$

$$\frac{\partial \overline{U_\theta^*}}{\partial t^*} + \overline{U_r^*}\frac{\partial \overline{U_\theta^*}}{\partial r} = V\left(\frac{\partial^2 \overline{U_\theta^*}}{\partial r^{*2}} + \frac{1}{r^*}\frac{\partial \overline{U_\theta^*}}{\partial r^*} - \frac{\overline{U_\theta^*}}{r^{*2}}\right) - \left[\frac{\partial \overline{U_r' U_\theta'}}{\partial r^*} - \frac{2\overline{U_\theta' U_r'}}{r^*}\right] + \frac{\sigma\mu_0^2 H_0^2(m\overline{U_z^*} - \overline{U_\theta^*})}{1+m^2}$$

(3.111)

3.8 Non-Dimensionalization

To non-dimensionalize equations (3.93), (3.110) and (3.111). The following scaling variables are applied in the non- dimensionalization process:

$$t = \frac{t^* U_0^2}{v} \qquad r = \frac{r^* U_0}{v} U_i = \frac{U_i^*}{U_0}; \theta = \frac{T^* - T_\infty^*}{T_W^* - T_\infty^*} \tag{3.112}$$

The (*) superscript denotes the dimensional variables, U_o is the reference velocity, L is the chord length of the porous aerofoil wing, $T_w^* - T_\infty^*$ is the temperature difference between the surface and the free stream temperature.

Using the scaling variables above yields the following equations:

$$\frac{\partial U_z^*}{\partial t^*} = \frac{\partial U_z^*}{\partial U_z}\frac{\partial U_z}{\partial t}\frac{\partial t}{\partial t^*} = \frac{U_0^3}{v}\frac{\partial U_z}{\partial t} \tag{3.113}$$

$$\frac{\partial U_\theta^*}{\partial t^*} = \frac{\partial U_\theta^*}{\partial U_\theta}\frac{\partial U_\theta}{\partial t}\frac{\partial t}{\partial t^*} = \frac{U_0^3}{v}\frac{\partial U_\theta}{\partial t} \tag{3.114}$$

$$\frac{\partial U_z^*}{\partial r^*} = \frac{\partial U_z^*}{\partial U_z}\frac{\partial U_z}{\partial r}\frac{\partial r}{\partial r^*} = \frac{U_0^2}{v}\frac{\partial U_z}{\partial r} \tag{3.115}$$

$$\frac{\partial U_\theta^*}{\partial r^*} = \frac{\partial U_\theta^*}{\partial U_\theta}\frac{\partial U_\theta}{\partial r}\frac{\partial r}{\partial r^*} = \frac{U_0^2}{v}\frac{\partial U_\theta}{\partial r} \tag{3.116}$$

$$\frac{\partial T^*}{\partial t^*} = \frac{\partial T^*}{\partial \theta}\frac{\partial \theta}{\partial t}\frac{\partial t}{\partial t^*} = (T_W^* - T_\infty^*)\frac{U_0^2}{v}\frac{\partial \theta}{\partial t} \tag{3.117}$$

$$\frac{\partial^2 U_z^*}{\partial r^{*2}} = \frac{\partial}{\partial r}\left(\frac{U_0^2}{v}\frac{\partial U_z}{\partial r}\right)\frac{\partial r}{\partial r^*} = \frac{U_0^3}{v^2}\frac{\partial^2 U_z}{\partial r^2} \tag{3.118}$$

$$\frac{\partial^2 U_\theta^*}{\partial r^{*2}} = \frac{\partial}{\partial r}\left(\frac{U_0^2}{v}\frac{\partial U_\theta}{\partial r}\right)\frac{\partial r}{\partial r^*} = \frac{U_0^3}{v^2}\frac{\partial^2 U_\theta}{\partial r^2} \tag{3.119}$$

$$\frac{\partial T^*}{\partial r^*} = \frac{\partial T^*}{\partial \theta}\frac{\partial \theta}{\partial r}\frac{\partial r^*}{\partial r} = \frac{U_0(T_W^*-T_\infty^*)}{v}\frac{\partial \theta}{\partial r} \tag{3.120}$$

$$\frac{\partial^2 T^*}{\partial r^{*2}} = \frac{\partial}{\partial r}\left(\frac{U_0(T_W^*-T_\infty^*)}{v}\frac{\partial \theta}{\partial r}\right)\frac{\partial r}{\partial r^*} = \frac{U_0^2(T_W^*-T_\infty^*)}{v^2}\frac{\partial^2 \theta}{\partial r^2} \tag{3.121}$$

Substituting equations (3.113), (3.115) and (3.118) into (3.110) yields:

$$\frac{U_0^3}{v}\frac{\partial U_z}{\partial t} + \overline{U_r^*}\frac{U_0^2}{v}\frac{\partial U_z}{\partial r} = V\left(\frac{U_0^3}{v^2}\frac{\partial^2 U_z}{\partial r^2} + \frac{1}{r^*}\frac{U_0^2}{v}\frac{\partial U_z}{\partial r}\right) - \left[\frac{1}{r^*}\frac{\partial \overline{U_z' U_r'}}{\partial r^*}\right] + \beta g(T_W^* - T_\infty^*) -$$

$$\frac{\sigma\mu_0^2 H_0^2(\overline{U_z^*}+m\overline{U_\theta^*})}{1+m^2} \tag{3.122}$$

On rearranging equation (3.122) becomes:

$$\frac{\partial U_z}{\partial t} + \overline{U_r^*}\frac{1}{U_0}\frac{\partial U_z}{\partial r} = V\left(\frac{1}{v}\frac{\partial^2 U_z}{\partial r^2} + \frac{1}{r^*}\frac{1}{U_0}\frac{\partial U_z}{\partial r}\right) - v\left[\frac{1}{U_0^3 r^*}\frac{\partial \overline{U_z' U_r'}}{\partial r^*}\right] + \frac{\beta g v(T_W^*-T_\infty^*)}{U_0^3} -$$

$$\frac{\sigma\mu_0^2 H_0^2 v(\overline{U_z^*}+m\overline{U_\theta^*})}{U_0^3(1+m^2)} \tag{3.123}$$

On employing non-dimensional parameters equation (3.123) gives:

$$\frac{\partial U_z}{\partial t} + \frac{1}{U_0}\bar{U}_r^*\frac{\partial U_z}{\partial r} = v\left(\frac{1}{v}\frac{\partial^2 U_z}{\partial r^2} + \frac{1}{r^*}\frac{1}{U_0}\frac{\partial U_z}{\partial r}\right) - v\left[\frac{1}{U_0^3 r^*}\frac{\partial \bar{U}_{z'}^* \bar{U}_{r'}^*}{\partial r^*}\right] + \frac{Gr}{Re^2 Pr} + \frac{M^2(\bar{U}_z^*+m\bar{U}_\theta^*)}{U_0(1+m^2)} \tag{3.124}$$

where $Gr = \frac{g\beta(T_w^* - T_\infty^*)L^3}{\nu^2}$, $Pr = \frac{\nu}{\alpha}$, $Re = \frac{U_0 L}{\nu}$, $LU_o = \frac{\nu^2}{\alpha}$ and $M^2 = \frac{\sigma\mu_0^2 H_0^2 v}{U_0^2}$.

Substituting equations (3.114), (3.116) and (3.119) into (3.111) yields:

$$\frac{U_0^3}{v}\frac{\partial U_\theta}{\partial t} + \overline{U_r^*}\frac{U_0^2}{v}\frac{\partial U_\theta}{\partial r} = V\left(\frac{U_0^3}{v^2}\frac{\partial^2 U_\theta}{\partial r^2} + \frac{1}{r^*}\frac{U_0^2}{v}\frac{\partial U_\theta}{\partial r} - \frac{\overline{U_\theta^*}}{r^{*2}}\right) - \left[\frac{\partial \overline{U_r' U_\theta'}}{\partial r^*} - \frac{2\overline{U_\theta' U_r'}}{r^*}\right] +$$

$$\frac{\sigma\mu_0^2 H_0^2(m\overline{U_z^*}-\overline{U_\theta^*})}{1+m^2} \tag{3.125}$$

This on re-arranging, equation (3.125) gives:

$$\frac{\partial U_\theta}{\partial t} + \overline{U_r^*}\frac{1}{U_0}\frac{\partial U_\theta}{\partial r} = v\left(\frac{1}{v}\frac{\partial^2 U_\theta}{\partial r^2} + \frac{1}{r^*}\frac{1}{U_0}\frac{\partial U_\theta}{\partial r} - v\frac{\overline{U_\theta^*}}{U_0^3 r^{*2}}\right) - v\left[\frac{\partial \overline{U_r' U_\theta'}}{U_0^3\partial r^*} - \frac{2\overline{U_\theta' U_r'}}{U_0^3 r^*}\right] +$$

$$v\frac{\sigma\mu_0^2 H_0^2\left(m\overline{U_z^*}-\overline{U_\theta^*}\right)}{U_0^3(1+m^2)} \tag{3.126}$$

On introducing the non-dimensional parameters to equation (3.126) gives:

$$\frac{\partial U_\theta}{\partial t} + \overline{U_r^*}\frac{1}{U_0}\frac{\partial U_\theta}{\partial r} = \frac{\partial^2 U_\theta}{\partial r^2} + \frac{1}{r^*}\frac{v}{U_0}\frac{\partial U_\theta}{\partial r} - v^2\frac{\overline{U_\theta^*}}{U_0^3 r^{*2}} - v\left[\frac{\partial\overline{U_r' U_\theta'}}{U_0^3\partial r^*} - \frac{2\overline{U_\theta' U_r'}}{U_0^3 r^*}\right] + \frac{M^2\left(m\overline{U_z^*} - \overline{U_\theta^*}\right)}{U_0(1+m^2)}$$

(3.127)

where $M^2 = \frac{\sigma\mu_0^2 H_0^2 v}{U_0^2}$.

Substituting equations (3.117) , (3.120) and (3.121) into (3.93) yields:

$$(T_w^* - T_\infty^*)\frac{U_0^2}{v}\frac{\partial\theta}{\partial t} + \overline{u_r}\frac{U_0(T_w^* - T_\infty^*)}{v}\frac{\partial\theta}{\partial r} = \frac{k}{\rho C_p}\left(\frac{U_0^2(T_w^* - T_\infty^*)}{v^2}\frac{\partial^2\theta}{\partial r^2} + \frac{1}{r^*}\frac{U_0(T_w^* - T_\infty^*)}{v}\frac{\partial\theta}{\partial r}\right) - \left(\frac{\partial\overline{U_r' T'}}{\partial r^*}\right)$$

(3.128)

This on re-arranging gives:

$$\frac{\partial\theta}{\partial t} = \frac{k}{\rho C_p}\frac{1}{v}\frac{\partial^2\theta}{\partial r^2} + \left(\frac{1}{r^*} - \overline{u_r}\right)\frac{\partial\theta}{U_0\partial r} - \frac{v\partial\overline{U_r' T}}{(T_w^* - T_\infty^*)U_0^2\partial r} \tag{3.129}$$

Now, we introduce dimensionless variables:

$\theta^* = \dfrac{\theta - T_\infty^*}{T_w^* - T_\infty^*}$, $r^* = \dfrac{r}{R}$, $t^* = \dfrac{t}{t_c}$ normalized time, with t_c as a characteristic time scale,

$\bar{u}_r^* = \dfrac{\bar{u}_r}{U_0}, \theta'^* = \dfrac{\theta'}{T_w^* - T_\infty^*}$, $U_{r'}^* = \dfrac{U_{r'}}{U_0}$.

Now, substituting these dimensionless variables into Equation (3.129), we get:

$$\frac{\partial\theta^*}{\partial t^*} = \frac{1}{RePr}\left(\frac{\partial^2\theta^*}{\partial r^{*2}} + \frac{1}{r^{*2}} - \frac{\bar{u}_r^*}{r^*}\frac{\partial\theta^*}{\partial r^*} - \frac{1}{Pr}\frac{\bar{U}_{r'}^*\theta'^*}{\partial r^*}\right) \tag{3.130}$$

Here, Re and Pr are the Reynolds and Prandtl numbers, respectively, defined as:

$Re = \dfrac{U_0 R}{v}, Pr = \dfrac{\mu C_p}{k}$ .Where μ is the dynamic viscosity.

This equation is now non-dimensionalized, making it easier to analyze and solve without the need to consider specific scales of temperature, distance, and time.

There was need to solve equations (3.124), (3.127) and (3.130). However, the solution of these equations is not currently possible due to the Reynolds stress terms in (3.124) and (3.127). These terms were first resolved, to be able to work out the solution of these equations. The Reynolds stresses in (3.127) and (3.124) are respectively $v\left[\frac{\partial\overline{U_{r'}U_{\theta'}}}{U_0^3\partial r^*}-\frac{2\overline{U_{\theta'}U_{r'}}}{U_0^3 r^*}\right]$ and $v\left[\frac{1}{U_0^3 r^*}\frac{\partial\bar{U}_{z'}^*\bar{U}_{r'}^*}{\partial r^*}\right]$. The Boussinessque approximation was adopted $\tau_t=-\rho\overline{uv}=A_\tau\frac{dU}{dy}$, A_τ is not a property of the fluid like μ but depends on the mean velocity U. To resolve the Reynolds stresses using the Boussinessque approximation, making the assumption that the fluctuating velocity components are much smaller compared to the mean flow velocities. The Boussinessque hypothesis states that the fluctuating components of velocity can be neglected everywhere except in the momentum equations, where they appear in the form of Reynolds stresses. In the Boussinessque approximation, the Reynolds stress tensor can be expressed as:

$$\overline{u_{i'}u_{j'}}=-\rho\overline{u_{i'}u_{j'}}\delta_{ij} \tag{3.131}$$

Where δ_{ij} is the Kronecker delta, which equals 1 if $i=j$ and 0 otherwise. Now, applying this approximation to resolve the Reynolds stresses in the given equation. Substituting the Boussinessque approximation into the Reynolds stress terms and simplify accordingly.

Given the Boussinessque approximation:

$$\overline{U_{r'}U_{\theta'}}=-\rho\overline{U_{r'}U_{\theta'}} \tag{3.132}$$

Substituting this into the Reynolds stress term: $-v\left[\frac{\partial\overline{U_{r'}U_{\theta'}}}{U_0^3\partial r^*}-\frac{2\overline{U_{\theta'}U_{r'}}}{U_0^3 r^*}\right]$.

Becomes:

$$-\nu\left[\frac{\partial(-\rho\overline{U_{r'}U_{\theta'}})}{U_0^3\partial r^*}-\frac{2(-\rho\overline{U_{\theta'}U_{r'}})}{U_0^3 r^*}\right]=-\nu\left[-\frac{\rho}{U_0^3}\frac{\partial\overline{U_{r'}U_{\theta'}}}{\partial r^*}-\frac{2\rho}{U_0^3 r^*}\overline{U_{\theta'}U_{r'}}\right] \tag{3.133}$$

On turning to semi empirical methods then lead to the use of the Prandtl mixing length hypothesis that for a long time has been an important tool in the analysis of turbulent boundary layers. Prandtl assumed that this momentum was transported by eddies which moved in the$y$-direction over a distance l without interaction (i.e. momentum is assumed to be conserved over distance *l*) and then mixed with existing fluid at the new location. To incorporate the Prandtl mixing length hypothesis into the resolved Reynolds stress term, next is to express the Reynolds stresses in terms of the Prandtl mixing length, which is a characteristic length scale used in turbulence modeling. The Prandtl mixing length hypothesis assumes that the Reynolds stresses can be expressed as a function of the distance from the wall, typically represented by the mixing length *l*.

The Prandtl mixing length hypothesis states that the Reynolds stress components can be expressed as:

$$\rho\overline{u_{i'}u_{j'}}=-\rho l^2\frac{\partial\overline{u_i}}{\partial x_j}. \tag{3.134}$$

At this stage further assumption is taken:

a) for $x_j > 3$ we neglect the viscous term in the shear stress,

b) $l = kx_j$ where k is the von Karman constant, sometimes referred to as the Karman constant, finally have:

$$\rho\overline{u_i u_j} = -\rho k^2 x_j^2 (\frac{\partial U_i}{\partial x_j})^2 \tag{3.135}$$

Hence:

$$\overline{u_i u_j} = -k^2 x_j^2 (\frac{\partial U_i}{\partial x_j})^2 \tag{3.136}$$

From (3.135) we deduce that:

$$\overline{u_\theta u_r} = -k^2 r^2 (\frac{\partial U_\theta}{\partial r})^2 \qquad (3.137)$$

$$\overline{u_z u_r} = -k^2 r^2 (\frac{\partial u_z}{\partial r})^2 \qquad (3.138)$$

Where *l* is the Prandtl mixing length, and x_j represents the coordinate direction.

Assuming that the Reynolds stress components $\overline{U_{r'} U_{\theta'}}$ and $\overline{U_{\theta'} U_{r'}}$ are proportional to the derivative of the mean velocity $\overline{U_r}$ with respect to the radial direction, as per the Prandtl mixing length hypothesis. Now, substituting this form of the Reynolds stress term back into the equation: Now (3.124) under (3.138) becomes:

$$\frac{\partial U_z}{\partial t} + \frac{1}{U_0}\overline{U}_r^*\frac{\partial U_z}{\partial r} = v\left(\frac{1}{v}\frac{\partial^2 U_z}{\partial r^2} + \frac{1}{r^*}\frac{1}{U_0}\frac{\partial U_z}{\partial r}\right) - v\left[\frac{1}{U_0^3 r^*}\frac{\partial}{\partial r^*}(-k^2 r^2 \left(\frac{\partial u_z}{\partial r}\right)^2)\right] + \frac{Gr}{Re^2 Pr} + \frac{M^2(\overline{U}_z^* + m\overline{U}_\theta^*)}{U_0(1+m^2)} \qquad (3.139)$$

Likewise, (3.127) under (3.132) yields:

$$\frac{\partial U_\theta}{\partial t} + \overline{U_r^*}\frac{1}{U_0}\frac{\partial U_\theta}{\partial r} = \frac{\partial^2 U_\theta}{\partial r^2} + \frac{1}{r^*}\frac{v}{U_0}\frac{\partial U_\theta}{\partial r} - v^2\frac{\overline{U_\theta^*}}{U_0^3 r^{*2}} - \frac{\rho v}{U_0^3}\frac{\partial}{\partial r^*}\left(-\rho l^2\frac{\partial \overline{U_r}}{\partial r^*}\right) - \frac{2\rho v}{U_0^3 r^*}\left(-\rho l^2\frac{\partial \overline{U_r}}{\partial r^*}\right) + \frac{M^2\left(m\overline{U_z^*} - \overline{U_\theta^*}\right)}{U_0(1+m^2)} \qquad (3.140)$$

Equations (1.139), (1.140) and (3.130) in cylindrical coordinates respectively simplifies to:

$$\frac{\partial U_z}{\partial t} + \frac{1}{U_0}\overline{U}_r^*\frac{\partial U_z}{\partial r} = v\left(\frac{1}{v}\frac{\partial^2 U_z}{\partial r^2} + \frac{1}{r^*}\frac{1}{U_0}\frac{\partial U_z}{\partial r}\right) - v\left[\frac{1}{U_0^3 r^*}\frac{\partial}{\partial r^*}(-k^2 r^2 \left(\frac{\partial u_z}{\partial r}\right)^2)\right] + \frac{Gr}{Re^2 Pr} + \frac{M^2(\overline{U}_z^* + m\overline{U}_\theta^*)}{U_0(1+m^2)} \qquad (3.141)$$

$$\frac{\partial U_\theta}{\partial t} + \overline{U_r^*}\frac{1}{U_0}\frac{\partial U_\theta}{\partial r} = \frac{\partial^2 U_\theta}{\partial r^2} + \frac{1}{r^*}\frac{v}{U_0}\frac{\partial U_\theta}{\partial r} - v^2\frac{\overline{U_\theta^*}}{U_0^3 r^{*2}} - \frac{\rho v}{U_0^3}\frac{\partial}{\partial r^*}\left(-\rho l^2\frac{\partial \overline{U_r}}{\partial r^*}\right) - \frac{2\rho v}{U_0^3 r^*}\left(-\rho l^2\frac{\partial \overline{U_r}}{\partial r^*}\right) + \frac{M^2\left(m\overline{U_z^*} - \overline{U_\theta^*}\right)}{U_0(1+m^2)} \qquad (3.142)$$

$$\frac{\partial \theta^*}{\partial t^*} = \frac{1}{RePr}\left(\frac{\partial^2 \theta^*}{\partial r^{*2}} + \frac{1}{r^{*2}} - \frac{\bar{u}_r^*}{r^*}\frac{\partial \theta^*}{\partial r^*} - \frac{1}{Pr}\frac{\bar{U}_{r'}^*\theta'^*}{\partial r^*}\right) \tag{3.143}$$

With the Reynolds stresses resolved next is to seek a numerical solution of equations (3.141), (3.142) and (3.143) subject to the boundary and initial conditions below:

3.9 Boundary and Initial Conditions

From equation (3.112) the non-dimensional form of (3.95) becomes:

$$t < 0 : U_z = 0, U_\theta = 0, \theta = 0 \; everywhere \tag{3.144}$$

$$t \geq 0 : U_z = 1, U_\theta = 0, \theta = 1 \text{ at } r = \frac{1}{2} \tag{3.145}$$

$$U_z \to 0, U_\theta \to 0, \theta \to 0 \text{ as } r \to \infty \tag{3.146}$$

The need to solve equations (3.141), (3.142) and (3.143), subject to equations (3.144), (3.145) and (3.146). However, the solution of these equations is not currently possible due to the Reynolds stress terms. These terms were first resolved so as to be able to work out the approximate solution of these equations by a direct numerical method. The momentum equations are resolved using Prandtl mixing length hypothesis. The Reynolds stresses in the energy conservation equation are computed in terms of Turbulent Prandtl number and Prandtl mixing length hypothesis. Thus equations (3.141) — (3.143) become:

$$\frac{\partial U_z}{\partial t} + \frac{1}{U_0}\bar{U}_r^*\frac{\partial U_z}{\partial r} = v\left(\frac{1}{v}\frac{\partial^2 U_z}{\partial r^2} + \frac{1}{r^*}\frac{1}{U_0}\frac{\partial U_z}{\partial r}\right) - v\left[\frac{1}{U_0^3 r^*}\frac{\partial}{\partial r^*}(-k^2 r^2\left(\frac{\partial u_z}{\partial r}\right)^2)\right] +$$

$$\frac{Gr}{Re^2 Pr} + \frac{M^2(\bar{U}_z^* + m\bar{U}_\theta^*)}{U_0(1+m^2)} \tag{3.147}$$

$$\frac{\partial U_\theta}{\partial t} + \overline{U_r^*}\frac{1}{U_0}\frac{\partial U_\theta}{\partial r} = \frac{\partial^2 U_\theta}{\partial r^2} + \frac{1}{r^*}\frac{v}{U_0}\frac{\partial U_\theta}{\partial r} - v^2\frac{\overline{U_\theta^*}}{U_0^3 r^{*2}} - \frac{\rho v}{U_0^3}\frac{\partial}{\partial r^*}\left(-\rho l^2\frac{\partial \overline{U_r}}{\partial r^*}\right) -$$

$$\frac{2\rho v}{U_0^3 r^*}\left(-\rho l^2\frac{\partial \overline{U_r}}{\partial r^*}\right) + \frac{M^2\left(m\overline{U_z^*} - \overline{U_\theta^*}\right)}{U_0(1+m^2)} \tag{3.148}$$

$$\frac{\partial\theta^{*}}{\partial t^{*}}=\frac{1}{RePr}\left(\frac{\partial^{2}\theta^{*}}{\partial r^{*2}}+\frac{1}{r^{*2}}-\frac{\bar{u}_{r}^{*}}{r^{*}}\frac{\partial\theta^{*}}{\partial r^{*}}-\frac{1}{Pr}\frac{\bar{U}_{r'}^{*}\theta'^{*}}{\partial r^{*}}\right) \tag{3.149}$$

$$t < 0: U_z = 0, U_\theta = 0, \theta = 0, everywhere \tag{3.150}$$

$$t \geq 0: U_z = 1, U_\theta = 0, \theta = 1, \text{ at } r = \frac{1}{2} \tag{3.151}$$

$$U_z \to 0, U_\theta \to 0, \theta \to 0, \text{ as } r \to \infty \tag{3.152}$$

3.10 Finite Difference Scheme

Considering that the systems of partial differential equations (3.147) — (3.149) are highly non-linear their solutions are approximated by finite difference method. In the following finite difference scheme the primary velocity $\overline{U_z}$ is denoted by U and the secondary velocity $\overline{U_\theta}$ is denoted by V to reduce the subscripts as i and j are used as subscripts, i corresponding to r as j corresponds to t.

Time derivative using forward difference:

$$\frac{\partial U}{\partial t}\approx\frac{U_{i}^{n+1}-U_{i}^{n}}{\Delta t} \tag{3.153}$$

First spatial derivative using central difference:

$$\frac{\partial U}{\partial r}\approx\frac{U^{n}_{i+1}-U^{n}_{i-1}}{2\Delta r} \tag{3.154}$$

Second spatial derivative using central difference:

$$\frac{\partial^{2}U}{\partial r^{2}}\approx\frac{U^{n}_{i+1}-2U^{n}_{i}+U^{n}_{i-1}}{\Delta r^{2}} \tag{3.155}$$

Where i and j refer to r and t respectively. r have been substituted with $i\Delta r$ .The equivalent finite difference scheme for equation (3.147) — (3.149) are respectively:

$$\frac{U_i^{n+1}-U^n{}_i}{\Delta t}+\frac{1}{U_0}\overline{U_r^*}\frac{U^n{}_{i+1}-U^n{}_{i-1}}{2\Delta r}=\nu\left(\frac{U^n{}_{i+1}-2U^n{}_i+U^n{}_{i-1}}{\Delta r^2}+\frac{1}{r^*}\frac{1}{U_0}\frac{U^n{}_{i+1}-U^n{}_{i-1}}{2\Delta r}\right)+\frac{Gr}{Re^2Pr}+\frac{M^2(\overline{U^*}+m\overline{V^*})}{U_0(1+m^2)}$$

(3.156)

$$U_{(i,j+1)}=U_{(i,j)}+\Delta t\left(\frac{U_{(i+1,J)}-2U_{(i,j)}+U_{(i-1,J)}}{(\Delta r)^2}+\frac{1}{i\Delta r}\frac{U_{(i+1,J)}-U_{(i,J)}}{\Delta r}\right)+$$

$$k^2 i(\Delta r)(\Delta t)\left(\frac{U_{(i+1,j)}-U_{(i,j)}}{\Delta r}\right)^2+\Delta t\left\{\frac{Gr}{Re^2Pr}+M^2\frac{(U_{(i,j)}+mV_{(i,j)})}{U_0(1+m^2)}\right\} \quad (3.157)$$

Forward Difference for Time Derivative:

$$\frac{\partial V}{\partial t}\Big|_i^n\approx\frac{V_i^{n+1}-V_i^n}{\Delta t} \quad (3.158)$$

Central Difference for First Derivative in Space:

$$\frac{\partial V}{\partial r}\Big|_i^n\approx\frac{V_{i+1}^n-V_{i-1}^n}{2\Delta r} \quad (3.159)$$

Central Difference for Second Derivative in Space:

$$\frac{\partial^2 V}{\partial r^2}\Big|_i^n\approx\frac{V_{i+1}^n-2V_i^n+V_{i-1}^n}{\Delta r^2} \quad (3.160)$$

$$\frac{V_i^{n+1}-V_i^n}{\Delta t}+\frac{\overline{U_r^*}}{U}\frac{V_{i+1}^n-V_{i-1}^n}{2\Delta r}=\frac{V_{i+1}^n-2V_i^n+V_{i-1}^n}{\Delta r^2}+\frac{v}{r^*U}\frac{V_{i+1}^n-U_{i-1}^n}{2\Delta r}-\frac{M^2(m\overline{U^*}-\overline{V^*})}{U_0(1+m^2)} \quad (3.161)$$

$$V_{(i,j+1)}=V_{(i,j)}+\Delta t\left(\frac{V_{(i+1,J)}-2V_{(i,J)}+V_{(i-1,J)}}{(\Delta r)^2}+\frac{1}{i\Delta r}\frac{V_{(i+1J)}-V_{(i,J)}}{\Delta r}-\frac{V_{(i,J)}}{(i\Delta r)^2}\right)+$$

$$2k^2(i\Delta r)^2(\Delta t)\left(\frac{V_{(i+1,j)}-V_{(i,j)}}{\Delta r}\right)\left(\frac{V_{(i+1,j)}-2V_{(i,j)}+V_{(i-1,j)}}{(\Delta r)^2}\right)-\Delta t M^2\frac{(mU_{(i,j)}-V_{(i,j)})}{U_0(1+m^2)} \quad (3.162)$$

Assume a uniform grid in * with grid points r_i^* such that $r_i^*=i\Delta r$, where Δr is the spacing between grid points and $i=0,1,2,\ldots,N$.

The time derivative will be approximated using a forward difference.

$$\frac{\partial \theta^*}{\partial t^*} \approx \frac{\theta_i^{n+1} - \theta_i^n}{\Delta t} \tag{3.163}$$

where θ_i^n is the value of θ^* at position i and time step n, and Δt is the time step size.

Second spatial derivative :

$$\frac{\partial^2 \theta^*}{\partial (r^*)^2} \approx \frac{\theta_{i+1}^n - 2\theta_i^n + \theta_{i-1}^n}{(\Delta r)^2} \tag{3.164}$$

First spatial derivative using central difference:

$$\frac{\partial \theta^*}{\partial r^*} \approx \frac{\theta_{i+1}^n - \theta_{i-1}^n}{2\Delta r} \tag{3.165}$$

Term involving fluctuations:

$$\frac{\overline{U}_{r'}^* \theta'^*}{\partial r^*} \approx \frac{\overline{U}_{r'}^* \theta'^*}{\Delta r} \text{ at } r_i^* \tag{3.166}$$

Finite Difference Equation Substituting these approximations into the PDE, we get:

$$\frac{\theta_i^{n+1} - \theta_i^n}{\Delta t} = \frac{1}{RePr}\left(\frac{\theta_{i+1}^n - 2\theta_i^n + \theta_{i-1}^n}{(\Delta r)^2} + \frac{1}{(r_i^*)^2} - \frac{\overline{u}_r^*}{r_i^*}\frac{\theta_{i+1}^n - \theta_{i-1}^n}{2\Delta r} - \frac{1}{Pr}\frac{\overline{U}_{r'}^* \theta'^*}{\Delta r} \right) \tag{3.167}$$

Rearranging for θ_i^{n+1} Solving for θ_i^{n+1}, we express the future state in terms of the current and neighboring states:

$$\theta_i^{n+1} = \theta_i^n + \Delta t\left[\frac{1}{RePr}\left(\frac{\theta_{i+1}^n - 2\theta_i^n + \theta_{i-1}^n}{(\Delta r)^2} + \frac{1}{(r_i^*)^2} - \frac{\overline{u}_r^*}{r_i^*}\frac{\theta_{i+1}^n - \theta_{i-1}^n}{2\Delta r} - \frac{1}{Pr}\frac{\overline{U}_{r'}^* \theta'^*}{\Delta r} \right)\right] \tag{3.168}$$

This scheme can now be used to step forward in time iteratively. Note that this discretization is first-order accurate in time and second-order in space. Stability and convergence of this scheme will be analyzed based on the specific values of Re, Pr, Δr, Δt, and other parameters.

$$\theta_{(i,j+1)} = \theta_{(i,j)} + \frac{\Delta t}{RePr}\left(\frac{\theta_{(i+1,j)} - 2\theta_{(i,j)} + \theta_{(i-1,j)}}{(\Delta r)^2} + \frac{1}{i\Delta r}\frac{\theta_{(i+1,j)} - \theta_{(i,j)}}{\Delta r}\right) +$$

$$\frac{k^2(\Delta t)(i\Delta r)^2}{RePr^2}\left(\frac{U_{(i+1,j)} - U_{(i,j)}}{\Delta r}\right)\left(\frac{\theta_{(i+1,j)} - \theta_{(i,j)}}{\Delta r}\right)$$

(3.169)

The boundary and initial conditions take the form:

$j < 0: U_{(i,j)} = 0, V_{(i,j)} = 0, \theta_{(i,j)} = 0$, everywhere (3.170)

$j \geq 0: U_{(i,j)} = 1, V(i,j) = 0, \theta_{(i,j)} = 1$, at $i = \frac{\mathrm{Re}}{2}$ (3.171)

$U_{(i,j)} \to 0, V_{(i,j)} \to 0, \theta_{(i,j)} \to 0$, as $i \to \infty$ (3.172)

Using the boundary and initial conditions we determine the values for consecutive grid points for primary velocity, secondary velocities, and temperature that is $U_{(i,j+1)}, V_{(i,j+1)}$ and $\theta_{(i,j+1)}$ in component form.

The approximate solution was computed using a computer program and the results are displayed in graphs as shown in figures 4.1,4.2 4.3,4.4,4.5,4.6, and 4.7

CHAPTER FOUR

RESULTS AND DISCUSSION

4.1 Introduction

In this chapter we present the numerical results obtained upon employing the program mentioned in section 3.6. The trends observed upon varying various fluid properties are discussed and explained. Mathematical modeling of porous aerofoil using Navier Stokes equations was done and numerical simulations of the formulated mathematical problem were carried out using FEATOOL to verify the analytic results on the system of equations presented in Chapter Three. CFD investigation consisted of three stages. Starting from pre-processing stage where 3-D geometry of porous wing model was drawn using ANSYS Design Modular and the grids were generated by OPENFOAM-CFD. The second stage was simulation by FLUENT solver using Finite Volume Approach. Finally, third step was the post-processing stage; in which the aerodynamic characteristics like Drag coefficient (CD), Lift coefficient (CL) and Lift-to-Drag ratio (L/D) were defined at the various angle of attack for porous wing.

4.2 Primary Velocity Profiles

Since the problem has been non-dimensionalized, there is no justification for any particular choice of the default values of the fluid properties. Of interest is how changes in these properties affect the flow variables. The results of the simulation show the airflow velocity distribution in each airfoil that is affected by the angle of attack. With the variation of the attack angle 0^0, 2^0, 4^0, 6^0 and 8^0, it is concluded that, the larger the angle of attack, the maximum air velocity distribution in each airfoil tends to increase

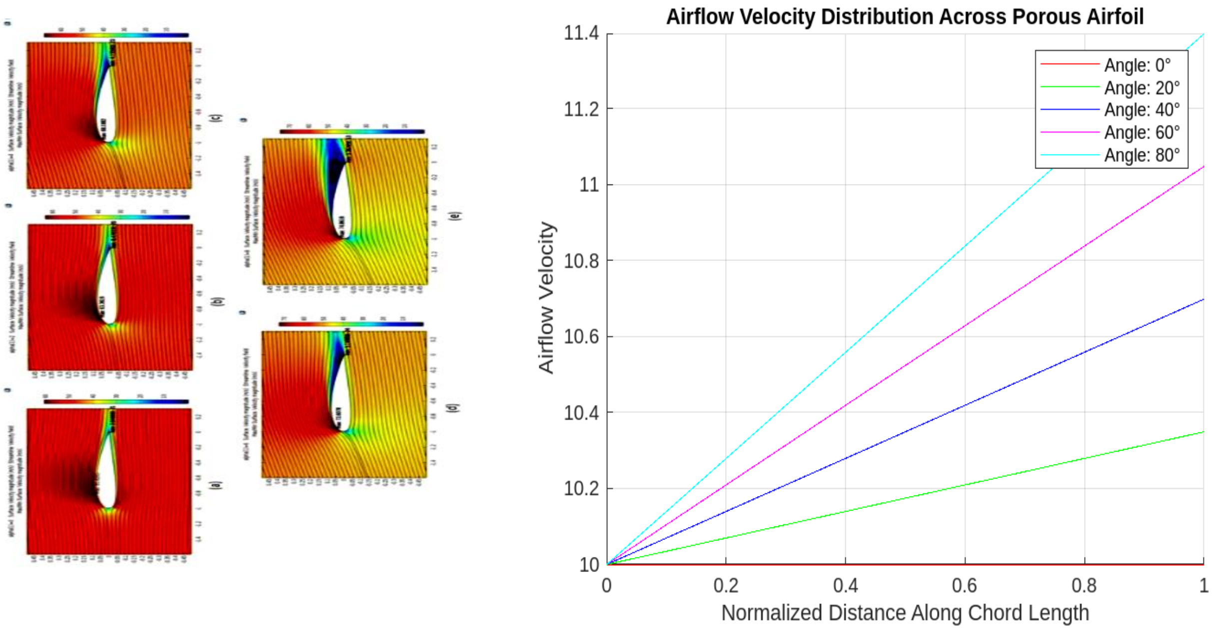

Figure 4.1: *Airflow around the NACA Airfoil 2412 at the Angle of attack 0, Angle of attack 20, Angle of attack 40, Angle of attack 60 and Angle of attack 80.*

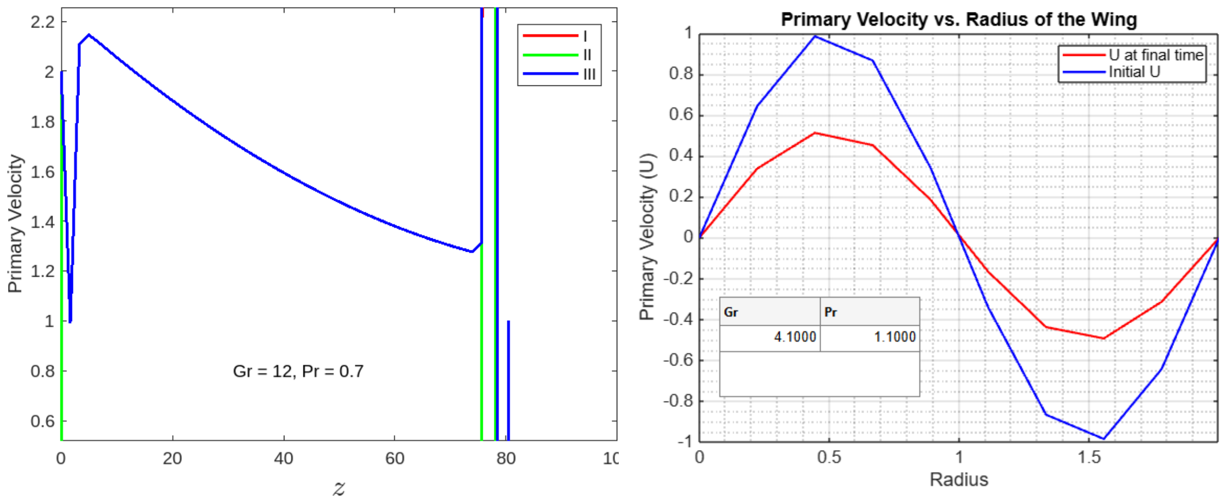

Figure 4.2: *Primary velocity profiles within a moving porous aerofoil wing*

From figure 4.2 it is noted that:

(i) Primary velocity is not affected by magnetic parameter and Hall parameter.

(ii) There is an increase in primary velocity profiles when Grashof number and time parameter are increased.

(iii) There is no change in primary velocity when Prandtl number is varied.

4.3 Secondary Velocity Profiles

Figures 4.3 illustrate the effects of parameter variation on the secondary mean velocity component

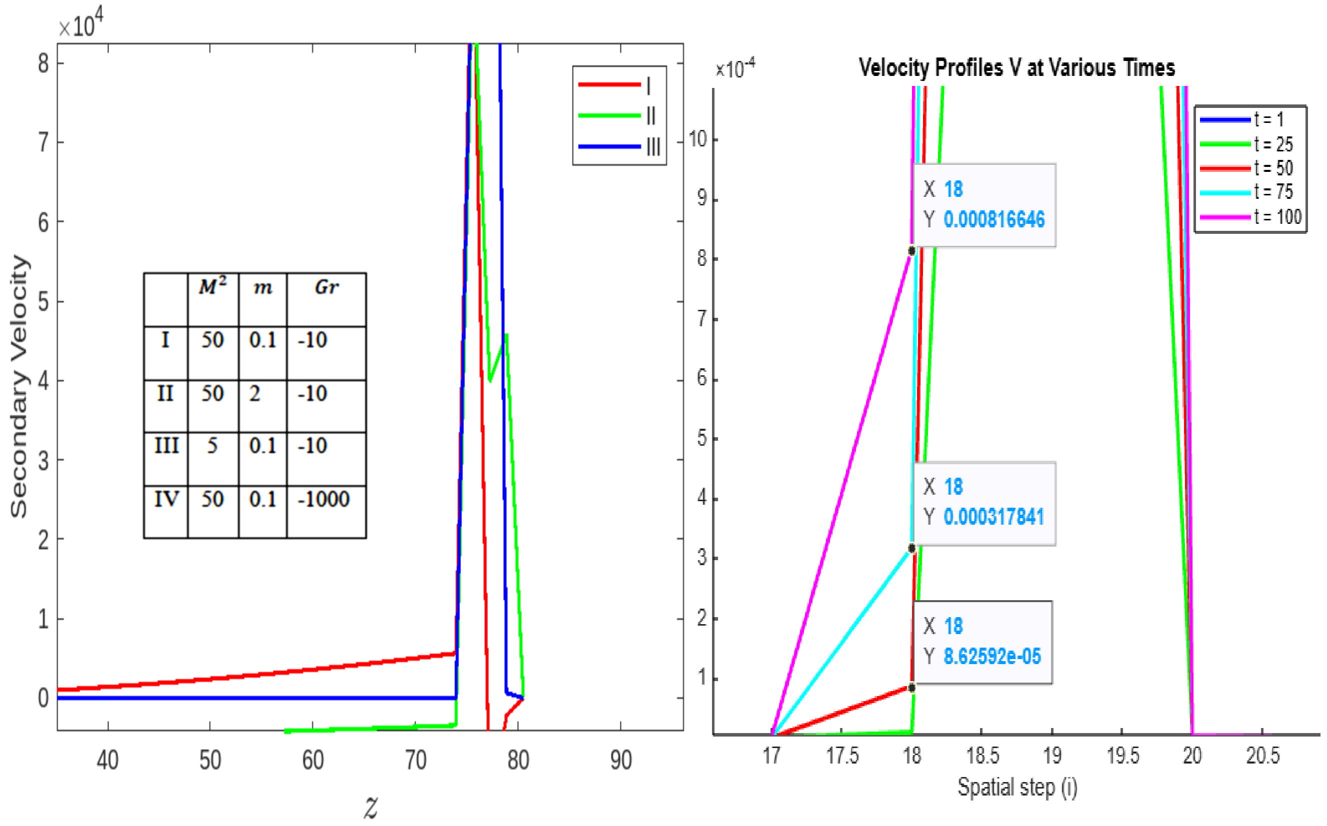

Figure 4.3: *Secondary velocity profiles with cooling of the cylinder*

From figure 4.3 it is noted that:

(i) The secondary velocity profiles increase in magnitude with increase in time parameter and magnetic parameter.

(ii) Variation in Grashof number does not affect secondary velocity profiles

(iii) There is no variation in velocity profiles with variation in Prandtl.

(iv) There is decrease in the secondary velocity profiles with increase in Hall parameter.

4.4 Temperature Profiles

The influence of different physical parameters like Grashof number, magnetic parameter, thermal radiation, Prandtl number, Eckert number, Soret number and Schmidt number on velocity, temperature and concentration is discussed by using graphical representations.

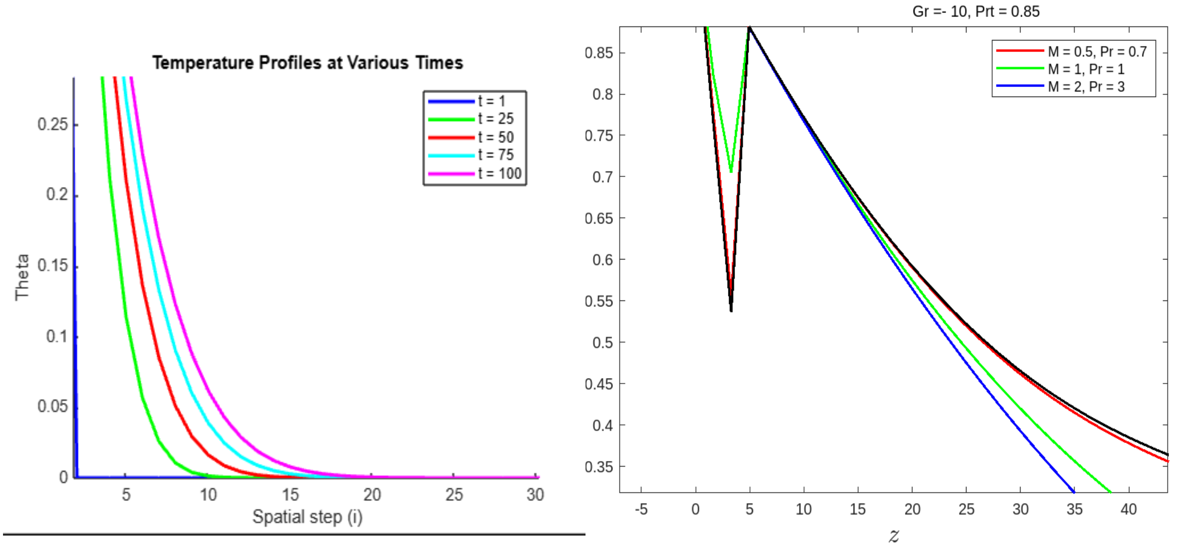

Figure 4.4: *Temperature profiles*

From figure 4.4 it is noted that:

(i) There is no observable variation in temperature profiles with variation in magnetic parameter and Hall parameter.

(ii) There is increase in temperature profiles with increase in time parameter.

(iii) There is decrease in temperature profiles with increase in Grashof number.

(iv) Increase in Prandtl number leads to decrease in temperature profiles.

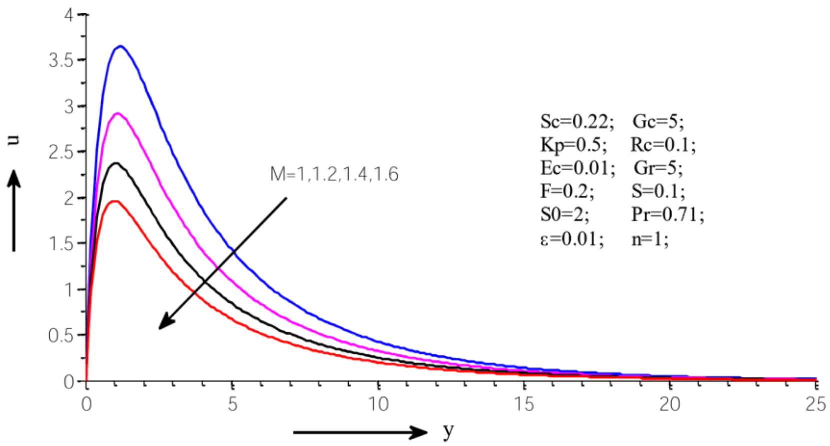

Figure 4.5: *Effect of magnetic parameter on velocity*

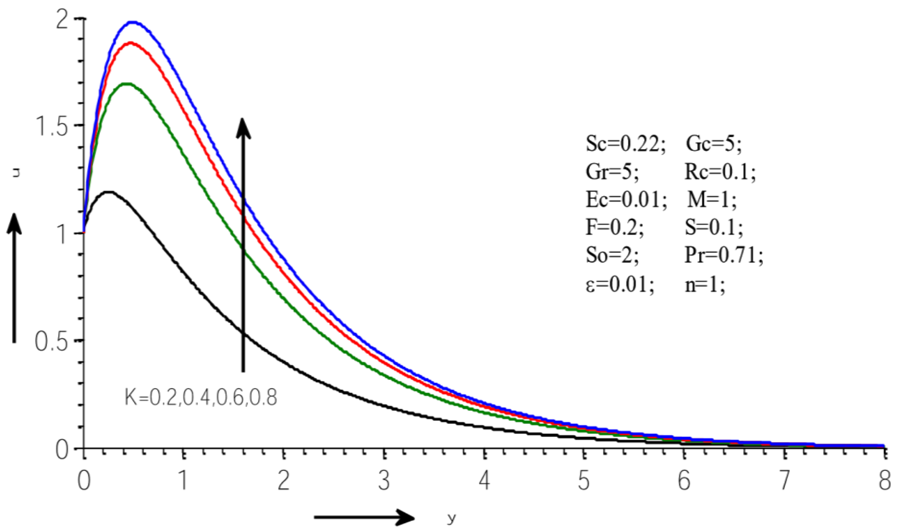

Figure 4.6: *Effect of Eckert number on temperature*

Velocity of the fluid reduces for increasing values of Prandtl number and magnetic parameter. Temperature of the fluid grows for rising values of Eckert number, but a reverse effect is noticed in the case of Prandtl number and radiation absorption parameter. Skin friction decreases with an increase of Eckert number and Schmidt number but a reverse effect is noticed in the case of radiation absorption parameter and magnetic parameter.

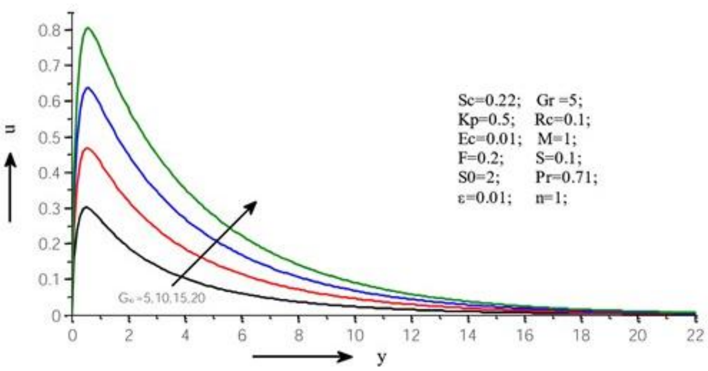

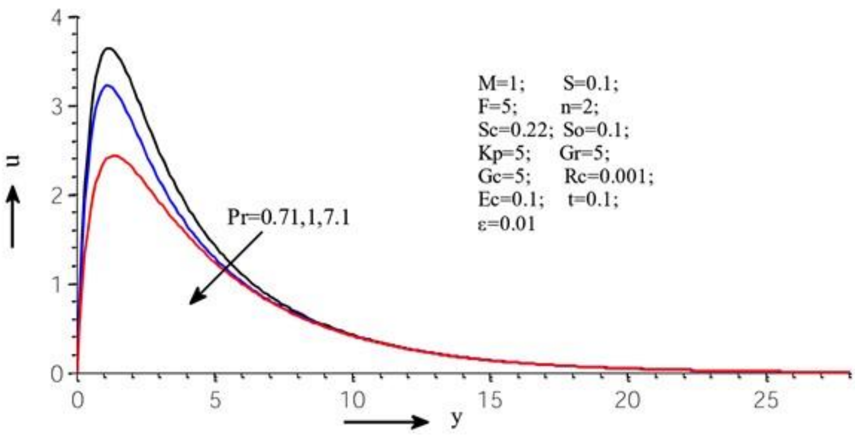

Figure 4.7: *Effect of Prandtl and Grashof number on velocity*

CHAPTER FIVE

SUMMARY, CONCLUSIONS AND RECOMMENDATIONS

5.1 Introduction

This chapter provides a comprehensive summary of the research findings, draws conclusive interpretations of the results obtained from the numerical simulations, and puts forward relevant recommendations for further research. The study investigated the behavior of magnetohydrodynamic (MHD) turbulent fluid flow over a porous aerofoil wing design subjected to an external magnetic field. With the increasing use of porous surfaces in aerospace design, particularly in high-magnetic-field environments such as near the Earth's poles or in space, understanding the complex interplay of forces influencing fluid behavior in such systems is of significant practical importance. This chapter ties together the objectives of the study, the insights gained, and avenues for future exploration.

5.2 Summary

The study applied a numerical approach to analyze how variations in specific flow parameters namely the magnetic parameter (M), Hall parameter, Grashof number (Gr), and Prandtl number (Pr) influence the velocity and temperature profiles in a magnetohydrodynamic turbulent flow environment. The wing was modeled as a porous medium to reflect modern aerofoil designs that enhance cooling, drag reduction, and control over turbulent boundary layers.

Key observations include:

i) Primary Velocity Profiles: An increase in the Grashof number, which reflects the buoyancy force due to temperature differences, led to a notable increase in primary velocity. This is expected, as greater thermal gradients enhance fluid motion. The Hall parameter, representing the Hall current effect in the presence of magnetic fields, showed negligible influence on primary velocity. This suggests that the Lorentz force components due to Hall currents predominantly affect secondary flows.

ii) Secondary Velocity Profiles: Secondary velocity decreased as the Hall parameter increased. This implies that enhanced Hall currents may divert momentum from transverse (secondary) flow components. No significant changes were observed in secondary velocity profiles with varying Grashof numbers, indicating that buoyancy effects are largely aligned with the direction of primary flow.

iii) Temperature Profiles: The temperature distribution remained mostly unaffected by changes in magnetic and Hall parameters, implying that the thermal boundary layer is more influenced by thermal properties of the fluid and not significantly altered by electromagnetic interactions. However, the Prandtl number, which defines the ratio of momentum diffusivity to thermal diffusivity, had a significant effect. As Prandtl number decreased, the thermal boundary layer thickened, leading to a more gradual temperature gradient. These findings collectively demonstrate how the behavior of electrically conducting fluids over porous surfaces can be strategically manipulated by tuning certain parameters, which is critical in aero-thermal system design.

5.3 Conclusions

The magnetohydrodynamic turbulent fluid flow over a porous aerofoil wing design within a magnetic field has been numerically investigated. The effects of various flow parameters on the mean velocities and mean temperature were obtained. Variation of Prandtl number significantly varied the temperature profile while it had no observable effect on the velocity profiles. It was found that the primary velocity increases with decreasing magnetic parameter (M), increases with increase in Hall parameter and also increases with increase in Grashoff number. The secondary velocity increases with decreasing magnetic parameter (M), decreases with increasing Hall parameter and the change in Grashoff number as no effect. It was also found that the temperature profile decreases with decreasing magnetic Parameter (M), decreases with increasing Hall parameter and increases with decrease in Prandtl number.

This investigation has successfully addressed the primary objective of analyzing the influence of magnetic and thermal parameters on the flow and heat transfer characteristics of a hydromagnetic turbulent fluid over a porous aerofoil.

The conclusions of the study are :

A decrease in the magnetic parameter resulted in increased primary and secondary velocity profiles. This is due to a reduction in the Lorentz force, which generally acts to dampen fluid motion. Conversely, temperature profiles exhibited a declining trend with decreasing magnetic parameter, suggesting that magnetic fields provide a resistance not just to fluid motion but also to heat transport.

The Hall effect had a dual nature: while it enhanced primary flow velocities, it suppressed secondary flow development. This supports the understanding that Hall currents introduce anisotropy in the current distribution, thereby modifying flow structures.

Temperature profiles tended to decline with increasing Hall parameter, albeit slightly, likely due to altered convective heat transport paths.

The Grashof number significantly increased the primary velocity, highlighting its dominant role in buoyancy-driven flow enhancement. It did not impact secondary velocity or temperature profiles to a significant degree.

Lower Prandtl numbers increased the thermal boundary layer thickness and led to higher temperatures throughout the flow domain. Velocity profiles remained largely unchanged with varying Prandtl numbers, reinforcing the decoupling between thermal and momentum diffusivity in such regimes.

Overall, the study has demonstrated that manipulating specific physical parameters can effectively control fluid motion and heat transport in hydromagnetic systems. These insights are particularly useful in aerospace engineering, energy systems, and cooling technologies for electronic devices operating under magnetic fields.

5.4 Recommendations

Although the study has successfully modeled and analyzed key features of MHD fluid flow over a porous aerofoil, certain limitations remain, primarily due to the simplifications made during numerical modeling. To bridge these gaps and enhance real-world applicability, the following recommendations are proposed:

Consideration of Compressibility: Real fluid flows, especially at high speeds in aerospace applications, are often compressible. Future work should include compressible fluid dynamics to better reflect operational conditions.

5.5 Suggestions for Further Research

To further broaden the scope and depth of understanding in this field, the following areas are suggested for future exploration:

Non-Newtonian Fluid Behavior: Investigating MHD flow with non-Newtonian fluids would simulate scenarios in advanced materials or biological flows where viscosity is not constant.

Inclined Magnetic Fields: This study assumed a uniform magnetic field aligned perpendicularly. Investigating magnetic fields at various angles could reveal more complex interactions and control strategies.

Rotational Effects: Incorporating rotational effects such as a spinning wing or rotating plate will simulate real aerofoil dynamics more accurately, especially in applications involving propulsion or atmospheric turbulence.

Three-Dimensional Flow Modeling: Extending the model from two-dimensional to three-dimensional flow analysis would capture vortices and cross-sectional behaviors, leading to more accurate simulations.

Transient Flow Analysis: This study focused on steady-state conditions. A transient (time-dependent) analysis would help understand dynamic behaviors and system responses to parameter changes.

Nano-fluid Incorporation: Use of nano-fluids (fluids embedded with nanoparticles) in MHD systems can significantly enhance thermal conductivity and may improve cooling and control mechanisms.

REFERENCES

Ahmed, T. (2013). Computational study of flow around a NACA 0012 wing flapped at different flap angles with varying Mach numbers. *Global Journals of Research in Engineering*, *13*(J4), 5-15.

Aldheeb, M. A., Asrar, W., Sulaeman, E., & Omar, A. A. (2016). A review on aerodynamics of non-flapping bird wings. *Journal of Aerospace Technology and Management*, *8*(1), 7–17.

Alsahlan, A., & Abdulkarim, T. (2017). Aerofoil design for unmanned high-altitude aft-swept flying wings. *Journal of Aerospace Technology and Management*, *9*, 335–345.

Amrit, A., Leifsson, L., & Koziel, S. (2018). Multi-fidelity aerodynamic design trade-off exploration using point-by-point Pareto set identification. *Aerospace Science and Technology*, *79*, 399–412.

Argyropoulos, C. D., & Markatos, N. C. (2015). Recent advances on the numerical modelling of turbulent flows. *Applied Mathematical Modelling*, *39*(2), 693-732.

Ayton, L. J., & Chaitanya, P. (2019). An analytical and experimental investigation of aerofoil–turbulence interaction noise for plates with spanwise-varying leading edges. *Journal of Fluid Mechanics*, *865*, 137–168.

Blakey-Milner, B., Gradl, P., Snedden, G., Brooks, M., Pitot, J., Lopez, E., ... & du Plessis, A. (2021). Metal additive manufacturing in aerospace: A review. *Materials & Design*, *209*, 110008.

Bronshtein, I. N., Semendyayev, K. A., & Musiol, G. (2015). Handbook of mathematics (6th ed.).

Chaudhary, R., & Jain, A. (2007). Combined heat and mass transfer effects on MHD free convection flow past an oscillating plate embedded in porous medium. *Romanian Journal of Physics*, *52*(5), 505–524.

Chebos, C., Sigey, J., Okelo, J., Okwoyo, J., & Giterere, K. (2016). Numerical investigation of unsteady MHD free convective flow past an oscillating vertical porous plate with oscillatory heat flux. *The SIJ Transactions on Computer Networks & Communication Engineering*, *04*(01), 01–09.

Chen, L., & Zonca, F. (2016). Physics of Alfvén waves and energetic particles in burning plasmas. *Reviews of Modern Physics*, *88*(1),1–12.

Domínguez, I., & Burguete, J. (2018). Instabilities triggered in different conducting fluid geometries due to slowly time-dependent magnetic fields. *Chaos: An Interdisciplinary Journal of Nonlinear Science*, *28*(7), 075514.

Fan, T. O. N. G., Weiyang, Q. I. A. O., Weijie, C. H. E. N., Cheng, H., Renke, W. E. I., & Xunnian, W. A. N. G. (2018). Numerical analysis of broadband noise reduction with wavy leading edge. *Chinese Journal of Aeronautics*, *31*(7), 1489-1505.

Foias, C., Manley, O., Rosa, R., & Temam, R. (2001). *Navier-Stokes equations and turbulence* (Vol. 83). Cambridge University Press, 1-23.

Frost, W. (2013). *Heat transfer at low temperatures*. Springer Science & Business Media.

Gaffar, S., Abdul, V. R., & Prasad, E. K. (2017). Computational study of Jeffrey's non-Newtonian fluid past a semi-infinite vertical plate with thermal radiation and heat generation/absorption. *Ain Shams Engineering Journal*, *8*, 277–294.

Goldstein, M. E. (2014). Effect of free-stream turbulence on boundary layer transition. *Philosophical Transactions of the Royal Society A: Mathematical, Physical and Engineering Sciences*, *372*(2020), 20130354.

Jithendra, S. R. C., Satyanarayana, K. V. V., Varun Kumar, G., Mahboob, S., & Bhaskar, A. (2020). Flow variation on naca 6412 aerofoil with surface modifications. I-Manager's. *Journal on Mechanical Engineering*, *10*(3), 1-7.

Johnson, O. B., & Oluwaseun, L. I. (2020). Crank-Nicolson and modified Crank-Nicolson scheme for one dimensional parabolic equation. *International Journal of Applied Mathematics and Theoretical Physics*, *6*(3), 35-40.

Jordán, J. Z. (2006). Numerical study of an unsteady free convective magnetohydrodynamic flow of a dissipative fluid along a vertical plate subject to a constant heat flux. *International Journal of Engineering Science*, *44*(18–19), 1380–1393.

Joshi, S. N., & Gujarathi, Y. S. (2016). A review on active and passive flow control techniques. *International Journal on Recent Technologies in Mechanical and Electrical Engineering*, *3*(4), 1–6.

Jha, B., & Aina, B. (2018). Impact of induced magnetic field on magnetohydrodynamic (MHD) natural convection flow in a vertical annular micro-channel in the presence of radial magnetic field. *Propulsion and power research*, *7*(2), 171-181.

Keshri, O. P., Kumar, A., & Gupta, V. K. (2018). Magento-solutal convection in Newtonian fluid layer with solutal modulated boundaries. *International Journal of Non-Linear Mechanics*, *107*, 86–93.

Kim, M. G., Seo, D. C., & Chung, H. T. (2021). A CFD study on flow control of ammonia injection for denitrification processes of SCR systems in coal-fired power plants. *Energies*, *14*(5), 1352.

Klose, B., Jacobs, G. B., Tank, J., & Spedding, G. (2018). Low Reynolds number airfoil aerodynamics: three different flow patterns within an angle of attack range of four degrees. In *2018 Fluid Dynamics Conference* (p. 3731).

Kong, W., Dong, H., Wu, J., Zhao, Y., & Jin, Z. (2022). Experimental Study on the Effect of Porous Media on the Aerodynamic Performance of Airfoils. *Aerospace*, *10*(1), 1-8.

Li, D., Zhao, S., Da Ronch, A., Xiang, J., Drofelnik, J., Li, Y., … Breuker, R. D. (2018). A review of modelling and analysis of morphing wings. *Progress in Aerospace Sciences*, *100*, 46–62.

Li, Q., Maeda, T., Kamada, Y., Murata, J., Kawabata, T., Shimizu, K., … Kasuya, T. (2016). Wind tunnel and numerical study of a straight-bladed Vertical Axis Wind Turbine in three-dimensional analysis (Part II: For predicting flow field and performance). *Energy (Oxford, England)*, *104*, 295–307.

Li, Z., Tang, T., Liu, Y., Arcondoulis, E. J. G., & Yang, Y. (2020). Numerical study of aerodynamic and aeroacoustic characteristics of flow over porous coated cylinders: Effects of porous properties. *Aerospace Science and Technology*, *105*(106042), 106042.

Łukaszewicz, G., & Kalita, P. (2016). Navier–Stokes Equations. *Advances in Mechanics and Mathematics, 34*.

Manda, A. Y., Chada, J. S. R., Surapaneni, S. P., & Geeri, S. (2020). Flow behaviour on aerofoils using CFD. *Journal of Mechanical Engineering, Automation and Control Systems*, *1*(1), 26–36.

Maswai, R. C. (2015). Mhd turbulent flow in presence of inclined magnetic field past a rotating semi-infinite plate.

Mukuna, W. O., Kwanza, J., Sigey, J., & Okello, J. A. (2017). Analysis of heat and mass transfer rates of hydromagnetic turbulent fluid flow over an immersed infinite horizontal cylinder with Hall current. *Journal of Engineering Research and Technology*, *3*(13), 207–212.

Pandit, A. R. (2015). Magneto-hydrodynamics (MHD) generation. In *National Conference on Recent Research in Engineering and Technology (NCRRET-2015)* ,2348–4470.

Prasath, M. S., & Angelin, I. (2017). Effect of dimples on aircraft wing. *Global Research and Development Journal for Engineering*, *2*(5), 234–242.

Radespiel, R., Burnazzi, M., Casper, M., & Scholz, P. (2016). Active flow control for high lift with steady blowing. *The Aeronautical Journal*, *120*(1223), 171–200.

Rajesh, V., Chamkha, A. J., Bhanumathi, D., & Varma, S. V. K. (2013). Radiation and chemical reaction effects on unsteady mhd free convection flow of a dissipative fluid past an infinite vertical plate with Newtonian heating. *Computational Thermal Sciences An International Journal*, *5*(5), 355–367.

Rasal, S. K., & Katwate, R. R. (2017). Numerical analysis of lift & drag performance of NACA0012 wind turbine aerofoil. *International Research Journal of Engineering and Technology*, *4*(6), 2892–2896.

Rasool, G., Shafiq, A., Hussain, S., Zaydan, M., Wakif, A., Chamkha, A. J., & Bhutta, M. S. (2022). Significance of Rosseland's Radiative Process on Reactive Maxwell Nanofluid Flows over an Isothermally Heated Stretching Sheet in the Presence of Darcy–Forchheimer and Lorentz Forces: Towards a New

Perspective on Buongiorno's Model. *Micromachines*, *13*(3), 368. https://doi.org/10.3390/mi13030368

Rasoulian, M. A., Rasteh, A., Farokhipour, A., Mansoori, Z., Saffar-Avval, M., Haj, A., & Ahmadi, G. (2018). Numerical 3D simulation of developing turbulent stratified gas-liquid flow in curved pipes consisting of entrained particles through this type of flow. *Scientia Iranica*, *25*(6: Special Issue Dedicated to Professor Goodarz Ahmadi), 3243-3257.

Rosti, M. E., Cortelezzi, L., & Quadrio, M. (2015). Direct numerical simulation of turbulent channel flow over porous walls. *Journal of Fluid Mechanics*, *784*, 396–442.

Saraf, A. A. K., Singh, B. M. P., & Chouhanr, C. T. S. (2018). Study of flow separation on airfoil with bump. *International Journal of Applied Engineering Research*, *13*(16), 12868–12872.

Singh, D., Gajghat, R. H., & Manik, M. K. (2019). Experimental investigation to examine the effect of shape and size of dimples at suction surface of aerofoil. *International Journal of Scientific & TechnologyResearch*, *8*(12), 521–534.

Soler, R., Carbonell, M., Ballester, J. L., & Terradas, J. (2013). Alfvén waves in a partially ionized two-fluid plasma. *The Astrophysical Journal*, *767*(2), 171.

Sreejith, B. K., & Sathyabhama, A. (2018). Numerical study on effect of boundary layer trips on aerodynamic performance of E216 airfoil. Engineering science and technology. *An International Journal*, *21*(1), 77–88.

Tamaro, S., Zamponi, R., Ragni, D., Teruna, C., & Schram, C. (2021). Experimental investigation of turbulent coherent structures interacting with a porous airfoil. *Experiments in Fluids*, *62*(5),1-8.

Temam, R. (2001). *Navier-Stokes equations: theory and numerical analysis* (Vol. 343). American Mathematical Society, (1-9)

Teruna, C., Avallone, F., Ragni, D., Rubio-Carpio, A., & Casalino, D. (2021). Numerical analysis of a 3-D printed porous trailing edge for broadband noise reduction. *Journal of Fluid Mechanics*, *926*(A17),1-17.

Tulus, Khairani, C., Marpaung, T. J., & Suriati. (2019). Computational analysis of fluid behaviour around airfoil with Navier-Stokes equation. *Journal of Physics. Conference Series*, *1376*(1), 012003.

Wang, Y., Hao, N. S., Lu, X. Y., Tong, F., & Song, Y. B. (2021). Airfoil self-noise reduction by gradient distributed porous trailing edges. *Journal of Aerospace Engineering*, *34*(6), 04021075.

Wauters, J., & Degroote, J. (2018). On the study of transitional Low-Reynolds number flows over airfoils operating at high angles of attack and their prediction using transitional turbulence models. *Progress in Aerospace Sciences*, *103*, 52–68.

Wood, B. D., He, X., & Apte, S. V. (2020). Modeling turbulent flows in porous media. *Annual Review of Fluid Mechanics*, *52*(1), 171–203.

Wood, E. F., Roundy, J. K., Troy, T. J., van Beek, L. P. H., Bierkens, M. F. P., Blyth, E., … Whitehead, P. (2011). Hyperresolution global land surface modeling: Meeting a grand challenge for monitoring Earth's terrestrial water. *Water Resources Research*, *47*(5), 1-10.

Yasuda, T., Fukui, K., Matsuo, K., Minagawa, H., & Kurimoto, R. (2019). Effect of the Reynolds number on the performance of a NACA0012 wing with leading edge protuberance at low Reynolds numbers. *Flow Turbulence and Combustion*, *102*(2), 435–455.

Zaheer, Z., Roy, K. E. R., Nair, G. S., Ragipathi, V., & Niranjan, U. V. (2019). CFD analysis of the performance of different airfoils in ground effect. *Journal of Physics. Conference Series*, *1355*(1), 012006.

Zargar, O. A., Lin, T., Zebua, A. G., Lai, T.-J., Shih, Y.-C., Hu, S.-C., & Leggett, G. (2022). The effects of surface modification on aerodynamic characteristics of airfoil DU 06 W 200 at low Reynolds numbers. *International Journal of Thermofluids*, *16*, 100208.

APPENDICES

Appendix I : OpenFoam Codes

```
OpenFOAM for Windows 20.09 (v2)

gideon kirui@DESKTOP-1S1DNJ4 /path/to/your/case/directory$
 # Step 1: Create the case directory and navigate into it

gideon kirui@DESKTOP-1S1DNJ4 /path/to/your/case/directory
$ mkdir -p turbulentFlow
cd turbulentFlow

# Step 2: Copy the mesh files (generated using a meshing tool) into the case directory

# Step 3: Set up the case files
cp -r $FOAM_TUTORIALS/incompressible/simpleFoam/pitzDaily .
cd pitzDaily

# Step 4: Modify the necessary files
# Modify the '0/U' file to set the inflow velocity boundary condition
# Modify the '0/p' file to set the pressure boundary condition
# Modify the 'constant/transport Properties' file to set the properties of the porous media
# Modify the 'system/fvSchemes' file to select suitable numerical schemes
# Modify the 'system/fvSolution' file to specify the solver settings and convergence criteria

# Step 5: Run the simulation
simpleFoam

z0=0;
zend=80.5;
zn=50; dz=(zend-z0)/(zn-1);
%dz=0.01;
z = z0:dz:zend;
%Generate array t values
t0=0; tend=1;
%creating corresponding time step
%tn=50; dt=(tend-t0)/(tn-1);
dt=0.2;
t = t0:dt:tend;
Co = 0.6;

%==PARAMETERS (Default value in parenthesis)=====
Pr1 = 0.7; % Prandtl number {5,(10),100,}
Pr2 = 0.7; % Prandtl number {5,(10),100,}
Pr3 = 0.7; % Prandtl number {5,(10),100,}
Pr4 = 0.9; % Prandtl number {5,(10),100,}
Prt1 = 0.95; %{(0.5), 1}
Prt2 = 0.95; %{(0.5), 1}
Prt3 = 0.95; %{(0.5), 1}
Prt4 = 0.9; %{(0.5), 1}
M1 = 50; % {1, 2, 5, (10), 20, 50}
m1 = 1; %Hall parameter {0.1, 0.5, 1,(2)}
M2 = 50; % {1, 2, 5, (10), 20, 50}
m2 = 2; %Hall parameter {0.1, 0.5, 1,(2)}
M3 = 5; % {1, 2, 5, (10), 20, 50}
m3 = 1; %Hall parameter {0.1, 0.5, 1,(2)}
M4 = 50; % {1, 2, 5, (10), 20, 50}
m4 = 1; %Hall parameter {0.1, 0.5, 1,(2)}
Gr = 1*9; % {1*10^4 Case of cooling the plate:(-1*10000) Case of heating the plate};
%INTITIAL CONDITIONS AT t < 0
u = zeros(length(z),length(t));
v = zeros(length(z),length(t));
theta = zeros(length(z),length(t));
% BOUNDARY CONDITIONS AT z = 0
v(:,1)=03;
velo=linspace(0,1,length(z));
temp=linspace(1,0,length(z));
for iz=1:length(z)
theta(iz,1)=(temp(iz).^2);
u(iz,1)=(velo(iz).^2);
end
%INTITIAL CONDITIONS AT t = 0
u(1:2,1:length(t)) = 02;
v(1:2,1:length(t)) = 01;
theta(1:2,1:length(t)) = 1;
%BOUNDARY CONDITIONS AT INFINITY (z = 2.5)
for i = length(z)-1:length(z)
u(i,1:length(t)) = 1;% for z tends to inf
v(i,1:length(t)) = 0;% for z tends to inf
theta(i,1:length(t)) = 0; % for z tends to inf
end
%COMPUTATION OF VARIABLES

loop = 1;
Usum11 = zeros(length(z),length(t),loop);
Usum21 = zeros(length(z),length(t),loop);
Usum31 = zeros(length(z),length(t),loop);
Usum41 = zeros(length(z),length(t),loop);
```

```
Vsum11 = zeros(length(z),length(t),loop);
Vsum21 = zeros(length(z),length(t),loop);
Vsum31 = zeros(length(z),length(t),loop);
Tsum11 = zeros(length(z),length(t),loop);
Tsum21 = zeros(length(z),length(t),loop);
Usum12 = zeros(length(z),length(t),loop);
Usum22 = zeros(length(z),length(t),loop);
Usum32 = zeros(length(z),length(t),loop);
Usum42 = zeros(length(z),length(t),loop);
Vsum12 = zeros(length(z),length(t),loop);
Vsum22 = zeros(length(z),length(t),loop);
Vsum32 = zeros(length(z),length(t),loop);
Tsum12 = zeros(length(z),length(t),loop);
Tsum22 = zeros(length(z),length(t),loop);
Usum13 = zeros(length(z),length(t),loop);
Usum23 = zeros(length(z),length(t),loop);
Usum33 = zeros(length(z),length(t),loop);
Usum43 = zeros(length(z),length(t),loop);
Vsum13 = zeros(length(z),length(t),loop);
Vsum23 = zeros(length(z),length(t),loop);
Vsum33 = zeros(length(z),length(t),loop);
Tsum13 = zeros(length(z),length(t),loop);
Tsum23 = zeros(length(z),length(t),loop);
Usum14 = zeros(length(z),length(t),loop);
Usum24 = zeros(length(z),length(t),loop);
Usum34 = zeros(length(z),length(t),loop);
Usum44 = zeros(length(z),length(t),loop);
Vsum14 = zeros(length(z),length(t),loop);
Vsum24 = zeros(length(z),length(t),loop);
Vsum34 = zeros(length(z),length(t),loop);
Tsum14 = zeros(length(z),length(t),loop);
Tsum24 = zeros(length(z),length(t),loop);
uk1 = zeros(length(z),length(t),loop);
vk1 = zeros(length(z),length(t),loop);
thetak1 = zeros(length(z),length(t),loop);
uk2 = zeros (length(z),length(t),loop);
vk2 = zeros(length(z),length(t),loop);
thetak2 = zeros(length(z),length(t),loop);
uk3 = zeros (length(z),length(t),loop);
vk3 = zeros(length(z),length(t),loop);
thetak3 = zeros(length(z),length(t),loop);
uk4 = zeros (length(z),length(t),loop);
vk4 = zeros(length(z),length(t),loop);

thetak4 = zeros(length(z),length(t),loop);
for n = 1:loop
uk1(1:length(z),1:length(t),1) = u(1:length(z),1:length(t));
vk1(1:length(z),1:length(t),1) = v(1:length(z),1:length(t));
thetak1(1:length(z),1:length(t),1) = theta(1:length(z),1:length(t));
uk2(1:length(z),1:length(t),1) = u(1:length(z),1:length(t));
vk2(1:length(z),1:length(t),1) = v(1:length(z),1:length(t));
thetak2(1:length(z),1:length(t),1) = theta(1:length(z),1:length(t));
uk3(1:length(z),1:length(t),1) = u(1:length(z),1:length(t));
vk3(1:length(z),1:length(t),1) = v(1:length(z),1:length(t));
thetak3(1:length(z),1:length(t),1) = theta(1:length(z),1:length(t));
uk4(1:length(z),1:length(t),1) = u(1:length(z),1:length(t));
vk4(1:length(z),1:length(t),1) = v(1:length(z),1:length(t));
thetak4(1:length(z),1:length(t),1) = theta(1:length(z),1:length(t));
for j = 1:length(t)
for i = length(z)-1:-1:2
%Computing Primary Velocity (u)
[Usum11(i,j,n),Usum21(i,j,n),Usum31(i,j,n),Usum41(i,j,n)] =Ueqn1(uk1(i+1,j,n),uk1(i,j,n),uk1(i-1,j,n),vk1(i,j,n),dz,i*dz,M1,m1,Gr,thetak1(i,j,n),dt);
uk1(i,j+1,n)=uk1(i,j,n)+Co*dt*(Usum11(i,j,n)+Usum21(i,j,n)+Usum31(i,j,n)+Usum41(i,j,n));
[Vsum11(i,j,n),Vsum21(i,j,n),Vsum31(i,j,n)] =Veqn1(vk1(i+1,j,n),vk1(i,j,n),vk1(i-1,j,n),uk1(i,j,n),dz,M1,m1,i*dz,dt);
vk1(i,j+1,n)= vk1(i,j,n)+Co*dt*(Vsum11(i,j,n)+Vsum21(i,j,n)-Vsum31(i,j,n));
[Tsum11(i,j,n),Tsum21(i,j,n)] = Teqn1(thetak1(i+1,j,n),thetak1(i,j,n),thetak1(i-1,j,n),uk1(i+1,j,n),uk1(i-1,j,n),i*dz,dz,Pr1, Prt1,dt);
thetak1(i,j+1,n) = thetak1(i,j,n)+Co*dt*(Tsum11(i,j,n)+Tsum21(i,j,n));
[Usum12(i,j,n),Usum22(i,j,n),Usum32(i,j,n),Usum42(i,j,n)] =Ueqn2(uk2(i+1,j,n),uk2(i,j,n),uk2(i-1,j,n),vk2(i,j,n),dz,i*dz,M2,m2,Gr,thetak2(i,j,n),dt);
uk2(i,j+1,n)=uk2(i,j,n)+Co*dt*(Usum12(i,j,n)+Usum22(i,j,n)+Usum32(i,j,n)+Usum42(i,j,n));
[Vsum12(i,j,n),Vsum22(i,j,n),Vsum32(i,j,n)] =Veqn2(vk2(i+1,j,n),vk2(i,j,n),vk2(i-1,j,n),uk2(i,j,n),dz,M2,m2,i*dz,dt);
vk2(i,j+1,n)= vk2(i,j,n)+Co*dt*(Vsum12(i,j,n)+Vsum22(i,j,n)-Vsum32(i,j,n));
[Tsum12(i,j,n),Tsum22(i,j,n)] = Teqn2(thetak2(i+1,j,n),thetak2(i,j,n),thetak2(i-1,j,n),uk2(i+1,j,n),uk2(i-1,j,n),i*dz,dz,Pr2, Prt2,dt);
thetak2(i,j+1,n) = thetak2(i,j,n)+Co*dt*(Tsum12(i,j,n)+Tsum22(i,j,n));
[Usum13(i,j,n),Usum23(i,j,n),Usum33(i,j,n),Usum43(i,j,n)] =Ueqn3(uk3(i+1,j,n),uk3(i,j,n),uk3(i-1,j,n),vk3(i,j,n),dz,i*dz,M3,m3,Gr,thetak3(i,j,n),dt);
uk3(i,j+1,n)=uk3(i,j,n)+Co*dt*(Usum13(i,j,n)+Usum23(i,j,n)+Usum33(i,j,n)+Usum43(i,j,n));
[Vsum13(i,j,n),Vsum23(i,j,n),Vsum33(i,j,n)] = Veqn3(vk3(i+1,j,n),vk3(i,j,n),vk3(i-1,j,n),uk3(i,j,n),dz,M3,m3,i*dz,dt);
vk3(i,j+1,n)= vk3(i,j,n)+Co*dt*(Vsum13(i,j,n)+Vsum23(i,j,n)-Vsum33(i,j,n));
[Tsum13(i,j,n),Tsum23(i,j,n)] =Teqn3(thetak3(i+1,j,n),thetak3(i,j,n),thetak3(i-1,j,n),uk3(i+1,j,n),uk3(i-1,j,n),i*dz,dz,Pr3, Prt3,dt);
thetak3(i,j+1,n) = thetak3(i,j,n)+Co*dt*(Tsum13(i,j,n)+Tsum23(i,j,n));
[Usum14(i,j,n),Usum24(i,j,n),Usum34(i,j,n),Usum44(i,j,n)] =Ueqn4(uk4(i+1,j,n),uk4(i,j,n),uk4(i-1,j,n),vk4(i,j,n),dz,i*dz,M4,m4,Gr,thetak4(i,j,n),dt);
uk4(i,j+1,n)=uk4(i,j,n)+Co*dt*(Usum14(i,j,n)+Usum24(i,j,n)+Usum34(i,j,n)+Usum44(i,j,n));
[Vsum14(i,j,n),Vsum24(i,j,n),Vsum34(i,j,n)] = Veqn4(vk3(i+1,j,n),vk4(i,j,n),vk4(i-1,j,n),uk4(i,j,n),dz,M4,m4,i*dz,dt);
vk4(i,j+1,n)= vk4(i,j,n)+Co*dt*(Vsum14(i,j,n)+Vsum24(i,j,n)-Vsum34(i,j,n));
[Tsum14(i,j,n),Tsum24(i,j,n)] = Teqn4(thetak4(i+1,j,n),thetak4(i,j,n),thetak4(i-1,j,n),uk4(i+1,j,n),uk4(i-1,j,n),i*dz,dz,Pr4, Prt4,dt);
thetak4(i,j+1,n) = thetak4(i,j,n)+Co*dt*(Tsum14(i,j,n)+Tsum24(i,j,n));
end
end
uk1(:,:,n+1) = uk1(:,:,n);
vk1(:,:,n+1) = vk1(:,:,n);
thetak1(:,:,n+1) = thetak1(:,:,n);
uk2(:,:,n+1) = uk2(:,:,n);
vk2(:,:,n+1) = vk2(:,:,n);
thetak2(:,:,n+1) = thetak2(:,:,n);
uk3(:,:,n+1) = uk3(:,:,n);
vk3(:,:,n+1) = vk3(:,:,n);
thetak3(:,:,n+1) = thetak3(:,:,n);
thetak4(:,:,n+1) = thetak3(:,:,n);
end
% Plot the results
figure;
plot(Vsum34);
```

```
xlabel('Spatial step (i)');
ylabel('U');
title('Final U profiles');
legend(['M = ' num2str(M_values(1)) ', Pr = ' num2str(Pr_values(1))], ...
    ['M = ' num2str(M_values(2)) ', Pr = ' num2str(Pr_values(2))], ...
    ['M = ' num2str(M_values(3)) ', Pr = ' num2str(Pr_values(3))]);

% CONSTRUCTING THE PRIMARY VELOCITY PROFILES
figure(1)
plot(z(1:length(z)), uk1(1:length(z), floor(0.5 * length(t)), loop), 'r', 'LineWidth', 1.5);
hold on;
plot(z(1:length(z)), uk2(1:length(z), floor(0.5 * length(t)), loop), 'g', 'LineWidth', 1.5);
plot(z(1:length(z)), uk3(1:length(z), floor(0.5 * length(t)), loop), 'b', 'LineWidth', 1.5);
% plot(z(1:length(z)), uk4(1:length(z), floor(0.5 * length(t)), loop), 'k', 'LineWidth', 1.5);
ylim([0 1]);
xlabel('$z$', 'interpreter', 'latex', 'FontSize', 16, 'FontWeight', 'bold');
ylabel('Primary Velocity');
legend('I', 'II', 'III', 'IV');
text(30, .8, ' Gr = 12, Pr = 0.7');
hold off

% CONSTRUCTING THE SECONDARY VELOCITY PROFILES
figure(2)
plot(z(1:length(z)), vk1(1:length(z), floor(0.5 * length(t)), loop), 'r', 'LineWidth', 1.5);
hold on;
plot(z(1:length(z)), vk2(1:length(z), floor(0.5 * length(t)), loop), 'g', 'LineWidth', 1.5);
plot(z(1:length(z)), vk3(1:length(z), floor(0.5 * length(t)), loop), 'b', 'LineWidth', 1.5);
% plot(z(1:length(z)), vk4(1:length(z), floor(0.5 * length(t)), loop), 'k', 'LineWidth', 1.5);
xlabel('$z$', 'interpreter', 'latex', 'FontSize', 16, 'FontWeight', 'bold');
ylim([-0.4 1]);
ylabel('Secondary Velocity');
legend('I', 'II', 'III', 'IV');
 text(1, 0.9, 'Gr = 12');
hold off

% CONSTRUCTING THE TEMPERATURE PROFILES
figure(3)
plot(z(1:length(z)), thetak1(1:length(z), floor(0.5 * length(t)), loop), 'r', 'LineWidth', 1.5);
hold on;
plot(z(1:length(z)), thetak2(1:length(z), floor(0.5 * length(t)), loop), 'g', 'LineWidth', 1.5);
plot(z(1:length(z)), thetak3(1:length(z), floor(0.5 * length(t)), loop), 'b', 'LineWidth', 1.5);
plot(z(1:length(z)), thetak4(1:length(z), floor(0.5 * length(t)), loop), 'k', 'LineWidth', 1.5);
xlabel('$z$', 'interpreter', 'latex', 'FontSize', 16, 'FontWeight', 'bold');
ylim([0 1]);
ylabel('Temperature');

legend(['M = ' num2str(M_values(1)) ', Pr = ' num2str(Pr_values(1))], ...
    ['M = ' num2str(M_values(2)) ', Pr = ' num2str(Pr_values(2))], ...
    ['M = ' num2str(M_values(3)) ', Pr = ' num2str(Pr_values(3))]);

text(20, 0.9, 'Gr =- 10, Prt = 0.85');
hold off

save('Result.mat', 'uk1', 'uk2', 'uk3', 'vk1', 'vk2', 'vk3', 'thetak1', 'thetak2', 'thetak3', 'thetak4');



function [Usum11,Usum21,Usum31,Usum41] = Ueqn1(urr,urc,url,vrc,dz,z,M1,m1,Gr,thetarc,dt)
Usum11 = 2*dt*((urr-2*urc+url)/(dz*dz)+(0.32*z*(((urr-urc)./(2*dz)).^2)));
Usum21 = 2*dt*((urr-2*urc+url)/(dz*dz))*(((urr-url)/(2*dz)))*(z*z*0.32);
Usum31 = 2*dt*M1*M1*((m1*vrc-urc)/(1+m1*m1));
Usum41 = 2*dt*(Gr*thetarc);
end
function [Vsum11,Vsum21,Vsum31] = Veqn1(vrr,vrc,vrl,urc,dz,M1,m1,z,dt)
Vsum11 = 2*dt*((vrr-2*vrc+vrl)/(dz*dz)+(0.32*z*((vrr-vrc)/(2*dz)).^2));
Vsum21 = 2*dt*(((vrr-2*vrc+vrl)/(dz*dz)).*((vrr-vrc)/(2*dz)))*(z*z*0.32);
Vsum31 = 2*dt*(M1*M1)*((m1*urc+vrc)/(1+m1*m1));
end
function [Tsum11,Tsum21] = Teqn1(thetarr,thetarc,thetarl,urr,urc,z,dz,Pr1,Prt1,dt)
Tsum11 = (2*dt/(Pr1))*((thetarr-2*thetarc+thetarl)/(dz*dz));
Tsum21 = (0.32*z*z*2*dt/Prt1)*(((urr-urc)/(2*dz)).*((thetarr-thetarc)/(2*dz)));
end
function [Usum12,Usum22,Usum32,Usum42] = Ueqn2(urr,urc,url,vrc,dz,z,M2,m2,Gr,thetarc,dt)
Usum12 = 2*dt*((urr-2*urc+url)/(dz*dz)+(0.32*z*(((urr-urc)./(2*dz)).^2)));
Usum22 = 2*dt*((urr-2*urc+url)/(dz*dz))*(((urr-url)/(2*dz)))*(z*z*0.32);
Usum32 = 2*dt*M2*M2*((m2*vrc-urc)/(1+m2*m2));
Usum42 = 2*dt*(Gr*thetarc);
end
function [Vsum12,Vsum22,Vsum32] = Veqn2(vrr,vrc,vrl,urc,dz,M2,m2,z,dt)
Vsum12 = 2*dt*((vrr-2*vrc+vrl)/(dz*dz)+(0.32*z*((vrr-vrc)/(2*dz)).^2));
Vsum22 = 2*dt*(((vrr-2*vrc+vrl)/(dz*dz)).*((vrr-vrc)/(2*dz)))*(z*z*0.32);

Vsum32 = 2*dt*(M2*M2)*((m2*urc+vrc)/(1+m2*m2));
end
function [Tsum12,Tsum22] = Teqn2(thetarr,thetarc,thetarl,urr,urc,z,dz,Pr2,Prt2,dt)
Tsum12 = (2*dt/(Pr2))*((thetarr-2*thetarc+thetarl)/(dz*dz));
Tsum22 = (0.32*z*z*2*dt/Prt2)*(((urr-urc)/(2*dz)).*((thetarr-thetarc)/(2*dz)));
end
function [Usum13,Usum23,Usum33,Usum43] = Ueqn3(urr,urc,url,vrc,dz,z,M3,m3,Gr,thetarc,dt)
Usum13 = 2*dt*((urr-2*urc+url)/(dz*dz)+(0.32*z*(((urr-urc)./(2*dz)).^2)));
Usum23 = 2*dt*((urr-2*urc+url)/(dz*dz))*(((urr-url)/(2*dz)))*(z*z*0.32);
Usum33 = 2*dt*M3*M3*((m3*vrc-urc)/(1+m3*m3));
Usum43 = 2*dt*(Gr*thetarc);
end
function [Vsum13,Vsum23,Vsum33] = Veqn3(vrr,vrc,vrl,urc,dz,M3,m3,z,dt)
Vsum13 = 2*dt*((vrr-2*vrc+vrl)/(dz*dz)+(0.32*z*((vrr-vrc)/(2*dz)).^2));
Vsum23 = 2*dt*(((vrr-2*vrc+vrl)/(dz*dz)).*((vrr-vrc)/(2*dz)))*(z*z*0.32);
Vsum33 = 2*dt*(M3*M3)*((m3*urc+vrc)/(1+m3*m3));
end
function [Tsum13,Tsum23] = Teqn3(thetarr,thetarc,thetarl,urr,urc,z,dz,Pr3,Prt3,dt)
Tsum13 = (2*dt/(Pr3))*((thetarr-2*thetarc+thetarl)/(dz*dz));
```

```
Tsum23 = (0.32*z*z*2*dt/Prt3)*(((urr-urc)/(2*dz)).*((thetarr-thetarc)/(2*dz)));
end
function [Usum14,Usum24,Usum34,Usum44] = Ueqn4(urr,urc,url,vrc,dz,z,M4,m4,Gr,thetarc,dt)
Usum14 = 2*dt*((urr-2*urc+url)/(dz*dz)+(0.32*z*(((urr-urc)./(2*dz)).^2)));
Usum24 = 2*dt*((urr-2*urc+url)/(dz*dz))*(((urr-url)/(2*dz)))*(z*z*0.32);
Usum34 = 2*dt*M4*M4*((m4*vrc-urc)/(1+m4*m4));
Usum44 = 2*dt*(Gr*thetarc);
end
function [Vsum14,Vsum24,Vsum34] = Veqn4(vrr,vrc,vrl,urc,dz,M4,m4,z,dt)
Vsum14 = 2*dt*((vrr-2*vrc+vrl)/(dz*dz)+(0.32*z*((vrr-vrc)/(2*dz)).^2));
Vsum24 = 2*dt*(((vrr-2*vrc+vrl)/(dz*dz)).*((vrr-vrc)/(2*dz)))*(z*z*0.32);
Vsum34 = 2*dt*(M4*M4)*((m4*urc+vrc)/(1+m4*m4));
end

function [Tsum14,Tsum24] = Teqn4(thetarr,thetarc,thetarl,urr,urc,z,dz,Pr4,Prt4,dt)
Tsum14 = (2*dt/(Pr4))*((thetarr-2*thetarc+thetarl)/(dz*dz));
Tsum24 = (0.32*z*z*2*dt/Prt4)*(((urr-urc)/(2*dz)).*((thetarr-thetarc)/(2*dz)));
End

% Define angles of attack in degrees
angles = [0, 20, 40, 60, 80];

% Define the airfoil span (normalized distance along the chord length)
x = linspace(0, 1, 100);

% Define a base velocity (can be adjusted as per your model)
base_velocity = 10;

% Preallocate matrix for velocities
velocities = zeros(length(angles), length(x));

% Loop over each angle of attack
for i = 1:length(angles)
   % Calculate velocity distribution based on angle of attack
   % Here, we use a simple model: velocity increases with the angle of attack
   angle_rad = deg2rad(angles(i));
   velocities(i, :) = base_velocity * (1 + 0.1 * angle_rad * x);
end

% Plot the results
figure;
hold on;
colors = ['r', 'g', 'b', 'm', 'c'];
for i = 1:length(angles)
   plot(x, velocities(i, :), 'color', colors(i), 'DisplayName', sprintf('Angle: %d°', angles(i)));
end
hold off;

xlabel('Normalized Distance Along Chord Length');
ylabel('Airflow Velocity');
title('Airflow Velocity Distribution Across Airfoil');
legend('show');
grid on;
% Define parameters and constants
Delta_t = 03.01;  % Time step size
Delta_r = 20.1;   % Spatial step size
iMax = 100;       % Number of spatial steps
jMax = 100;       % Number of time steps
U0 = 1000;          % Constant U0
Gr = 100000010;         % Grashof number
Re = 1050;        % Reynolds number

% Define arrays for M and Pr values
M_values = [0.5, 1, 1.5];  % Different values of M
Pr_values = [0.7, 1, 1.3]; % Different values of Pr

% Initialize arrays to store results
U_final = zeros(iMax, length(M_values));

% Loop over different values of M and Pr
for idx = 1:length(M_values)
   M = M_values(idx);
   Pr = Pr_values(idx);

   % Initialize U for each simulation
   U = zeros(iMax, jMax);
   U(:, 1) = 0; % Initial condition for U

   % Time-stepping loop
   for j = 1:jMax-1
      for i = 2:iMax-1
         % Update U using the finite difference scheme
         U(i, j+1) = U(i, j) + Delta_t * ((U(i+1, j) - 2*U(i, j) + U(i-1, j)) / Delta_r^2 ...
            + 1/(i*Delta_r) * (U(i+1, j) - U(i, j)) / Delta_r) ...
            + 1/U0 * (U(i, j) / Delta_r * (U(i+1, j) - U(i, j))) ...
            + ((U(i+1, j) - 2*U(i, j) + U(i-1, j)) / Delta_r^2) ...
            + Gr / (Re^2 * Pr) ...
            + M^2 * ((U(i, j) + 0.1 * U(i, j)) / (U0 * (1 + 0.1^2)));
      end
   end

   % Store the final U profile
   U_final(:, idx) = U(:, end);
end

% Plot the results
figure;
plot(U_final);
xlabel('Spatial step (i)');
ylabel('U');
title('Final U profiles');
```

```
legend(['M = ' num2str(M_values(1)) ', Pr = ' num2str(Pr_values(1))], ...
       ['M = ' num2str(M_values(2)) ', Pr = ' num2str(Pr_values(2))], ...
       ['M = ' num2str(M_values(3)) ', Pr = ' num2str(Pr_values(3))]);

% Constants
delta_t = 0.00085; % Time step
delta_r = 0.075; % Spatial step
k = 1; % Example constant
Gr = 4.10; Re = 100; Pr = 1.1; M = 1; U_0 = 0.710; m = 1; % More constants
num_r = 10; % Number of spatial points
num_t = 10; % Number of time steps
r = linspace(0, 2, num_r); % Radius values
U = zeros(num_r, num_t); % Initialize U

% Initial condition
U(:, 1) = sin(pi * r); % Example initial condition

% Time-stepping loop
for j = 1:num_t-1
    for i = 2:num_r-1 % Avoiding boundary points
        term1 = (U(i+1, j) - 2*U(i, j) + U(i-1, j)) / delta_r^2;
        term2 = (1/i) * (U(i+1, j) - U(i, j)) / delta_r;
        term3 = k^2 * r(i) * (U(i+1, j) - U(i, j))^2 / delta_r;
        term4 = Gr / (Re^2 * Pr) + M^2 * (U(i, j) + m*U(i, j)) / (U_0 * (1 + m^2));
        U(i, j+1) = U(i, j) + delta_t * (term1 + term2 + term3 + delta_t * term4);
    end
end
% Plotting
figure;
plot(r, U(:, end), 'r', 'DisplayName', 'U at final time'); % Plotting the last time step
hold on;
plot(r, U(:, 1), 'b', 'DisplayName', 'Initial U'); % Initial condition for reference
xlabel('Radius');
ylabel('Primary Velocity (U)');
title('Primary Velocity vs. Radius of the Wing');
% Add the table to the figure
data = table(Gr', Pr', 'VariableNames', {'Gr', 'Pr'});
uitable('Data', data{:,:}, 'ColumnName', data.Properties.VariableNames, ...
    'RowName', [], 'Units', 'Normalized', 'Position', [0.16, 0.2, 0.3, 0.2]);

legend show;

grid on;
% Define the parameters
Re = 100;       % Reynolds number
Pr = 0.0007;        % Prandtl number
k = 1;          % Some constant related to your specific problem
Delta_t = 15.01; % Time step size
Delta_r = 34.91;  % Spatial step size
iMax = 100;     % Number of spatial steps
jMax = 100;     % Number of time steps

% Initialize arrays
theta = zeros(iMax, jMax);
U = zeros(iMax, jMax);

% Boundary and initial conditions
theta(:, 001) = 0; % Initial condition for all i when j<0 (assuming j starts from 1 in MATLAB)
U(:, 01) = 0;     % Initial velocity condition

% Specific conditions at i = Re/2 (adjust for MATLAB indexing, floor to nearest integer)
iMid = floor(Re/2/Delta_r);
if iMid <= iMax
    theta(iMid, :) = 1;
    U(iMid, :) = 1;
end

% Time-stepping loop
for j = 1:jMax-1
    for i = 2:iMax-1
        % Apply the scheme (4.79)
        theta(i, j+1) = theta(i, j) + Delta_t/(Re*Pr) * ...
            ((theta(i+1, j) - 2*theta(i, j) + theta(i-1, j)) / Delta_r^2 + ...
            1/(i*Delta_r) * (theta(i+1, j) - theta(i, j)) / Delta_r) + ...
            (k^2 * Delta_t * (i*Delta_r)^2) / (Re*Pr)^2 * ...
            ((U(i+1, j) - U(i, j)) / Delta_r) * ...
            ((theta(i+1, j) - theta(i, j)) / Delta_r);
    end
    % Boundary conditions as i -> infinity (approximate this by setting the last row to zero)
    theta(iMax, j+1) = 0;
end

% Select times at which to plot theta profiles
selectedTimes = [1, 25, 50, 75, 100]; % Example time steps to plot
colors = ['b', 'g', 'r', 'c', 'm']; % Colors for each plot
figure;
hold on;
for idx = 1:length(selectedTimes)
    plot(theta(:, selectedTimes(idx)), colors(idx), 'LineWidth', 2)
end
hold off;
xlabel('Spatial step (i)')
ylabel('Theta')
title('Temperature Profiles at Various Times')
legend(arrayfun(@(t) sprintf('t = %d', t), selectedTimes, 'UniformOutput', false), 'Location', 'northeast')
```

Appendix II : Letter of authorization for data collection

Appendix 2 : UoK graduate school clearance

UNIVERSITY OF KABIANGA
ISO 9001:2015 CERTIFIED
OFFICE OF THE DIRECTOR, BOARD OF GRADUATE STUDIES

REF: PGC/AM/008/19 **DATE: 12TH MAY, 2023**

Gideon Kimutai Kirui,
MAPS Department,
University of Kabianga,
P.O Box 2030- 20200,
KERICHO.

Dear Mr. Kirui,

RE: CLEARANCE TO COMMENCE FIELD WORK/DATA COLLECTION

I am pleased to inform you that the Board of Graduate Studies has considered and approved your Masters research proposal entitled **"Numerical Investigation of Turbulent Fluid Flow over a Porous Aerofoil Wing Design within a Magnetic Field"**. Subsequently the Board has also approved the following supervisors for appointments.

1. Dr. Wilys O. Mukuna, PhD
2. Prof. Maurice O. Oduor, PhD

You may now proceed to commence field work/data collection on condition that you obtain a research permit from NACOSTI and /or an ethical review permit from a relevant ethics review board.

You are also required to publish one (1) article in a peer reviewed journal, with all your supervisors, before your oral defense of thesis and to submit through your supervisors, and HoD, progress reports every three months, to the Director, Board of Graduate Studies.

Please note that it is the policy of the University that you complete your studies within two years from the date of registration. Do not hesitate to consult this office in case of any difficulties encountered in the course of your studies.

I wish you all the best in your research and hope that your study will yield original contribution for the betterment of humanity.

Yours Sincerely,

UNIVERSITY OF KABIANGA
12 MAY 2023
BOARD OF GRADUATE STUDIES

Dr. Ronald K. Rop
DIRECTOR, BOARD OF GRADUATE STUDIES.
RKR/hk

cc 1. Dean, SST
2. HOD, MAPS
3. Supervisors

Appendix III: NACOSTI research permit

REPUBLIC OF KENYA

NATIONAL COMMISSION FOR SCIENCE,TECHNOLOGY & INNOVATION

Ref No: 174054

Date of Issue: 29/September/2023

RESEARCH LICENSE

This is to Certify that Mr.. Gideon KIMUTAI Kirui of University of Kabianga, has been licensed to conduct research as per the provision of the Science, Technology and Innovation Act, 2013 (Rev.2014) in Kericho on the topic: NUMERICAL INVESTIGATION OF TURBULENT FLUID FLOW OVER A POROUS AEROFOIL WING DESIGN WITHIN A MAGNETIC FIELD for the period ending : 29/September/2024.

License No: NACOSTI/P/23/30067

174054

Applicant Identification Number

Director General
NATIONAL COMMISSION FOR SCIENCE,TECHNOLOGY & INNOVATION

Verification QR Code

NOTE: This is a computer generated License. To verify the authenticity of this document, Scan the QR Code using QR scanner application.

See overleaf for conditions

Appendix IV: Publication

IARJSET

International Advanced Research Journal in Science, Engineering and Technology

Impact Factor 8.066 ⁜ Peer-reviewed / Refereed journal ⁜ Vol. 1, Issue 1, September 2024

DOI 10.17148/IARJSET, ISSN (O) 2393-8021, ISSN (P) 2394-1588

NUMERICAL INVESTIGATION OF TURBULENT FLUID FLOW OVER A POROUS AEROFOIL WING DESIGN WITHIN A MAGNETIC FIELD

Kirui G. K[1], Mukuna W. O[1], Oduor M. O[1]

Department of Mathematics, Actuarial and Physical Science,

University of Kabianga,

P.O.Box 2030-20200 KERICHO, KENYA

Abstract: A mathematical model of turbulent fluid flow over a porous aerofoil wing design within a magnetic field is considered. The fluid flow was modelled using Navier stokes equations of conservation of momentum, energy and mass in cylindrical coordinates. The governing equations were then non-dimentionalized and gave rise to the non-dimensional parameters. Computational fluid dynamics (CFD) techniques was used to simulate the flow of air over a porous wing within a range of magnetic field strengths. Examinations of the effects of the magnetic field on key performance metrics such as lift, drag, and efficiency, as well as the overall flow structure of the wing was performed and found valuable insights into the use of porous aerofoil wings in the design of aircraft operating in high-magnetic field environments, such as those found in space or near the Earth's poles. Additionally, the outcomes of the research had wider implications for other domains investigating the impact of magnetic fields on fluid motion, such as in the design of magnetic resonance imaging systems or in the study of planetary motions. Aerofoil wings are an essential component of aircraft design, as they provide lift and enable flight. However, the flow of air over the wing is often turbulent, which can lead to decreased efficiency and performance. Porous aerofoil wings was proposed as a means of reducing turbulence, and the effects of such wings on fluid flow within a magnetic field have been thoroughly investigated. In this research, numerical investigation of the effects of a magnetic field on turbulent fluid flow over a porous aerofoil wing design was done. It is evident from the results that the primary velocities increase when the magnetic parameter was reduced. It was also found that the lift force increases when the Grashof number and Prandtl number decreases.

Keywords: Turbulent, Porous medium, Aerofoil, Prandtl number, Magneto hydrodynamics.

ACKNOWLEDGMENT

I gratefully acknowledge the funding received towards my MSc. from Higher Education Loans Board –(HELB), which enabled me to carry out this research.

IARJSET

International Advanced Research Journal in Science, Engineering and Technology

Impact Factor 8.066 ⨳ Peer-reviewed / Refereed journal ⨳ Vol. 1, Issue 1, September 2024

DOI 10.17148/IARJSET, ISSN (O) 2393-8021, ISSN (P) 2394-1588

REFERENCES

[1]. Ahmed, T. (2013). Computational study of flow around a NACA 0012 wing flapped at different flap angles with varying Mach numbers. *Global Journals of Research in Engineering*, *13*(J4), 5-15.

[2]. Aldheeb, M. A., Asrar, W., Sulaeman, E., & Omar, A. A. (2016). A review on aerodynamics of non-flapping bird wings. *Journal of Aerospace Technology and Management*, *8*(1), 7–17.

[3]. Alsahlan, A., & Abdulkarim, T. (2017). Aerofoil design for unmanned high-altitude aft-swept flying wings. *Journal of Aerospace Technology and Management*, *9*, 335–345.

[4]. Amrit, A., Leifsson, L., & Koziel, S. (2018). Multi-fidelity aerodynamic design trade-off exploration using point-by-point Pareto set identification. *Aerospace Science and Technology*, *79*, 399–412.

[5]. Blakey-Milner, B., Gradl, P., Snedden, G., Brooks, M., Pitot, J., Lopez, E., ... & du Plessis, A. (2021). Metal additive manufacturing in aerospace: A review. *Materials & Design*, *209*, 110008.

[6]. Chebos, C., Sigey, J., Okelo, J., Okwoyo, J., & Giterere, K. (2016). Numerical investigation of unsteady MHD free convective flow past an oscillating vertical porous plate with oscillatory heat flux. *The SIJ Transactions on Computer Networks & Communication Engineering*, *04*(01), 01–09.

[7]. Chen, L., & Zonca, F. (2016). Physics of Alfvén waves and energetic particles in burning plasmas. *Reviews of Modern Physics*, *88*(1),1–12.

[8]. Cortés-Domínguez, I., & Burguete, J. (2018). Instabilities triggered in different conducting fluid geometries due to slowly time-dependent magnetic fields. *Chaos: An Interdisciplinary Journal of Nonlinear Science*, *28*(7), 075514.

[9]. Frost, W. (2013). *Heat transfer at low temperatures*. Springer Science & Business Media.

[10]. Joshi, S. N., & Gujarathi, Y. S. (2016). A review on active and passive flow control techniques. *International Journal on Recent Technologies in Mechanical and Electrical Engineering*, *3*(4), 1–6.

[11]. Keshri, O. P., Kumar, A., & Gupta, V. K. (2018). Magento-solutal convection in Newtonian fluid layer with solutal modulated boundaries. *International Journal of Non-Linear Mechanics*, *107*, 86–93.

[12]. Klose, B., Jacobs, G. B., Tank, J., & Spedding, G. (2018). Low Reynolds number airfoil aerodynamics: three different flow patterns within an angle of attack range of four degrees. In *2018 Fluid Dynamics Conference* (p. 3731).

[13]. Manda, A. Y., Chada, J. S. R., Surapaneni, S. P., & Geeri, S. (2020). Flow behaviour on aerofoils using CFD. *Journal of Mechanical Engineering, Automation and Control Systems*, *1*(1), 26–36.

IARJSET
International Advanced Research Journal in Science, Engineering and Technology
Impact Factor 8.066 ⁝ Peer-reviewed / Refereed journal ⁝ Vol. 1, Issue 1, September 2024
DOI 10.17148/IARJSET, ISSN (O) 2393-8021, ISSN (P) 2394-1588

BIOGRAPHY

GIDEON KIMUTAI KIRUI was born in 1995 in Rift Valley Kenya. A Mathematics and Physics Teacher at Kabianga National school, Department of Mathematics and Science, he holds a First class degree in Education Science from Maasai Mara University. Being a science and engineering patron at Kabianga high school his research interests are in the areas of Differential Equations, Fluid Dynamics and Magnetohydrodynamics.

Born in 1977, Western Kenya, Dr. Wilys Mukuna is currently a Senior Lecturer at the Department of Mathematics, Actuarial and Physical Sciences, University of Kabianga Kenya. He holds a Doctor of Philosophy degree in Applied Mathematics from Jomo Kenyatta University of Agriculture and Technology. Engaged in teaching at both undergraduate and post graduate levels his research interests are in the areas of Computational fluid Dynamics and modelling

Prof. Maurice Owino is a Professor of Pure Mathematics in the Department of Mathematics, Actuarial and Physical Sciences. He is the Deputy Vice Chancellor in charge of Planning, Research and Development at the University of Kabianga. P.O.Box 2030-20200 Kericho, Kenya Tel.: +254721-753-991
Email:moduor@kabianga.ac.ke, morricearaka@yahoo.com